MODEL FOR INTERPRETATION OF PIPELINE SURVEY DATA

By

CHENCHEN QIU

A DISSERTATION PRESENTED TO THE GRADUATE SCHOOL
OF THE UNIVERSITY OF FLORIDA IN PARTIAL FULFILLMENT
OF THE REQUIREMENTS FOR THE DEGREE OF
DOCTOR OF PHILOSOPHY

UNIVERSITY OF FLORIDA

2003

ACKNOWLEDGMENTS

I would like to express my sincerest gratitude and appreciation to Dr. Mark E. Orazem for his support, inspiration and guidance in directing this study. His hard work and attention to detail were an excellent example during my studies. He always helped me to learn more and taught me the importance of thinking creatively. Many of the advances achieved during my graduate study would not have been possible without his support. I would also like to gratefully acknowledge Dr. Loc Vu Quoc for teaching me the boundary element method at the early stage of this work. Moreover, I wish to thank Dr. Anthony J. Ladd, Dr. Oscar D. Crisalle, and Dr. Darryl Butt for their time, useful discussions and guidance as members of the supervisory committee. I would like to acknowledge the financial support of the Pipeline Research Council, International and Gas Research Institute. My colleagues, Douglas P. Riemer, Kerry Allahar, Nelliann Perez-Garcia, Pavan Shukla, who have contributed to this research by their valuable discussions and friendship, are also gratefully acknowledged. Finally, I would like to thank my husband, Kuide Qin, for his unselfish support and understanding throughout my doctorate work, which would not have been possible without him. I would also like to thank my parents and my sister for their encouragement and inspiration. Even though they were half a planet away from me, they have always been with me in my heart.

TABLE OF CONTENTS

LIST OF TABLES

LIST OF FIGURES

Abstract of Dissertation Presented to the Graduate School
of the University of Florida in Partial Fulfillment of the
Requirements for the Degree of Doctor of Philosophy

MODEL FOR INTERPRETATION OF PIPELINE SURVEY DATA

By

Chenchen Qiu

December 2003

Chair: Mark E. Orazem
Major Department: Chemical Engineering

Pipeline corrosion annually costs the U.S. seven billions of dollars. Ninety percent of the cost is the capital, operation and maintenance. It is desirable to optimize this expenditure while ensuring that the integrity of the pipeline, which represents a valuable asset, is maintained. Regular inspection of pipelines using a variety of survey techniques is routinely conducted, but interpretation of the results is confounded by stochastic and systematic errors. The objective of the present work was to investigate use of *inverse* model that could interpret survey data in the context of the physics of the system.

An *inverse* analysis model was developed which provides a mathematical framework for interpretation of survey data in the presence of random noise. A boundary-element *forward* model was coupled with a weighted nonlinear regression algorithm to obtain pipe surface properties from two types of survey data: soil-surface potentials and local values of current flowing through the pipe. The *forward* model accounted for the passage of current through a three-dimensional

homogeneous medium and yielded soil surface potentials for given pipe/anode configurations and pipe coating properties. The number of regressed parameters was reduced by using a function for coating resistivity that allowed specification of coating defects. A weighted simulate-annealing nonlinear regression algorithm facilitated analysis of noisy data. A method to determine the appropriate number of fitted parameters was developed.

The model was demonstrated for synthetic data generated for a section of a coated underground pipeline electrically connected to a vertical sacrificial anode. The success of the regression was sensitive to the relative weighting applied in the objective function to the respective types of data. A generalized weighted and scaled objective function was proposed.

NOTATION

ϕ	Potential and potential distribution, V
ψ	Potential and potential distribution refer to the reference electrode, defined as $V - \phi$, V
ρ_k	Resistance reduction of the coating defect k, Ω·m
σ_k	The half width of the coating defect k, m
$\vec{n}$	Normal vector of boundary
c_j	Concentration of species j, mol/cm^3
D_j	Diffusion coefficient of species j, cm^2/s
F	Faraday's constant, 96487C/equiv
i	Current density, A/m^2
u_j	Mobility of species j, cm$^2 \cdot$ mol/J $\cdot$ s
V	Voltage distribution of pipe steel or anode metal, V
v	Bulk velocity, cm/s
x_k	Center point of the coating defects k, m
z_j	Charge number of species j
ρ	Resistivity of the pipe coating, Ω·m

CHAPTER 1
INTRODUCTION

In the U.S., there are 779,000 km (484,000 mi) of gas and liquid transmission pipelines. Seven billion of dollars is spent due to pipeline corrosion every year. 90% of the cost is the capital, operation and maintenance. It is desirable to optimize this expenditure while ensuring that the integrity of the pipeline, which represents a valuable asset, is maintained. Regular inspection of pipelines using a variety of survey techniques is routinely conducted, but interpretation of the results is confounded by stochastic and systematic errors.

The goal of this work was to develop a computer program that can be used to extract the condition of the pipe taking into account a wide variety of field data, such as potential and line current survey data. In addition, the intention of this preliminary effort was to establish a *proof of concept* which can motivate future development.

The pipeline protection techniques that are used most often are cathodic protection and coating. The normal use of computer programs for modeling of cathodic protection is to assess whether a pipeline with an assumed coating condition can be protected by a given cathodic protection design. In this strategy, called a *forward solution,* all physical properties of the pipe, anodes, ground beds, and the soil are assumed, and the corresponding distribution of current and potential on the pipe is calculated. Over-protected and under-protected sections of the pipeline can be identified in this way. Such programs can also be used to calculate the potential and the current density at other locations such as at the soil surface or at

the specified locations where coupons may be buried. This strategy lends itself well to answering "what if" questions. For example, "what will happen if discrete coating holidays expose five percent of the pipe surface?", or "what will happen if a new pipe is constructed in the right-of-way?"

The *forward* strategy is not appropriate, however, for the interpretation of field data to assess whether a given pipe is protected. The concept behind the approach developed in this work is to solve the *inverse problem* in which the properties of the pipe coating are inferred from measurements of the current and the potential distributions. This approach would allow interpretation of field data in a manner that would take into account the physical laws that constrain the flow of electrical current from anode to pipe.

In addition, the development of the *inverse* model can not proceed alone. Only when the *forward* model is well developed can the *inverse* model be able to interpret multiple kinds of survey data.

The basic concepts of the corrosion, corrosion protection methods, and pipeline survey methods are presented in Chapter 2.

Verification of published methods for model two-dimensional systems are presented in Chapter 3. This chapter includes the thin-plate method and the boundary element method to solve the two-dimensional Laplace's equation. The two--dimensional *inverse* model is also established in this chapter. This work involved the construction of the objective function, the formalism of regression strategies, and regression methods analysis.

The development of the *forward* and the *inverse* models for two-dimensional systems provided insights into the methods needed to address the *inverse* problem for pipelines. However, the two-dimensional *forward* model cannot describe precisely the geometry of the pipeline cathodic protection system. In addition, the

more sophisticated three-dimensional *forward* models such as CP3D,[1] PROCAT,[2] and OKAPPI[3] are not appropriate , since they require too much computation work for the *inverse* model. A simplified version of a *forward* is presented in Chapter 4. Both the *forward* model and *inverse* model are applied to soil surface potential survey data. For the *forward* part, a three-dimensional boundary element method with cylindrical elements was developed in this work. The simulated annealing method was shown to be ideally suitable for the three-dimensional *inverse* model. In addition, several strategies were explored to assess the confidence level of the *inverse* model results.

The *forward* model presented in Chapter 4 provided the foundation for an extended model, presented in Chapter 5, which accounted for the potential drop along the pipe steel. Both the potential on soil surface and the current density along the pipeline could be obtained from the *forward* model. An *inverse* model was created to apply these data. A new general form of the objective function was established by adding different weighting factors for each data point and by including the number of the data points.

Chapter 6 verifies the general form of the objective function built in Chapter 5. Off-potential on the soil surface was simulated in the *forward* model. Therefore, three kinds of data sets, *i.e.*, on-potential, off-potential and current density data, were used for the *inverse* model.

Summary of the study and future work are presented in Chapter 7.

CHAPTER 2
PIPELINE CORROSION, PROTECTION AND MEASUREMENTS

2.1 Introduction

The corrosion of metallic structures has significant impact on the U.S. economy in many fields. In 1975, Battelle-NBS's benchmark study estimated that the cost of corrosion was $70 billion per year, 4.2 percent of the nation's gross national product (GNP). If the effective and presently available corrosion technology can be applied, $10 billion of this cost could be avoided. From 1999 to 2001, the Federal Highway Administration (FHWA) indicated that the total direct cost of corrosion was about $276 billion per year, 3.1 percent of the U.S. gross domestic product (GDP). The indirect costs is unpredictable .[4]

Pipeline-related corrosion costs approximately $7.0 billion annually. There are 528,000 km (328,000 mi) of natural gas transmission pipelines, 119,000 km (74,000 mi) of crude oil transmission pipelines and 132,000 km (82,000 mi) of hazardous liquid transmission pipelines in the U.S.[4]

In the past few years, a number of gas and liquid pipeline failures have drawn people's attention to the pipeline safety. In order to preserve the asset of the pipeline and to avoid those failures which may jeopardize public safety, result in product loss, or cause property and environmental damage, some new regulations were established. Regular pipeline inspections, such as hydrostatic testing, direct assessment, and in-line inspection (ILI), are required. Furthermore, corrosion prediction models need to be developed in order to determine and prioritize the most effective corrosion preventive strategies.

Development of an understanding of cathodic protection of buried structures such as pipelines requires an understanding of the electrochemical reactions associated with corrosion. This section provides an overview of the principles of corrosion, methods for cathodic protection, and the criteria used to assess the effectiveness of corrosion-prevention strategies. Moreover, the pipeline survey methods are included.

2.2 Basic Concepts of Corrosion

Corrosion takes place in response to the tendency to reduce the overall free energy of a system. For example, when metal is in a dilute aerated neutral electrolyte atmosphere, moisture films, which contain oxygen and water, usually cover the metal surface. Some atoms in the metal surface tend to give out electrons and become ions in the moisture layer. In this way, they are in a lower energy state in solution than when they are in the lattice of the solid metal. At the same time the metal surface builds up a huge excess negative charge. These electrons move out from the metal and attach themselves to protons (H^+ ions) and molecules oxygen (O_2). The process repeats itself on various parts of the surface. Then the metal dissolves away as ions.[5] The primary constituent of pipeline-grade steels is iron. Therefore the overall corrosion reaction can be written in terms of dissolution of iron, *e.g.*,

$$2\mathrm{Fe} + \mathrm{O_2} + 2\mathrm{H_2O} \rightarrow 2\mathrm{Fe(OH)_2} \tag{2-1}$$

Reaction (2-1) can be considered as the result of two half-cell reactions. One is

$$\mathrm{Fe} \rightarrow \mathrm{Fe^{2+}} + 2\mathrm{e^-} \tag{2-2}$$

This is an oxidation reaction with an increase of oxidation state for iron from 0 to 2+. It is called an anodic reaction. The other is

$$2\mathrm{H_2O} + \mathrm{O_2} + 4\mathrm{e^-} \rightarrow 4\mathrm{OH^-} \tag{2-3}$$

This reaction is a reduction reaction with a decrease of oxidation state for O_2 to OH^-. It is defined to be a cathodic reaction.

The change in free energy associated with reaction (2-1) can be expressed in terms of a cell potential as

$$\Delta G = -nF\Delta E \tag{2-4}$$

where n is the number of electrons exchanged in the reaction, F is Faraday's constant, 96487 coulombs/equivalent,[6] and E is the electrochemical potential. According to the Nernst equation, obtained by neglecting both activity coefficients and liquid-junction potential,[7,8]

$$\Delta E = \Delta E^0 - \frac{RT}{nF}\ln(\prod(a_i^{s_i})) = \Delta E^0 - \frac{RT}{nF}\ln(\prod(c_i^{s_i})) \tag{2-5}$$

where E^0 is the equilibrium potential, and a_i is the activity of the species i, s_i is the stoichiometric coefficient of species i, and c_i is the concentration of the species i. For reaction (2-2), the potential in Nernst equation form is

$$E_a = E^0_{Fe^{2+}/Fe} - \frac{RT}{2F} ln\left(\left[Fe^{2+}\right]\right) \tag{2-6}$$

Likewise, for reaction (2-3), the potential in Nernst equation form is

$$E_c = E^0_{O_2/OH^-} - \frac{RT}{4F} ln\left(\frac{\left[OH^-\right]^4}{P_{O_2}}\right) \tag{2-7}$$

where a means anodic reaction and c refers to the cathodic reaction. To the whole reaction, where $n_a = 2$ and $n_c = 4$,

$$\Delta G = 2\Delta G_a + \Delta G_c = -2n_aFE_a - n_cFE_c = -4F(E_a + E_c) \tag{2-8}$$

For the two half-cell reactions, E_a and E_c are positive. Hence, the free energy of the overall reaction must be negative, which means the corrosion reaction occurs spontaneously.

2.3 Corrosion Protection

To control the corrosion situations, several methods have been proved effective, which include coating and cathodic protection.

2.3.1 Coating

Electrically insulating materials can be use to cover the pipe surface and thereby isolate the pipe metal from contact with the surrounding electrolyte. In this way, a high electrical resistance in the anode-cathode circuit is added. Theoretically, since no significant corrosion current flows from the anode to the cathode, no corrosion would occur. Many kinds of materials have been applied as coatings, such as enamels, tapes, and plastic coating. Recent improvements in pipeline coating materials will also reduce the risk of a corrosion-related failure. However, a recent survey of major pipeline companies indicated that about 30% of the primary loss of the pipeline protection was due to coating deterioration.[4] Therefore, coating alone can not provide full protection for the pipeline. Practically, effective pipeline corrosion control comprises use of good coatings along with cathodic protection as a secondary defense.

2.3.2 Cathodic Protection

In 1824, Sir Humphrey Davy successfully protected copper against corrosion from seawater by using iron anodes. It was the first application of cathodic protection (CP) and, at that time, it had no theoretical foundation. From that beginning, CP has been applied to marine and underground structures, water storage tanks, pipelines, oil platform supports, reinforcing steel and many other facilities exposed to a corrosive environment. By now, the theory of CP is well established. Natural gas and oil companies have already been using CP for economic, as well as safety reasons, since the 1930's. The Pipeline Safety Act of 1972 made the appli-

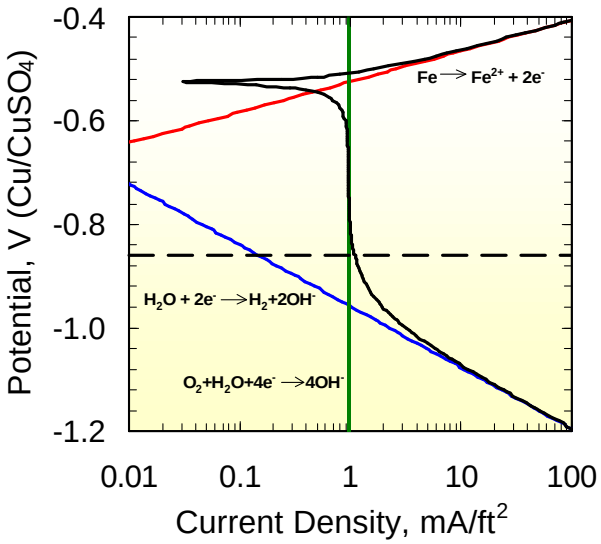

Figure 2-1: Polarization curve of the cathodic protection.

cation of CP on pipelines transporting hazardous material mandatory for safety concerns.

Cathodic protection results from cathodic polarization of a corroding metal surface to reduce the corrosion rate. In this system, the corrosion potential reduces the rate of the half-cell reaction (2-2) with an excess of electrons, which drives the equilibrium from right to left. The excess of electrons also increases the rate of oxygen reduction and OH^- production by reaction (2-3) in a similar manner during cathodic polarization. Cathodic protection reduces the corrosion rate of a metallic structure by reducing its corrosion potential, bringing the metal closer to an immune state, which is represented by the black curve in Figure 2-1.

Two methods are usually used to achieve this goal.[6] There include sacrificial anode and impressed current.

Sacrificial Anode. One method to provide CP is to connect a sacrificial metal (with a higher natural electromotive force) through a metallic conductor or a wire to the structure intended to be protected (as Figure 2-2). Magnesium is a common sacrificial or galvanic anode. This type of galvanic cathodic protection relies on the

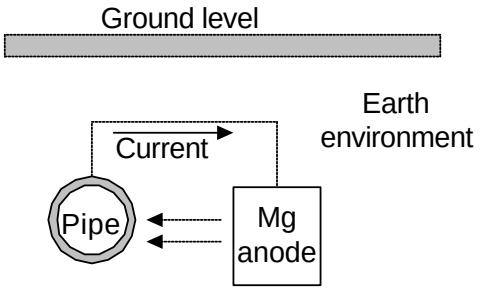

Figure 2-2: Sacrificial electrode CP.

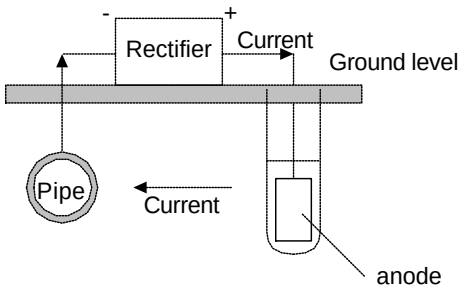

Figure 2-3: Impressed current CP.

natural electrical potential between the two metals to cause the cathodic protection current to flow. Since the driving voltage is limited to the very small potential difference existing between the metals, and the current output is relatively low, this type of cathodic protection is normally associated with very small or very well coated structures.

Impressed-Current. The second common method to provide CP involves use of impressed-current. It relies on an external direct current source such as a rectifier or battery (as Figure 2-3). An anode material, placed in the electrolyte with the protected structure, is made more positive than the structure by connecting both the anode and the structure to the direct current supply. Any conductive materials can be utilized as an impressed current anode, but since corrosion takes place at the anode, materials with very low consumption rates are most desirable.

2.4 Cathodic Protection Criteria

As the cathodic protection is widely used, the reliable criteria need to be developed to direct the cathodic protection systems to an optimum level. The criteria are based on the potential differences between the pipeline and its environment. Two criteria will be introduced in this section, -850mV and 100mV potential creteria.

2.4.1 -850mV Potential Criterion

The criteria for protecting steel pipe, RP-10-69, was established by NACE in 1969. It was revised later in 1972, 1983 and again in 1996. It defines a negative potential at least 850mV with respect to a saturated copper/copper sulfate reference electrode(CSE) when CP is applied. This criterion is mostly used since the potential measurements with current applied requires minimum equipment, personnel and takes less time to obtain in the field survey.

Normally, the desired potential range of the cathodic protection for a pipeline is between -850mV and -1200mV measured with respect to a $Cu/CuSO_4$ reference electrode located at the surface of the steel or coating defects.[9] If excessive amounts of cathodic protection are applied, the direct reduction of water becomes thermodynamically possible, *e.g.*,

$$2H_2O + 2e^- \rightarrow H_2 + 2OH^- \tag{2-9}$$

Hydrogen is evolved upon the metal, and, at large cathodic over-potentials, a small fraction of hydrogen can enter the metal, which makes the metal brittle. This undesirable process is called “hydrogen embrittlement”. If the pipeline has a coating, the developing hydrogen gas bubble can exert tremendous pressure. When the pressure is created under the torn coating, a stripping action exposes the metal and results in rapid deterioration. Obviously, if smaller amounts of CP

is applied (resulting in potential less negative than −850mV), the structure will not be fully protected. In addition, the −850mV criterion does not directly address the polarization. It is valid only when the effect of IR drop has been considered and eliminated.

2.4.2 100mV Potential Criterion

The 100mV polarization criterion was first proposed by S.P. Ewing in 1951.[10] The criterion means that the change in potential polarization to protect pipeline is always less than 100mV. To utilize this criterion, the IR drop effect at measurement area needs to be estimated. Normally, coupons are used to get the IR drop values by measuring the potentials when the coupon is "on" and "off", and comparing the two potentials curves to establish the potential differences between the two curves, which is the IR drop value. Recent research in the UK has shown that the applied current density could be reduced by 25% after three month of using the 100mV criterion and by 65% after one year, without losing any protection.[11]

2.5 Pipeline Measurements

Cathodic protection design should be based on actual data. Monitoring methods are necessary to investigate the corrosive conditions and to evaluate the degree of the applied CP. The techniques used include measurement of potential along the ground above the pipe, measurement of current flowing through the pipes, and use of auxiliary electrodes, such as a reference electrode and coupon.

2.5.1 Potential Survey

Construction of a potential survey involves measuring the potential difference between the pipe and a reference electrode at the ground surface level. The reference electrode is moved to different locations to sample many positions at ground level near the pipe. In this way, a mapping of potential is created which can be

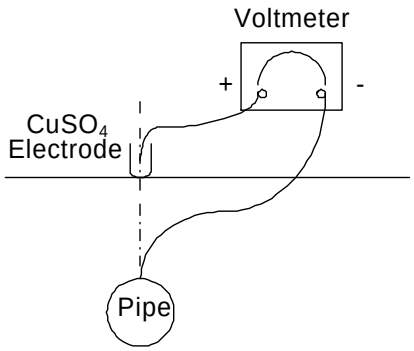

Figure 2-4: Potential survey method.

used to identify regions where the pipe is grossly under-protected. The survey involves use of a voltmeter and a reference electrode which is typically based on the $Cu/CuSO_4$ reaction. A schematic representation of the survey method is presented in Figure 2-4.[12] Potential survey measures the potentials between buried pipeline and environment.[9] This survey needs an appropriate voltmeter with its negative terminal connected to the pipeline and the positive terminal connected to a reference electrode.

The procedure involves moving the reference electrode at 3 to 10 ft intervals down the full length of the pipe and using the trailing cable to determine distance and to connect to the pipeline. A vast quantity of data is gathered by a data logger. From the survey readings, the worst corrosion takes place where the readings are the highest (less negative value) and little or no corrosion should take place where the potential is more negative.

For this measurement, the location of the reference electrode (half-cell) is important.[13] The most desirable place is directly above the pipeline. If the reference half-cell is placed $2 \sim 3$ meters to the side of the pipeline, the measured potential will be a group of scattered data as the second curve shown in Figure 2-5. In such a case, it is difficult to make a judgement. To avoid this case, measurements on both sides of the pipe may be required to make sure that the over the pipe potentials

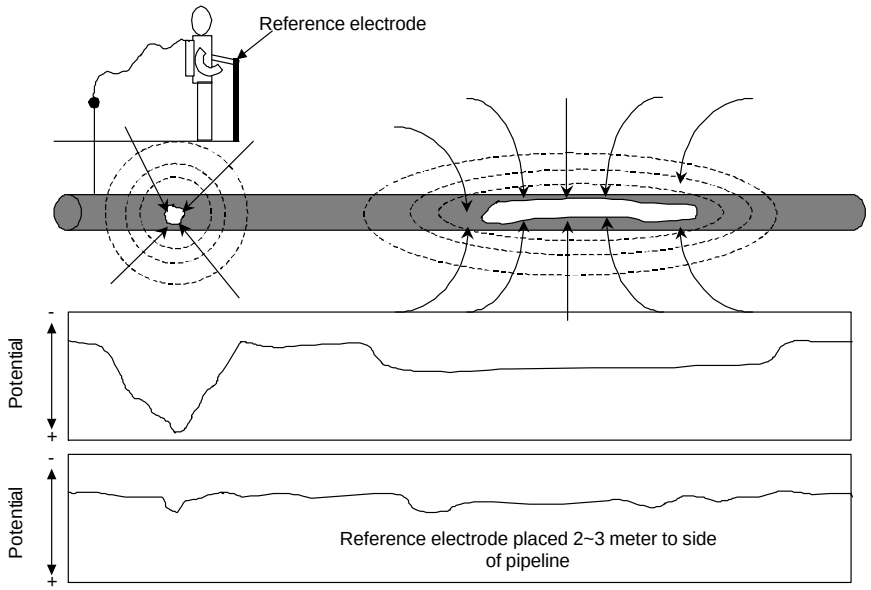

Figure 2-5: Pipe-to-soil potential survey method and importance of the half-cell location.

are taken as close to the pipes as possible.

An instant off-potential (IR-free) survey[9,14] is used to eliminate the potential drop through the soil in the pipe to soil potential measurement by interrupting the flow of protective current to the pipeline. This technique can be used to determine the effectiveness of the cathodic protection system. It is based on the principle that the IR effect in the potential measurement decays almost instantaneously, while the pipe-to-soil interface polarization decays relatively slowly, thus allowing the correct pipe-to-soil potential to be measured free of the IR error.

2.5.2 Line Current Survey

The line current survey technique is used to measure the electrical current flowing on the pipe. If corrosion is taking place on a pipeline, current will flow to the line at some points and flow out of the line at others. For small local cells, the current path may be too short to detect. For large cells, the current may follow the pipe for hundreds or thousands of feet. It is these long line currents that can be detected in a line current survey.

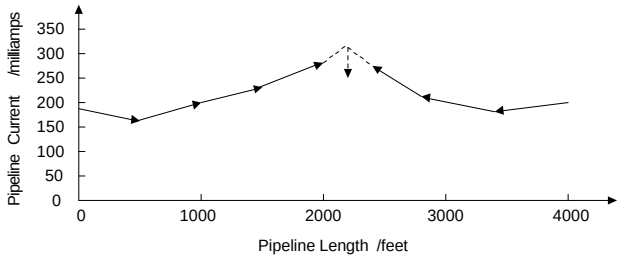

Figure 2-6: Line current survey.

Because the pipe itself has some resistance to the flow of electric current, there will be a voltage drop in the pipe if current is flowing through the pipe steel. Normally, the voltage drops are very small. Thus the span of the two test points is often fixed at 100 feet to increase the span resistance.

Knowing the span resistance of the pipe being surveyed, the voltage drops may be converted to equivalent current by the application of Ohm's Law:

$$I(\text{current}) = \frac{\text{E(potential)}}{\text{R(resistance)}} \tag{2-10}$$

The values of current together with the direction of flow then may be plotted as function of line length.[9] From Figure 2-6, it is noted that in one area current flows from both directions toward a particular point on the line. This point must be a place of current discharge.

2.5.3 Other Survey Techniques

The airborne cathodic monitoring systems (ACMS)[15] detect upset conditions on the pipelines protected by impressed current. Sensitive and filtered magnetic field coils are installed on a helicopter, which continuously measure the magnetic field generated by the ripple from an alternating current source. The principle is based on

$$B = (\frac{\mu_0}{2\pi})\frac{I}{R} \tag{2-11}$$

where B is the magnetic field generated by the impressed current I, R is the distance from the center of the pipe to the sensor installed on the helicopter, and the

constant $\mu_0/2\pi$ is the permeability of the medium. Thus, if the magnetic field can be measured along with the distance, then the current can be calculated.

In addition, use of an insulated coupon is a variation of the instant-off potential to soil method. The coupon usually is buried close to the protected structures to have the same characteristic of the chemical environment and electrical field as those at the structure surface. The exposed coupon surface simulates a coating defect. Cathodic protection current to the coupon can be interrupted without any effect on the protected structures. In this way, the difficulties of the instant-off potential-to-soil method can be eliminated.

2.6 Conclusions

A brief introduction of the corrosion situations was given in this chapter. The basic concepts of corrosion were explained. The pipeline protection techniques, especially the cathodic protection technique, have been introduced. In addition, the commonly used pipeline survey methods, such as potential survey, line current survey, airborne cathodic monitoring systems and coupons, are also summarized.

CHAPTER 3
APPLICATION OF TWO-DIMENSIONAL FORWARD AND INVERSE MODELS TO CORROSION

3.1 Introduction

Given the governing equation and the boundary conditions to estimate the potential and current density distribution on the soil surface by solving the governing equation directly is known as the *forward* model. In contrast, in an *inverse* problem, usually a model or a governing equation and measurements of some variables are given, such as the potential and current density measurements. Boundary conditions and the rest of the variables may not be known explicitly. The purpose of the inverse model is to identify the unknown parameters using the information from the measurements. It is a type of ill-conditioned problem in which the solution is extremely sensitive to the measured data.

In this chapter, the *forward* and *inverse* models applied in the literature are reviewed and reproduced. Two methods were studied, the thin plate approximation method and the boundary element method. The experiences of developing and evaluating these models are summarized.

3.2 Thin Plate Method

3.2.1 Introduction

Inglese[16,17] solved the *inverse* problem for two electrode separated by a small gap, a, as following:

$$\begin{cases} \bigtriangledown^2\phi = 0 & in \ \ \Omega; \\ \phi(x) = \phi_0(x) & x \in [0,1], y = 0; \\ \phi_n(x) + \gamma(x)\phi(x) = f(x) & x \in [0,1], y = a; \\ \phi_n(0,y) = \phi_n(1,y) = 0 & y \in [0,a] \end{cases} \tag{3-1}$$

where γ is the corrosion coefficient, which represents the corrosion rate, ϕ is the potential, and ϕ_n is the outward normal flux and a is the thickness of the domain. The goal was to find γ from the potential ϕ_0 on the accessible boundary $x \in [0,1], y = 0$.

The author introduced the thin plate approximation (TPA) method. The idea is to perform an expansion of the solution γ in terms of powers of the thickness of the domain Ω. Owing to the assumption that the thickness a is much smaller than 1 ($a \ll 1$), higher order terms of the expansion can be ignored. Inglese deduced a formula of γ as function of $\phi_{xx}(x,0)$, which is the second derivative of ϕ with respect to x.

$$\gamma_{TPA}(x) = \frac{\phi_{xx}(x,0) + \phi_0(x)}{\phi(x,0)} \tag{3-2}$$

In order to prove the accuracy of equation (3-2), the direct problem was solved for a prescribed corrosion rate give by

$$\gamma(x) = \exp(-100(x-0.25)^2) \tag{3-3}$$

First of all, for the *forward* part, $\phi(x,0)$ is calculated according to the given $\gamma(x)$. After that, ϕ_{xx}, ϕ_0 can be obtained without problems. For the *inverse* part, the

corrosion rate γ was obtained from equation (3-2) and it can be compared with the value of $\gamma(x)$ from equation (3-3).

3.2.2 Evaluation Process

The domain of Ω in x direction is $[0,1]$ and in y direction is $[0,a]$. To simplify the problem, the y direction is normalized to $[0,1]$. Thus, the decomposed form of equations (3-1) is:

$$\begin{cases} a^2\phi_{xx} + \phi_{yy} = 0 & in \ \ \Omega; \\ \phi_x(0,y) = 0 & ; \\ \phi_x(1,y) = 0 & ; \\ \phi_y(x,0) = -a^2\tilde{\phi} & ; \\ \phi_y(x,1) + a^2\widetilde{\gamma}(x)\phi(x,1) = 0 & ; \\ a\widetilde{\gamma}(x) = \exp[-100(x-0.25)^2] & . \end{cases} \tag{3-4}$$

To solve equation (3-4), the Laplace's equation with Robin boundary conditions, two methods were tested. One was the separation of variables method and the other was the finite difference method. However, the separation variable method failed for this kind of problem because a contradiction occurs between the result and boundary condition $\phi_y(x,0) = -a^2 \neq 0$.

To apply the finite difference method as shown in Figure 3-1, we set

$$\begin{cases} \phi_{i,j} \cong \phi(x_i, y_j) \\ x_i = ih \\ y_j = jh \\ \Delta x = \Delta y \end{cases} \tag{3-5}$$

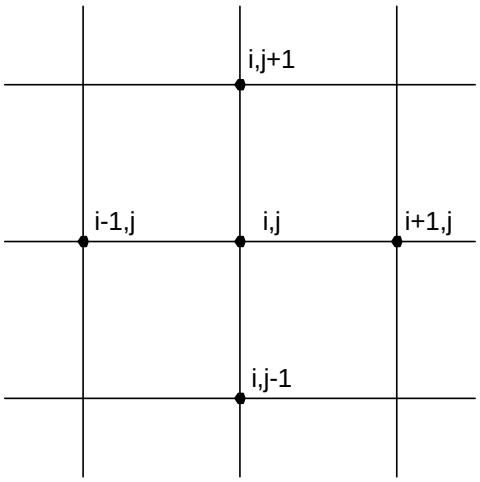

Figure 3-1: Finite difference method.

Therefore,

$$\begin{cases} \phi_{x,x} & = \frac{1}{\Delta x^2}(\phi_{i+1,j} - 2\phi_{i,j} + \phi_{i-1,j}) \\ \phi_{y,y} & = \frac{1}{\Delta y^2}(\phi_{i,j-1} - 2\phi_{i,j} + \phi_{i,j+1}) \\ \phi_x(1,y) & = \phi_{-1,j} - \phi_{1,j} \\ \phi_y(x,0) & = \phi_{i,1} - \phi_{i,-1} \end{cases} \tag{3-6}$$

Equation (3-4) becomes:

$$\begin{cases} \phi_{i,j-1} + a^2\phi_{i+1,j} - 2(a^2+1)\phi_{i,j} + a^2\phi_{i-1,j} + \phi_{i,j+1} = 0 & ; \\ \phi_{-1,j} - \phi_{1,j} = 0 & j = 0,1,\cdots N; \\ \phi_{N+1,j} - \phi_{N-1,j} = 0 & j = 0,1,\cdots N; \\ \phi_{i,1} - \phi_{i,-1} = -2ha^2\widetilde{\phi} & i = 0,1,\cdots N; \\ \frac{1}{2h}[-\phi_{i,N-1} + \phi_{i,N+1}] = -a^2\widetilde{\gamma}(ih)\phi(i,N) = -a\gamma(ih)\phi_{i,N} & i = 0,1,\cdots N; \\ a\widetilde{\gamma}(x) = \exp[-100(x-0.25)^2] & . \end{cases} \tag{3-7}$$

the solution to equation (3-7) yields $\phi_{x,x}(x,0)$, $\phi(x)$ and $\phi(x,0)$. Due to the normalization in y direction, correspondingly, equation (3-2) will be,

$$\gamma \cong \frac{a\phi_{xx}(x,0) + \phi(x)}{\phi(x,0)} \tag{3-8}$$

The results are shown in Figure 3-2. Where the solid curve represents $\gamma(x) =$

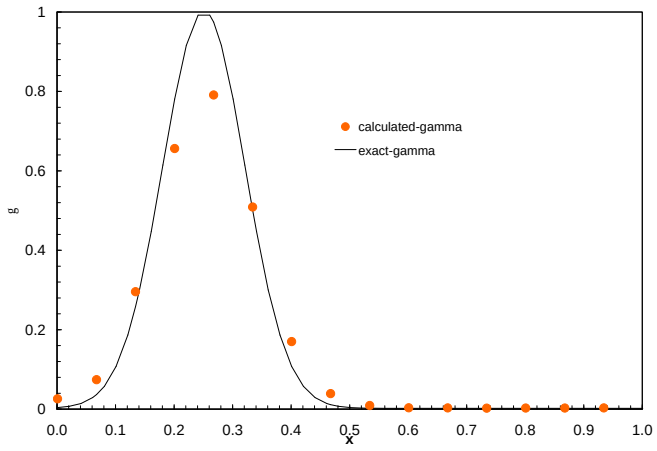

Figure 3-2: Comparisons of the *forward* and *inverse* results of TPA method. $\exp[-100(x-0.25)^2]$ and the points represent $\gamma(x)$ calculated from the ϕ and its derivatives according to equation (3-8).

3.2.3 Summary

This method is only useful for two-dimension problem of a thin strip and for three-dimension problem of a thin plate since the instability increases dramatically with thickness a. Therefore, this method is inapplicable to the buried underground pipeline under cathodic protection system. In addition, the corrosion parameter γ provides an inadequate description of the corrosion problem. These limitations show that TPA method is not suitable for this application.

3.3 Two-Dimensional Boundary Element Method

3.3.1 Introduction

Aoki *et al.*,[18,19] solved a two-dimensional *inverse* problem. The nonlinear relationship between the potential and current density was assumed to be known on the boundary of cathode as equation (3-9) and anode as equation (3-10).

$$q = q_{0c}\{\exp\left(\frac{\phi_c - \phi}{\beta_c}\right) - \exp\left(\frac{\phi_c - \phi}{-\alpha_c}\right)\} \tag{3-9}$$

$$q = q_{0a}\{\exp\left(\frac{\phi_a - \phi}{\beta_a}\right) - \exp\left(\frac{\phi_a - \phi}{-\alpha_a}\right)\} \tag{3-10}$$

Both the ϕ-potential and q-current density were unknown. Aoki applied a Newton-Raphson iterative procedure and used singular value decomposition (SVD) method to get ϕ and q. Where q_{0a}, q_{0c}, ϕ_c, ϕ_a, β_a, β_c, α_a and α_c are parameters. Except for the parameter to represents the connecting position of two electrodes, four parameters are used for each electrode. Thus, these parameters need to be fitted in the *inverse* process.

Kenji and Aoki[20,21] simplified equations (3-9) and (3-10) by using an inverse hyperbolic sine function. The polarization curves for anode and cathode turn out to be,

$$f(q) = \alpha_1 \sinh^{-1} q + \beta_1 \tag{3-11}$$

$$f(q) = \alpha_2 \sinh^{-1} q + \beta_2 \tag{3-12}$$

where α_1, β_1, α_2, and β_2 are the parameters. The number of parameters was reduced a factor of 2. The authors used a conjugate gradient method to minimize the objective function (3-13)

$$g(\alpha_i, \beta_i, x_0) = \sum_{j=1}^{k} (\bar{\phi}_j - \phi_j)^2 \qquad (i = 1, 2) \tag{3-13}$$

where $\bar{\phi}_j$ and ϕ_j represent measured potential and calculated potential respectively. x_0 is the connecting point of two electrodes. However, the results of the fitted parameters and their standard deviations were not given. In order to improve the accuracy of the results, the authors checked the eigen values of the Hessian matrix of the objective function at the convergence point and found that three of the five eigen values were approaching zero. In other words, the five parameters of the objective function actually occupied about a two-dimensional sub-domain

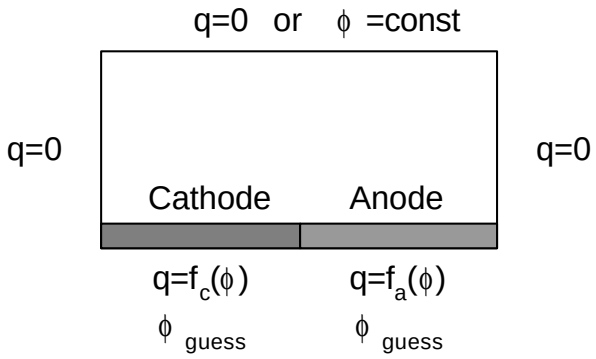

Figure 3-3: Schematic representation of the two-dimensional problem.

instead of a five-dimensional domain. This is the reason that the results cannot be close to the exact solutions and why it is difficult to give the accuracy of the parameters. In addition, an *a priori* technique was used in their work. *A priori* means the probable values of some parameters that need to be estimated are known. In such cases, one may want to perform a fit that takes this advance information properly into account, neither completely freezing a parameter at a predetermined value nor completely leaving it to be determined by the data set.

3.3.2 Evaluation Process

The procedure of evaluating the *inverse* model described by the literature took place in two stages. At the first stage, a *forward* model for the two-dimensional system was created, which was similar to the work of Aoki *et al.* 's.[18,20] Based on the *forward* model, the second stage involved testing the regression approaches and comparing them.

3.3.3 Two-Dimensional Problem

The two-dimensional problem studied here is in a rectangular domain as shown in Figure 3-3, which is by described Aoki *et al.* .[18,20] The lower horizontal boundary consists of a cathode and an anode. The cathode may be considered to play the role of the pipeline, and the anode plays the role of a sacrificial anode. The upper

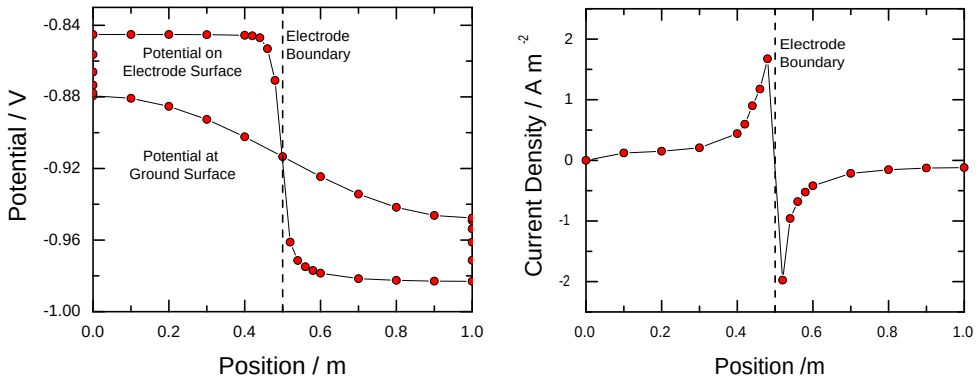

(a) (b)

Figure 3-4: Reproducing results for the two-dimensional *forward* model: a) Potentials at the boundary of domain; b) Current density along the electrode surface.

horizontal boundary can be considered as the soil surface. Neither the potential ϕ nor current density q are known on the electrode boundary, but the nonlinear relationship between them is known. The nonlinear relationship between potential ϕ and current density q is the polarization curve of the electrodes, which are given as equations (3-9) and (3-10). The parameters are $q_{0c} = q_{0a} = 1\text{Am}^{-2}$, $\phi_c = 0.845\text{V}$, $\phi_a = -0.985\text{V}$, $\alpha_c = 0.001\text{V}$, $\alpha_a = 0.025\text{V}$, $\beta_c = 0.05\text{V}$ and $\beta_a = 0.05\text{V}$. The parameters α, β and q_0 are polarization parameters to be obtained by the *inverse* technique described in section 3.4. The subscripts c and a represent the cathode and anode, respectively.

Potential within the interior of the system is governed by Laplace's equation. We followed Aoki's method, applying a Newton-Raphson iterative procedure for the *forward* problem. The potential and current density distributions from the *forward* model are shown in Figure 3-4. As seen in Figure 3.4(a), Aoki*et al.* showed that the variation of potential on the upper surface is much less than that seen on the electrode boundary.[18,20] It is evident that a large distance between the electrodes and the soil surface will blur the measurement data on the soil surface.

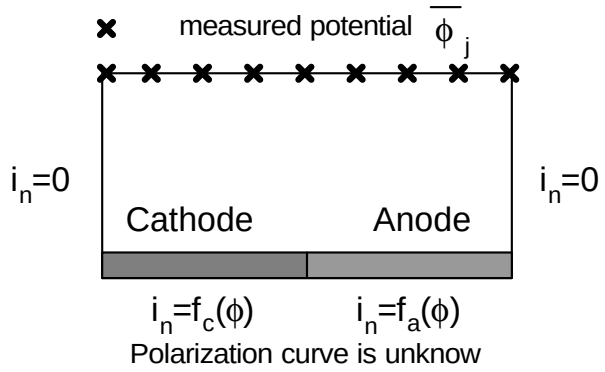

Figure 3-5: Schematic representation of the two-dimensional *inverse* model.

3.4 Inverse Analysis in Two Dimensions

The purpose of this portion of effort was to apply an *inverse* boundary element method to develop an efficient approach for identification of the polarization curve in a cathodic protection system. Different regression methods will be explored in this section.

3.4.1 Objective Function

An objective function, which describes the difference between the measured potential and calculated potential on the soil surface, was constructed as following

$$g(\alpha_i, \beta_i, x_0) = \sum_{j=1}^{k} (\bar{\phi}_j - \phi_j)^2 \qquad (i = 1, 2) \tag{3-14}$$

where $\bar{\phi}_j$ and ϕ_j represent measured and calculated soil surface potentials, respectively. For the two-dimensional *inverse* analysis, Aoki *et al.*[18,20] described it in Figure 3-5. The parameters of the polarization curves were not known. What was known is the measured potential on the soil surface. The goal of the *inverse* analysis is to identify the parameters of the polarization curves that would provide the minimum value for the objective function.

3.4.2 Regression Method Analysis

We tested several regression methods, including the *Levenberg-Marquart*, *conjugate gradient* and *quasi-Newton* methods. These methods, distinguished by the need to evaluate both the function value and the function gradient, were rejected for the pipeline *inverse* model. For the present problem, evaluation of the function gradient can only use finite-difference method, which requires extra calculations of the *forward* model. It inevitably adds significant work to the computation. Besides, the most serious deficiency was that these methods were found to be extremely sensitive to the value of an initial guess and to have a tendency to find local rather than global minima. The *downhill simplex* method requires evaluation only of the objective function itself, *i.e.,* the derivative of the objective function is not needed.

As the results of this work, it is shown that the *downhill simplex* method is the most robust one, independent of the measurement position and the initial guesses. It was successful for our two-dimensional *inverse* analysis and will be further developed for the three-dimensional problems.

3.4.3 Downhill Simplex Method

The downhill simplex method was first created by Nelder and Mead.[22] Only the objective function needs to be evaluated, no such need to its derivative. An objective function, which has N number of adjustable parameters, is evaluated for $N+1$ points. The $N+1$ points are generated by defining a starting point P_0, then other points are obtained by using

$$P_i = P_0 + \lambda_i e_i \tag{3-15}$$

where e_i are N unit vectors, λ_i are constants set according to the problem's characteristic length scale at different directions. The geometrical figure including $N+1$ vertices, all the interconnecting line segments and polygonal faces is called a 'sim-

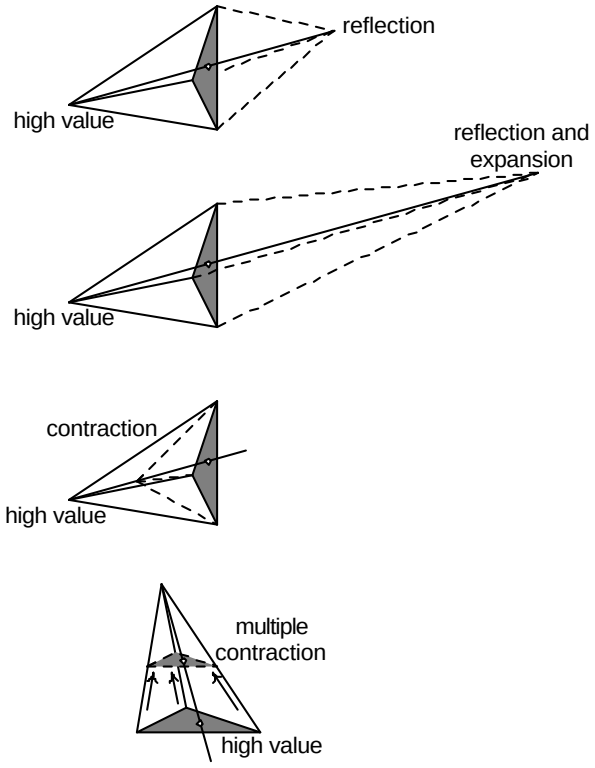

Figure 3-6: Schematic representation of the downhill simplex method.

plex'. According to the function values on $N+1$ points, by using steps, such as reflection, reflection and expansion, contraction and multiple contraction, as shown in Figure 3-6, one can find a new point to continue the function evaluation until the objective function encounters a minimum.

3.4.4 Accuracy of the Parameters

One of the important issues of the regression process is how to determine the accuracy of the parameters. For a χ^2 merit function

$$\chi^2(a_k) = \sum_{i=1}^{N} \left[\frac{\hat{y}_i - y_i}{\sigma_i} \right]^2 \tag{3-16}$$

a_k represents the parameters. $\hat{y}_i$ and y_i are the model and the measurement values respectively. δ_i is the standard deviation for the measurement data point y_i. In this section, we are going to discuss the uncertainties of the parameters a_k.

The variance and the covariance of parameter a_k are given as

$$\sigma^2_{a_k,a_j} = \sum_i^N (\sigma_i^2 \frac{\partial a_j}{\partial \hat{y}_i} \frac{\partial a_k}{\partial \hat{y}_i}), \qquad j,k = 1,2,\ldots,M \tag{3-17}$$

If $j = k$,

$$\sigma^2_{a_j} = \sum_i^N \sigma_i^2 (\frac{\partial a_j}{\partial \hat{y}_i})^2 \tag{3-18}$$

$\sigma^2_{a_j a_k}$ is a $M \times M$ matrix. We can set

$$\sigma^2_{a_j a_k} = [C] \tag{3-19}$$

The gradient of χ^2 with respect to the parameters a_k will be zero at the χ^2 minimum. Thus, from equation (3-16), we get

$$\frac{\partial \chi^2}{\partial a_k} = -2 \sum_{i=1}^N \frac{[\hat{y}_i - y_i]}{\sigma_i^2} \left(\frac{\partial \hat{y}_i}{\partial a_k} \right) \qquad k = 1,2,\ldots,M. \tag{3-20}$$

Taking an additional partial derivative gives

$$\frac{\partial^2 \chi^2}{\partial a_j \partial a_k} = 2 \sum_{i=1}^N \left[\frac{\partial \hat{y}_i}{\partial a_j} \frac{\partial \hat{y}_i}{\partial a_k} - (\hat{y}_i - y_i) \frac{\partial^2 \hat{y}_i}{\partial a_j \partial a_k} \right] \frac{1}{\sigma_i^2} \tag{3-21}$$

Note that the components of equation (3-21) depend both on the first derivatives and on the second derivatives of the basis functions with respect to their parameters. Inclusion of the second derivative term can in fact be destabilizing if the model fits badly. From this point on, we always define α_{jk} as

$$\alpha_{jk} = \frac{1}{2} \frac{\partial^2 \chi^2}{\partial a_j \partial a_k} = \sum_{i=1}^N \left[\frac{\partial \hat{y}_i}{\partial a_j} \frac{\partial \hat{y}_i}{a_k} \right] \frac{1}{\sigma_i^2} \tag{3-22}$$

Comparing equation (3-19) with equation (3-22), we get

$$[C] = [\alpha]^{-1} \tag{3-23}$$

The diagonal elements of the matrix $[\alpha]^{-1}$ are the uncertainties of the parameters. These methods will be used to estimate the uncertainties of the parameters in the next section.

Table 3.1: Regression result for two-dimensional *inverse* model described by Aoki *et al.* The underlined symbols represent the parameters estimated by regression.

Initial Parameters	Final Parameters	g	Standard Deviations
$\underline{\alpha_1 = -0.2}$, $\beta_1 = 0.7$, $\alpha_2 = -1.0$, $\beta_2 = 0.0$, $x_{connection} = 0.5$.	$\underline{\alpha_1 = -0.1}$, $\beta_1 = 0.7$, $\alpha_2 = -1.0$, $\beta_2 = 0.0$, $x_{connection} = 0.5$.	1.32603×10^{-12}	$\sigma_{\alpha_1} = 1.594 \times 10^{-6}$
$\alpha_1 = -0.1$, $\underline{\beta_1 = 0.1}$, $\alpha_2 = -1.0$, $\beta_2 = 0.0$, $x_{connection} = 0.5$.	$\alpha_1 = -0.1$, $\underline{\beta_1 = 0.7}$, $\alpha_2 = -1.0$, $\beta_2 = 0.0$, $x_{connection} = 0.5$.	1.32603×10^{-12}	$\sigma_{\beta_1} = 1.46 \times 10^{-6}$
$\underline{\alpha_1 = -0.2}$, $\beta_1 = 0.7$, $\underline{\alpha_2 = -1.3}$, $\beta_2 = 0.0$, $x_{connection} = 0.5$.	$\underline{\alpha_1 = -0.1576}$, $\beta_1 = 0.7$, $\underline{\alpha_2 = -1.2112}$, $\beta_2 = 0.0$, $x_{connection} = 0.5$.	7.25157×10^{-4}	$\sigma_{\alpha_1} = 3.16 \times 10^{+1}$ $\sigma_{\alpha_2} = 1.13 \times 10^{+3}$
$\underline{\alpha_1 = -0.2}$, $\underline{\beta_1 = 0.5}$, $\underline{\alpha_2 = -1.3}$, $\underline{\beta_2 = 0.1}$, $\underline{x_{connection} = 0.5}$.	$\underline{\alpha_1 = -0.164}$, $\underline{\beta_1 = 0.6632}$, $\underline{\alpha_2 = -1.0708}$, $\underline{\beta_2 = 0.497}$, $\underline{x_{connection} = 0.5}$.	7.35439×10^{-3}	$\sigma_{\alpha_1} = 1.18 \times 10^{+2}$ $\sigma_{\beta_1} = 3.16 \times 10^{+1}$ $\sigma_{\alpha_2} = 1.26 \times 10^{+3}$ $\sigma_{\beta_2} = 1.0 \times 10^{+2}$ $\sigma_{x_{connection}} = 4.35 \times 10^{+1}$

3.4.5 Regression Results

The results of the regression for the two-dimensional problem are presented in Table 3.1. The underlined symbols represent the parameters estimated by regression. It is clear that the number of independent parameters that can be obtained in a statistically significant manner is limited. When four parameters are fixed, the fifth could be obtained with high confidence. When two and more parameters were determined from the regression, the confidence interval became too large.

This analysis provided two important insights. The first was that the number of statistically significant parameters that could be obtained by regression was limited by the amount and quality of the data. The second was that the weighted regression procedure proposed in this work could provide an indication of when the number of statistically significant parameters was exceeded.

3.5 Conclusions

Different regression techniques, such as conjugate gradient method, quesi-Newton method and downhill simplex method, were compared. As the results of the studies in this chapter, the downhill simplex approach was shown to be the most robust method and it is independent of the initial guesses. It will be applied further for the three-dimension problem.

However, the results from all the regression procedures were insufficiently reliable. One possible reason may be the insufficiency of data, since only one series of potential data has been used. Future work will incorporate not only the on-potential data, but also the off-potential and the current survey data. The complex objective function to be minimized will be:

$$\chi^2(a_1,\ldots,a_m) = \left[\sum_{i=1}^{n_1}\frac{(\hat{y}_i-y_i)^2}{\sigma_i^2}\right]_{on-potential} + \left[\sum_{i=1}^{n_2}\frac{(\hat{y}_i-y_i)^2}{\sigma_i^2}\right]_{off-potential} + \left[\sum_{i=1}^{n_3}\frac{(\hat{y}_i-y_i)^2}{\sigma_i^2}\right]_{current} \quad (3\text{-}24)$$

where a_1,...,a_m are the parameters to be fitted, σ_i is the standard deviation of a measured value, and n_1, n_2, n_3 are the number of data points.

CHAPTER 4
DEVELOPMENT OF THREE-DIMENSIONAL FORWARD AND INVERSE MODELS FOR PIPELINE WITH POTENTIAL SURVEY DATA ONLY

4.1 Introduction

From the previous chapter, it is known that pipeline surveys are usually used to determine the adequacy of cathodic protection (CP) for the underground pipelines. However, these survey data may contain significant scatter or noise. The limitations of measurement techniques, instruments, and analysis methods make the data interpretation difficult. Therefore, the objective of this chapter is to develop a mathematical framework for interpretation of survey data in the presence of random noise.

There are two types of approaches used in modeling cathodic protection. A *forward* model yields the distribution of current and potential for a given system geometry and for given physical properties of pipes, anodes, ground beds, and soil. An *inverse* model yields system properties such as pipe coating resistivity given values for current and/or potential distributions.

The history of the development of analytic and numerical *forward* models for cathodic protection of pipelines encompasses more than fifty years. Waber *et al.*[23] derived an analytic model in the form of a Fourier series, which can only be used for simple geometries and boundary conditions. Pierson *et al.*[24] developed a series of analytic equations to account for attenuation for coated pipelines which extend the usual resistance formulas such as Dwight's equation.[9–26] Doig *et al.*[27] utilized the finite difference method to simulate the galvanic corrosion with com-

plex polarization. In the 1980's, Brebbia[28] developed the revolutionary boundary element method (BEM). The BEM has since been applied in many engineering fields because it is accurate, effective for both infinite and semi-infinite domains, and computationally efficient.[28,29] Aoki *et al.*[18,20,30] applied the BEM to both two--dimensional and three-dimensional systems. Telles *et al.*[31] improved the BEM for CP simulation by introducing the current density self-equilibrium limitation, which eliminated the need to discretize a boundary located at infinity. Brichau and Deconinck[3,32] coupled the internal and external Laplace equations which were solved by coupled BEM and finite element methods (FEM). Kennelley *et al.*[33,34] used FEM to model the influence on CP protection of discrete coating holidays that exposed bare steel. The concept of discrete holidays was extended to three dimensions using BEM by Orazem *et al.*[35–37] Riemer and Orazem[1,38–40] combined the advantages of the previous work in their development of the *CP3D* model. A distinguishing point of this software is that it can account for localized defects and yet is suitable for long pipelines and pipe networks. Some commercial programs are available such as PROCAT[2] and OKAPPI.[3] All the simulations described above solve Laplace's equation coupled with linear or nonlinear boundary conditions to obtain the potential distribution and current distribution. The analytic models can only be used for two-dimensional domains with simple geometries. The numerical models can be applied to almost any complex domain; thus, they are widely used. While many numerical models are based on the FEM, the newer generation of models use either BEM or a combination of BEM and FEM.

The use of computer programs to interpret pipe survey data in terms of the unknown condition of the pipe requires solution of the *inverse* problem, in which the properties of the pipe coating are inferred from measurements of current and potential distributions. This approach allows interpretation of field data in a manner

that would take into account the physical laws that constrain the flow of electrical current from anode to pipe. Aoki *et al.* has made significant contributions to the application of *inverse* model to CP. Their studies included simplifying the unknown parameters in the polarization curves, changing the form of objective function, and trying different kinds of minimization methods. To minimize the objective function, they have employed a variety of techniques conjugate gradient, fuzzy a priori,[20] and genetic algorithm methods.[41,42] Their work involves modeling protection of pipes, ships, and reinforcing steel in concrete structures.[41–42] Wrobel and Miltiadou describe the application of genetic algorithms to *inverse* problems, including identification of coating holidays.[44,45] Aoki *et al.* used an *inverse* BEM analysis to eliminate Ohmic error from measurement of polarization curves.[46]

The concept behind use of the *inverse* model for cathodic protection is related to the approach used to reconstruct the distribution of electrical resistance for medical, chemical process, and geological applications. For medical applications, the readings from an array of sensing electrodes are used to construct an image associated with conductivity variations within a body.[47–50] The technique is called electrical-impedance tomography.[51,52] Electrical-impedance tomography has also been used to determine the interfacial area for two-phase gas-liquid and particulate flows in chemical processes[53–56] and, through identifying the distribution of electrical resistivity, to identify composition distributions in laboratory and plant-scale process equipment.[57] Electrical-resistivity tomography is used to interpret cross-borehole resistivity measurements to obtain electrical resistivity distributions of geological formations.[58–64]Electrical resistivity is an important petroleum reservoir parameter because it is sensitive to porosity, type of pore fluid, and degree of saturation. While use of neural networks have been suggested,[65,66] most

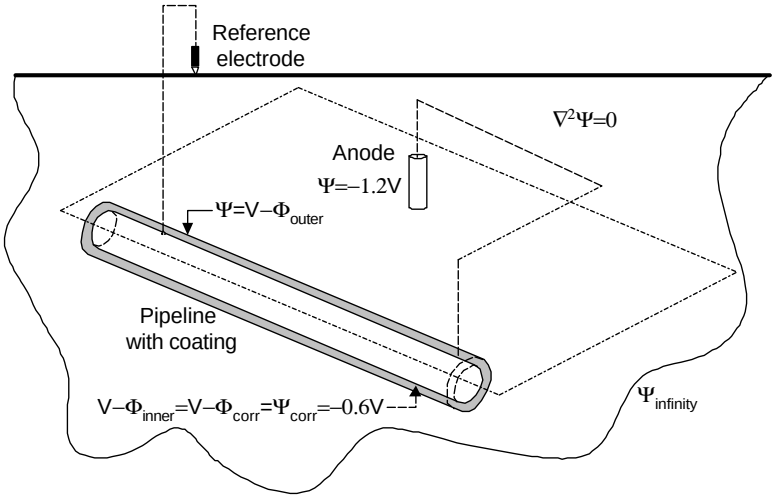

Figure 4-1: Schematic illustration of the pipe segment and anode used to test the *inverse* model.

approaches are based on non-linear regression.

In this chapter, the construction of the *forward* model, *inverse* model for CP system, theoretical basis and development of the three-dimensional BEM will be introduced.

4.2 Construction of the Forward Model

4.2.1 Cathodic Protection System

For the three-dimensional problem, a pipe was considered to be buried horizontally under the ground surface. A cylindrical vertical anode was placed a distance away from the pipe. The underground region was considered to be bounded by the soil surface and to extend infinitely in the other directions in the soil. The anode was connected to the pipe with a wire, as shown in Figure 4-1. The pipe was placed horizontally 1.0 m (4.75 feet) below the soil surface and had a diameter of 0.457 m (1.5 feet). The anode was placed in a vertical position and a distance away from the center of the pipe. The anode diameter was 0.152 m and the length was 1.0 m (3.28 feet). The soil resistivity was 100 Ωm. A 0.5 mm-thick coating was assumed to cover the side area of the pipe, with the exception that the two ends were assumed to be insulated. The potential of the pipe steel was assumed to

be uniform. This assumption, valid for the short pipe segments considered in this preliminary work, will need to be extended in future work. The *forward* model was used to calculate the potential that one might measure with a voltmeter connected to the pipeline and a $Cu/CuSO_4$ reference electrode (CSE).

4.2.2 Governing Equation and Boundary Conditions

The current density in a dilute electrolyte solution can be described as[8]

$$i = -F^2 \nabla\phi \sum_j z_j^2 u_j c_j - F \sum_j z_j D_j \nabla c_j + Fv \sum_j z_j c_j \tag{4-1}$$

where i is the current density vector, v is the bulk velocity, F is Faraday's constant, z_j is the charge for species j, u_j is the mobility for species j, c_j is the concentration for species j, and D_j is the diffusion coefficient for species j. In this study, only the electrode surfaces, such as pipe walls are considered. Since the velocity v is small in the soil, the convection can be neglected. In addition, concentration gradients only have a significant effect in the diffusion layer, which is close to the structure and is relatively thin comparing with the characteristic length of the system. Thus, concentration gradients generally are neglected in large-scale simulations. Therefore, the current density in the soil is

$$i = -F^2 \nabla\phi \sum_j z_j^2 u_j c_j \tag{4-2}$$

The conductivity of the electrolyte is defined to be

$$\kappa = F^2 \nabla \sum_j z_j^2 u_j c_j \tag{4-3}$$

The current density equation can be reduced to

$$i = -\kappa \nabla\phi \tag{4-4}$$

which is called Ohms Law. The conservation of charge in the bulk yields

$$\nabla \cdot i = 0 \tag{4-5}$$

Substituting equation(4-4) into equation (4-5)

$$\nabla \cdot (-\kappa \nabla \phi) = 0 \tag{4-6}$$

Thus

$$\kappa \nabla^2 \phi = 0 \tag{4-7}$$

Equation (4-7) is known as Laplace's equation for the electrochemical potential ϕ. The boundary conditions are shown in Figure 4-1. The corrosion potential of pipe steel is -0.6V. The sacrificial anode has a given potential of -1.2V.

4.2.3 Theoretical development

As mentioned previously, the *forward* model has to be efficient in terms of computer calculations due to its coupling with the *inverse* model. To achieve this goal, a linear relation, considering the coating covered pipe with various resistivity, is proposed in this section.

Linear Boundary Conditions

The polarization curve, which describes the relationship between the potential and the current density, indicates the corrosion condition on the pipe surface and is normally used as the boundary condition. It is not an easy task to determine the polarization curve since it strongly depends on a number of phenomena. Further more, the polarization curve can also be a function of time and history. The polarization curve used by Riemer and Orazem[1,39] had eight parameters. Amaya and Aoki *et al.*[20,21] simplified the polarization curve from the Butler-Volmer equation and reduced the parameters to four for one cathode and one anode system. However, if the corrosion condition along the pipe is not uniform, more polarization curves are needed. In present study, the polarization curve was substituted by a linear relationship between the potential drop and the current density over the pipe coating for three-dimensional simulation, shown in Figure 4-2.

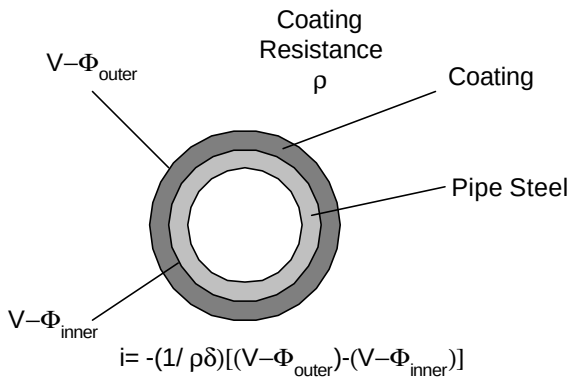

Figure 4-2: Linear relationship between potential drop and current density over the pipe coating.

$$i = -\frac{1}{\rho_c \delta}[(V - \phi_{\text{outer}}) - (V - \phi_{\text{inner}})] \tag{4-8}$$

where i is the current density along the pipe radical direction, ρ_c is the unit resistance of coating material, δ is the coating thickness, V is the potential of the pipe steel, assumed to be constant, ϕ is the potential in the electrolyte, $V - \phi_{\text{outer}}$ is the potential of the pipe referred to a reference electrode placed at the outside coating surface, and $V - \phi_{\text{inner}}$ is the potential of the pipe with respect to a reference electrode placed at the inside coating surface. Under the assumption that the current densities through the coating and those at the pipe steel surface are equal,

$$i = -\frac{[(V - \phi_{\text{outer}}) - (V - \phi_{\text{inner}})]}{R_{\text{c}}} = -\frac{[(V - \phi_{\text{inner}}) - (V - \phi_{\text{corr}})]}{R_{\text{kinetic}}} \tag{4-9}$$

where R_{c} and R_{kinetic} represent the coating and polarization resistance, respectively, and $V - \phi_{\text{corr}}$ is the corrosion potential. As $R_{\text{c}} \gg R_{\text{kinetic}}$,

$$(V - \phi_{\text{inner}}) - (V - \phi_{\text{corr}})] \approx 0 \tag{4-10}$$

Therefore,

$$i = -\frac{1}{\rho_c \delta}[(V - \phi_{\text{outer}}) - (V - \phi_{\text{corr}})] \tag{4-11}$$

Equation (4-11) provides a linear relationship between the potential and the current density. This linear boundary condition, replaces the nonlinear polarization

curve and greatly simplifies the calculations of *forward* model.

Description of the Pipe Surface

According to the coating-covered special feature of pipe, a coating resistance approximation was made. It allows the coating resistance to vary along the length of the pipe according to:

$$\rho = \rho_0 + \sum_k \rho_k e^{-(x-x_k)^2/2\sigma_k^2} \tag{4-12}$$

wherein ρ_0 refers to the average good coating resistance of the pipe, ρ_k represents the resistance reduction associated with coating defect k, x_k is the center point of the coating defect, and σ_k is the half width of the defect region. Equation (4-12) shows that if the coating position is close to a defect center x_k, *i.e.,* falling into the defect region $2\sigma_k$, the coating resistance decay is evident; whereas, if the coating position is far away from the defect center, the coating resistance decay is insignificant. The present approach has two significant advantages over assigning a resistivity to each cylindrical element. For instance, use of equation (4-12) to represent two coating defects on a 150 feet pipeline is shown in Figure 4-3. If the pipeline is discretized with a 10 foot space interval, only seven parameters are required ρ_0,ρ_1,x_1,σ_1,ρ_2,x_2 and σ_2 for the equation (4-12), as compared to 15 parameters are needed for an element-by-element coating resistivity estimation. If the pipeline is discretized with a 5 foot spacing, still these seven parameters are required, while it is now thirty parameters for the regular method. Likewise, if the space interval is decreased to be so small that it makes the resistivity value continuous, no more than these seven parameters are enough to describe resistivity along the whole pipeline. The degree of freedom for the problem is increased dramatically, and correspondingly, the required computational time is reduced.

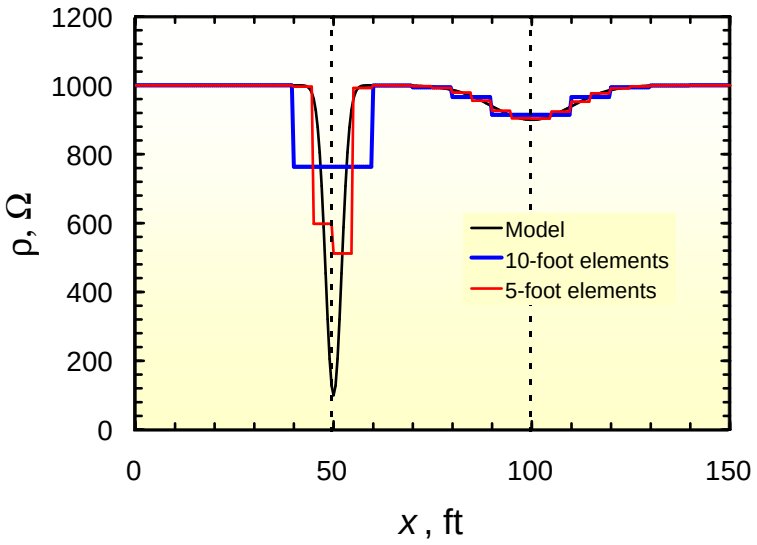

Figure 4-3: Schematic illustration of the pipe surface resistivity model.

4.3 Three-Dimensional Boundary Element Method

The theory for application of the boundary element method to the three-dimensional half-infinity multi-connected domain is introduced in this section. The linear cylindrical elements are adopted to discretize the pipe/anode surface in present study.

4.3.1 Infinity Domain

In the two-dimensional system, a closed rectangular domain was investigated. This kind of system, called an interior problem, is shown in Figure 4-4 and where S is the boundary of the volume V, the shaded area is the interior domain. $\vec{n}$ is the normal vector of the boundary S at that point. According to Brebbia *et al.* ,[29] the basic equation of boundary element method corresponding to the Laplace's equation is

$$c(x_s)u(x_s) = \int_s [q(y)u^*(x_s, y) - q^*(x_s, y)u(y)]dS(y) \tag{4-13}$$

Equation (4-13) is called boundary integral equation. Wherein x_s is the source point, y is the field point. $u^*(x_s, y)$ and $q^*(x_s, y)$ are the fundamental solutions of Green's function for potential and flux. u and q are the general solution of Laplace's function for potential and flux. $c(x_s)$ depends on the position of the

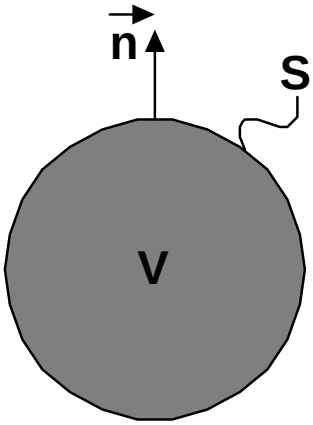

Figure 4-4: Interior problem.

source point x_s, as shown in equation (4-14),

$$c(x_s) = \begin{cases} x_s \notin V, & c(x_s) = 0 \\ x_s \in V, & c(x_s) = 1 \\ x_s \in S, & c(x_s) = \frac{\omega}{4\pi} \end{cases} \tag{4-14}$$

ω is the solid angle subtended by V at x_s, which is on the boundary S. For the three-dimensional system, the studied domain is outside the pipeline and the anode surface, and is between the soil at infinity. It is a multi-connected region of an interior problem, as shown in Figure 4-5. The boundary S can be considered to be the boundary of the pipeline or the anode. The boundary S_R can be the boundary at infinity. When $R \to \infty$, equation (4-13) is also valid for this case. For $x_s \in S$,

$$\begin{aligned} c(x_s)u(x_s) &= \int_s [q(y)u^*(x_s, y) - q^*(x_s, y)u(y)]dS(y) \\ &+ \lim_{R\to\infty} \int_{S_R} [q(y)u^*(x_s, y) - q^*(x_s, y)u(y)]dS(y) \end{aligned} \tag{4-15}$$

The fundamental solutions to the Green's function for three-dimensional problem at the boundary S_R are

$$\begin{aligned} u^*(x_s, y) &= \frac{1}{4\pi R} \\ q^*(x_s, y) &= \frac{\partial u^*(x_s, y)}{\partial n} = -\frac{1}{4\pi R^2} \end{aligned} \tag{4-16}$$

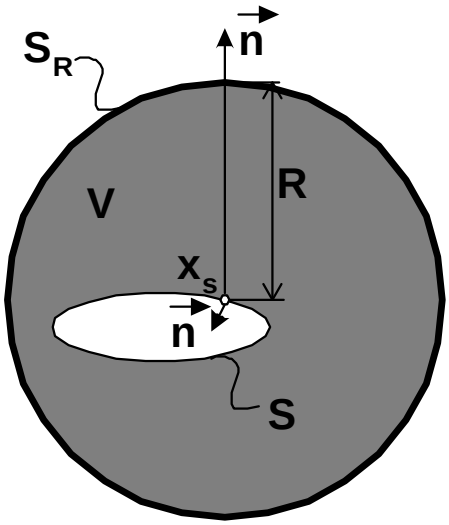

Figure 4-5: Multi connected region of interior problem.

And the general solution to the problem over the infinity boundary S_R are

$$\begin{aligned} u(y) &= Ku^*(x_s, y) + u_\infty \sim O(\frac{1}{R}) \\ q(y) &= \frac{-K}{4\pi R^2} \sim O(\frac{1}{R^2}) \end{aligned} \tag{4-17}$$

where K and u_∞ are two undetermined constants at the infinity boundary. K is the sum of source term (*e.g.*, electric charge) distributed over S,

$$K = \int_S q(y) dS(y) \sim O(1) \tag{4-18}$$

Equation (4-16) and (4-17) are introduced into equation (4-15). Since

$$\begin{aligned} &\lim_{R\to\infty} \int_{S_R} [q(y)u^*(x_s, y) - q^*(x_s, y)u(y)]dS(y) \\ &= \lim_{R\to\infty} \int_{S_R} [q(y)u^*(x_s, y) - q^*(x_s, y)(Ku^*(x_s, y) + u_\infty)]dS(y) \\ &= \lim_{R\to\infty} \int_{S_R} \{u^*(x_s, y)[q(y) - Kq^*(x_s, y)] - q^*(x_s, y)u_\infty\}dS(y) \end{aligned} \tag{4-19}$$

where the first term inside the bracket is

$$\begin{aligned} &\lim_{R\to\infty} \int_{S_R} u^*(x_s, y)[q(y) - Kq^*(x_s, y)]dS(y) \\ = \quad &\lim_{R\to\infty} \int_{S_R} \tfrac{1}{4\pi R}[O(\tfrac{1}{R^2}) - (-\tfrac{K}{4\pi R^2})]dS(y) \\ \sim \quad &\lim_{R\to\infty} [O(\tfrac{1}{R^3}) \cdot 4\pi R^2] \to 0 \end{aligned} \tag{4-20}$$

and the second term is

$$\begin{aligned}\lim_{R\to\infty}\int_{S_R} q^*(x_s,y)u_\infty dS(y) &= \lim_{R\to\infty} u_\infty(-\frac{1}{4\pi R^2}\cdot 4\pi R^2)\\ &= -u_\infty \end{aligned} \tag{4-21}$$

Then equation (4-15) becomes,

$$c(x_s)u(x_s)+\int_s[-q(y)u^*(x_s,y)+q^*(x_s,y)u(y)]dS(y)=u_\infty \tag{4-22}$$

Equation (4-22) indicates that the value of K has no important effect on the boundary S. To satisfy the pipeline and the anode CP system, the unit outward normal n on S in Figure 4-5 needs to change its direction. Correspondingly, equation (4-22) will be

$$c(x_s)u(x_s)+\int_s\{-q(y)u^*(x_s,y)+[-q^*(x_s,y)u(y)]\}+dS(y)=u_\infty \tag{4-23}$$

In addition, according to the physical condition, there is no current flow out of the soil surface, therefore, $K=0$ is given as boundary condition and u_∞ is unknown.

4.3.2 Half-Infinity Domain

The half-infinity domain is obtained by using a plane to split an infinite domain. Two half spaces lie on each side of the plane. Either the Dirichlet or Neumann boundary condition is satisfied at the plane. For the buried pipelines system, the underground soil domain is the half-space being studied. Since there is no net current flowing out of the soil into the air, the Neumann boundary condition vanishes at the soil surface. The Green's function can satisfy that condition by using the reflection properties.[29–70] If we set Ω^- to be the region $x\le 0$, $P\in\Omega^-$ and let $P'(-x,y,z)$ be the mirror image of a given source point $P(x,y,z)$ with respect to the plane $x=0$ (or $\partial\Omega$), P' becomes the reflected source point, and $r=|Q-P|$, $r'=|Q-P'|$ (see Figure 4-6). Q is the field point. Consequently, half-space fundamental solutions satisfying a homogeneous Neumann condition $H^N(P,Q)=0$

on $\partial\Omega$ can be deduced by adequate superposition of free-space fundamental solutions for sources at P and P', that is

$$\frac{\partial G^N(P,Q)}{\partial Q}\cdot n(Q) = H^N(P,Q)=0 \tag{4-24}$$

Here, the superscript N is for the Newmann boundary conditions; $n(Q)$ is the normal vector at point Q. Assuming two full free-space problems with $\forall Q\in\Omega^-$, equation (4-24) can be written as

$$\frac{\partial G^-(P,Q)}{\partial Q}\cdot n(Q_r) = H^-(P,Q)=(-\frac{1}{4\pi r^2})\cdot n(Q_r) \tag{4-25}$$

$$\frac{\partial G^+(P',Q)}{\partial Q}\cdot n(Q_{r'}) = H^+(P',Q)=(-\frac{1}{4\pi r'^2})\cdot n(Q_{r'}) \tag{4-26}$$

From Figure 4-7, the normal vectors $n(Q_r)$ and $n(Q_{r'})$ of $\vec{r}$ and $\vec{r'}$ at point Q are

$$n(Q_r) = 1 \tag{4-27}$$

$$n(Q_{r'}) = -1 \tag{4-28}$$

Meanwhile, according to the Neumann boundary condition given in equation (4-24)

$$H^N(P,Q) = H^-(P,Q)+H^+(P',Q)=0 \tag{4-29}$$

When $Q\in\partial\Omega$, $r=r'$, the fundamental solution in two full free-space have to be

$$G^-(P,Q) = \frac{1}{4\pi r} \tag{4-30}$$

$$G^+(P',Q) = \frac{1}{4\pi r'} \tag{4-31}$$

to satisfy equation (4-24), indicating that the two source intensities P and P' are equal and have the same sign. Therefore, the final form of the Green's function is

$$G^N(P,Q)=G^-(P,Q)+G^+(P',Q)=\frac{1}{4\pi}\left(\frac{1}{r}+\frac{1}{r'}\right) \tag{4-32}$$

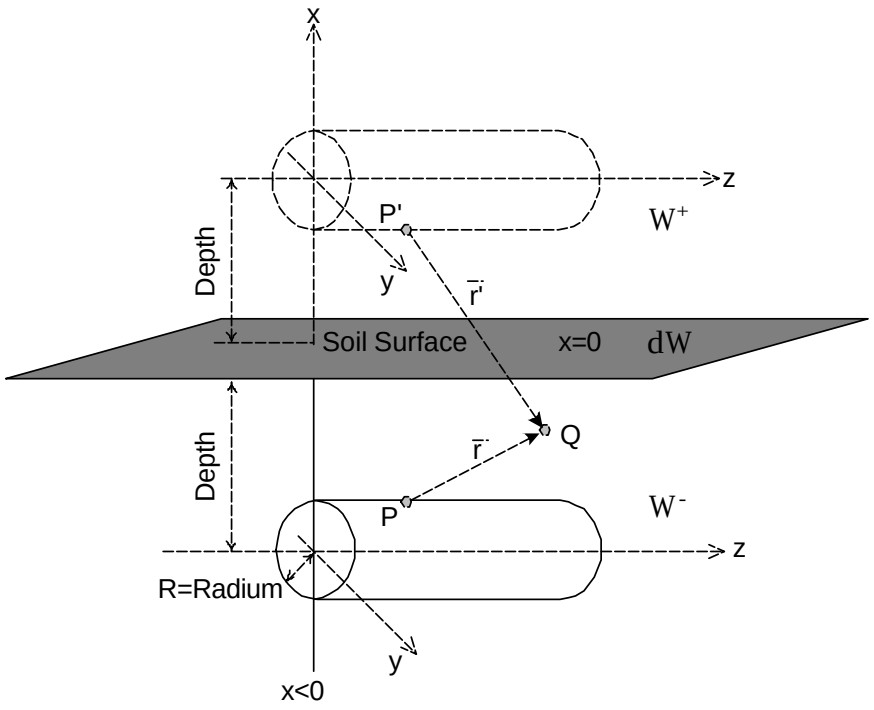

Figure 4-6: Schematic illustration of mirror reflection technique.

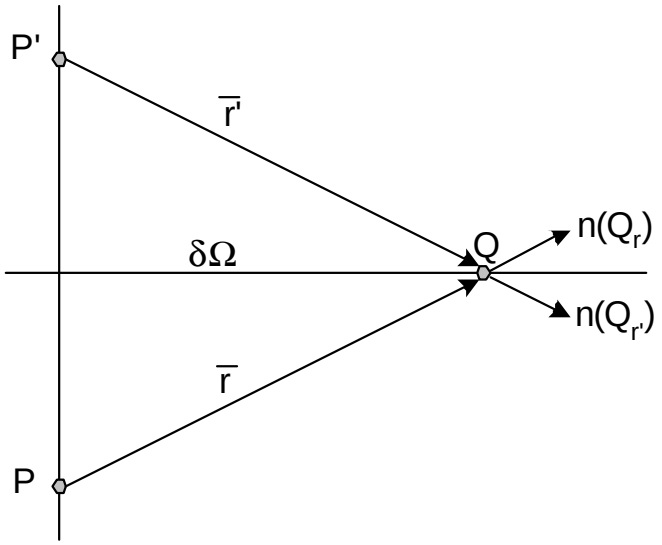

Figure 4-7: The Fundamental solution to the half-infinity domain satisfying the Neuman b.c's.

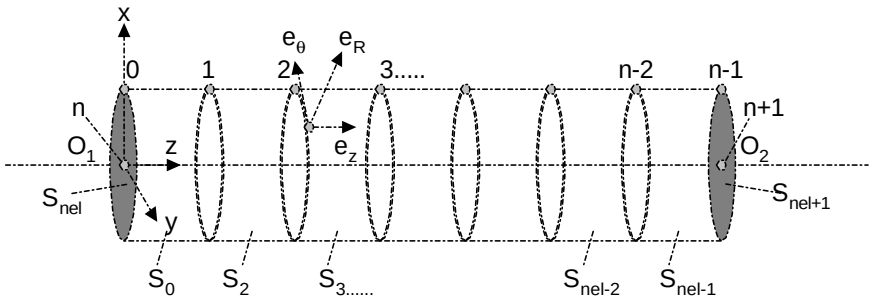

Figure 4-8: Pipe discretision and collocation points.

4.3.3 Boundary Discretization

Rectangular and triangular elements are commonly used in the literature for BEM meshes on the surface of a three-dimensional object. Aoki *et al.*[71] used 352 constant triangular elements to discretize the side area of a 160mm long, 155mm-diameter cylinder. Riemer and Orazem's model *CP3D* may involve thousands of elements to discretize a pipeline with discrete coating holidays. This level of detail is appropriate for a *forward* model, but it is inappropriate for an *inverse* model where the amount of data may be insufficient to extract a high level of details concerning the pipe condition. Besides, the model needs to be calculated not once, but thousands of times. To decrease the number of elements, a series of linear cylindrical elements were used to take advantage of the cylindrical shape of the pipe and the anode. The source points (also called collocation points) were localized on the cylindrical side area. At the two ends of the object–pipe/anode, the two discs were set as two constant circle elements. The center of each circle was a collocation point (see Figure 4-8). For the cylindrical elements, there was no variation along the circumference. The variation was only along the axial direction[72–75] such that the collocation points could be chosen at the reference line, which was on the top of the cylinder. The elements on the side area of the cylinder were from S_0 to (S_{nel-1}), and, at the two ends of the pipe, were the two circle areas S_{nel} and $S_{(nel+1)}$. The collocation points on the side area of cylinder were from 0 to $(n-1)$,

while two collocation points at the center of circles are counted as n and $(n+1)$. The relation between the number of elements and the number of nodes depends on the order of the interpolation functions, which can be constant, first-order or even higher order.

The identical mesh was used for the element separation because in the following *inverse* model, the position of the coating defects was distributed randomly along the pipeline. If the pipeline meshing depended on the position of coating defects, every time when the new coating defect positions would be assumed, the system would have to be remeshed. To save computational time, by using the identical mesh, the matrices G and H for the BEM need to be calculated only once.

4.3.4 Coordinates Definition and Transformation

In this program, two kinds of objects were defined, one is pipe, and the other is anode. The user needs to input the beginning point of the pipe/anode's axle to the program. Both the global coordinate and the local coordinate were used in this study. The global coordinates was set as: z axial parallel to the soil surface and directed to north direction; x axial perpendicular to the soil surface and pointed toward the sky. The y axial and z axial build the soil surface plane. The origin is on the soil surface. The angle between the pipe/anode's axle and soil surface is defined as the elevation angle θ_e. $\theta_e = 0^\circ$ means that the object is parallel to the soil surface. $\theta_e = 90^\circ$ (or $\theta_e = -90^\circ$) means that the object is perpendicular to the soil surface. The direction angle θ_d refers the angle between the pipe/anode's axle and z axial positive direction. The local coordinate is used when the collocation point and the field point are on the same object (*i.e.*, the pipe/anode), while the global coordinate is used when the collocation point and field point are on the different objects to clarify the relative positions of these objects.

Transformation between two different coordinates, such as the global and the

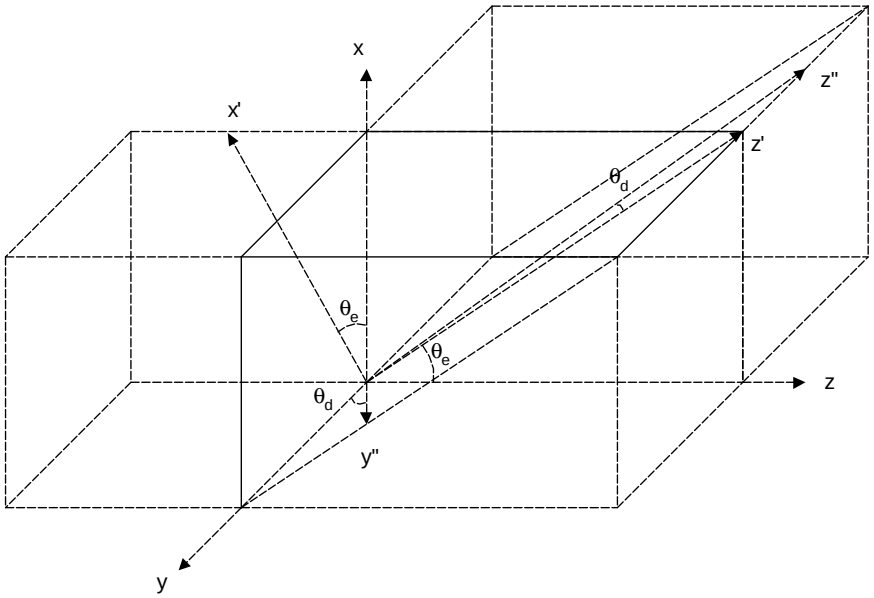

Figure 4-9: Coordinate rotation.

local coordinates or two different local coordinates, usually consists of two steps. One is origin transformation, which is to move from one original point to a new origin. The other is rotation, which is to rotate previous axials around the new origin. Coordinate rotation actually includes two rotations. Figure 4-9 shows the precedure to rotate a coordinate around a point and one axis. The first rotation is to rotate the x axis and the z axis about the y axis with elevation angle θ_e to get new x' axis and z' axis. The second rotation is to fix x', and to rotate y and z' axes with direction angle θ_d to get a new axes y'' and z''. Finally, coordinates (x, y, z) is converted to (x', y'', z'').

4.3.5 Discretization of Boundary Element Method

Rewriting equation (4-23) using P as source point, Q as field point and $\partial\Omega$ as boundary, we get

$$cu(P) + \int_{\partial\Omega} u(Q) q^*_{PQ} d(\partial\Omega) \quad = \quad \int_{\partial\Omega} q(Q) u^*_{PQ} d(\partial\Omega) + u_\infty \tag{4-33}$$

where u^* and q^* are the fundamental solution of the Green function, and they have the relation

$$q^*_{PQ} = \frac{\partial u^*_{PQ}}{\partial n_Q} \tag{4-34}$$

Discretizing equation (4-33),

$$c_i u_i(P) + \sum_{j=1}^{nel} \int_{S_j} u_j(Q) \frac{\partial u^*_{PQ}}{\partial n_Q} dS_j = \sum_{j=1}^{nel} \int_{S_j} q_j(Q) \partial u^*_{PQ} dS_j + u_\infty \tag{4-35}$$

where *nel* means the number of element. Since u and q of each linear cylindrical element vary linearly along the z axial direction, then

$$\begin{aligned} u(z) &= u_1(l-z) + u_2 z \\ q(z) &= q_1(l-z) + q_2 z \end{aligned} \tag{4-36}$$

where l is the length of the element. Let $t = \frac{z}{l}$, then u and q, the functions of z, can be transferred to be the functions of t,

$$\begin{aligned} u(t) &= l[u_1(l-t) + u_2 t] \\ &= l[u_1 N_1(t) + u_2 N_2(t)] \\ q(t) &= l[q_1(l-t) + q_2 t] \\ &= l[q_1 N_1(t) + q_2 N_2(t)] \end{aligned} \tag{4-37}$$

The basis functions can be extracted from equation (4-37),

$$\begin{aligned} N_1(t) &= 1 - t; \\ N_2(t) &= t. \end{aligned} \tag{4-38}$$

Upon substituting equation (4-37) into equation (4-35), the discretized boundary integral equation becomes

$$\begin{aligned} c_i u_i(P) &+ \sum_{j=1}^{nel} \int_{S_j} l_j [u_{j,1} N_1(t) + u_{j,2} N_2(t)] \frac{\partial u^*_{ij}}{\partial n_j} dS_j \\ &= \sum_{j=1}^{nel} \int_{S_j} l_j [q_{j,1} N_1(t) + q_{j,2} N_2(t)] u^*_{ij} dS_j + u_\infty \end{aligned} \tag{4-39}$$

Since the fundamental solutions are

$$\begin{aligned} u^*_{ij} &= \frac{1}{4\pi r_{ij}} \\ q^*_{ij} &= \frac{\partial u^*_{ij}}{\partial n_j} = \frac{1}{4\pi}\frac{\partial(\frac{1}{r_{ij}})}{\partial n_j} \end{aligned} \tag{4-40}$$

According to equation (4-39), we define

$$G_{ij} = \int_{S_j} \sum_{k=1}^{2} l_j q_{jk} N_k(t) u^*_{ij} dS_j \tag{4-41}$$

$$H_{ij} = \int_{S_j} \sum_{k=1}^{2} l_j u_{jk} N_k(t) q^*_{ij} dS_j \tag{4-42}$$

If the field point Q is on the cylindrical element side area, $dS_j = Rd\theta dt$, R is the radium of cylinder, then G_{ij} becomes

$$\begin{aligned} G_{ij} &= \int_0^1 \int_0^{2\pi} \sum_{k=1}^{2} l_j q_{jk} N_j(t) u^*_{ij} R d\theta dt \\ &= l_j(\frac{R}{4\pi}) \int_0^1 (\sum_{k=1}^{2} q_{jk} N_k(t)) dt \int_0^{2\pi} \frac{1}{r_{ij}} d\theta \end{aligned} \tag{4-43}$$

and H_{ij} becomes

$$\begin{aligned} H_{ij} &= \int_0^1 \int_0^{2\pi} \sum_{k=1}^{2} l_j u_{jk} N_k(t) q^*_{ij} R d\theta dt \\ &= l_j(\frac{R}{4\pi}) \int_0^1 (\sum_{k=1}^{2} u_{jk} N_k(t)) dt \int_0^{2\pi} \frac{\partial(\frac{1}{r_{ij}})}{\partial n_j} d\theta \end{aligned} \tag{4-44}$$

If the field point Q is on the circle elements, $dS_j = rdrd\theta$, $0 \le r \le R$, G_{ij} changes its form to

$$G_{ij} = q_j(\frac{1}{4\pi}) \int_0^R \int_0^{2\pi} \frac{1}{r_{ij}} r dr d\theta \tag{4-45}$$

and H_{ij} is in form

$$H_{ij} = u_j(\frac{1}{4\pi}) \int_0^R \int_0^{2\pi} \frac{\partial(\frac{1}{r_{ij}})}{\partial n_j} r dr d\theta \tag{4-46}$$

The boundary integral for G_{ij} and H_{ij} with the different positions of the source point P and the field point Q is shown in Appendix A.

In addition, adding the unknown potential at infinity u_∞ in equation (4-39) to H_{ij}, **H** matrix becomes

$$\mathbf{H} = \begin{bmatrix} H_{p,p} & H_{p,a} & -1 \\ H_{a,p} & H_{a,a} & -1 \end{bmatrix}_{(n_p+n_a)\times(n_p+n_a+1)} \tag{4-47}$$

where -1 column corresponds to u_∞. And the **G** matrix is

$$\mathbf{G} = \begin{bmatrix} G_{p,p} & G_{p,a} \\ G_{a,p} & G_{a,a} \end{bmatrix}_{(n_p+n_a)\times(n_p+n_a)} \tag{4-48}$$

The subscript p and a indicate the pipe and the anode respectively. The subscript (p,p) and (a,a) indicate that the collocation points and the field points are on the same object. While (p,a) means that the collocation points are on the pipe and the field points are on the anode. Likewise (a,p) means that the collocation points are on the anode and the field points are on the pipe. The number of node on the pipe and the anode are represented by n_p and n_a.

4.3.6 Row Sum Elimination

The diagonal elements of the matrix $\boldsymbol{H}$ are usually difficult to calculat since the linear or higher order elements have been used and the constant c_i in equation (4-14) involves the calculation of the solid angle subtended by the region V at x_s on S. In order to overcome this difficulty, Gibbs's theorem can be applied to find the values of the diagonal.[76] For a domain governed by Laplace's equation, if the potential is uniform throughout the domain, and its gradient of the potential is zero at infinity if it exists, the gradient of the potential will be equal to zero within the domain. For the three-dimensional potential problem, $u(y) \equiv 1$ is defined in the interior region. Since $q(y) = \frac{\partial u(y)}{\partial n} = 0$ on the boundary, $q(y) = 0$ in the domain. Thus equation (4-13) becomes

$$c(x_s) = -\int_s q^*(x_s, y) dS(y) \tag{4-49}$$

It means that,

$$\sum_{i,j} H_{i,j} = 0 \tag{4-50}$$

where the diagonal terms are unknown. The diagonal terms are now specified by the negative sum of the off-diagonal terms of each row

$$H_{i,i} = -\sum_{j \neq i} H_{i,j} \tag{4-51}$$

where j goes from one to the number of terms in a row.

The same technique used for the interior domain is applied to present work. Assuming $u(y) \equiv 1$, since $q(y) = \frac{\partial u(y)}{\partial n} = 0$ on the boundary and in the domain, equation (4-15) becomes

$$c(x_s) = -\int_s q^*(x_s, y) dS(y) - \lim_{R \to \infty} \int_{S_R} q^*(x_s, y) dS(y) \tag{4-52}$$

Additionally, since

$$\lim_{R \to \infty} \int_{S_R} q^*(x_s, y) dS(y) = (-\frac{1}{4\pi R^2})(4\pi R^2) = -1 \tag{4-53}$$

$c(x_s)$ in equation (4-52) becomes

$$c(x_s) = -\int_s q^*(x_s, y) dS(y) + 1 \tag{4-54}$$

which means that,

$$H_{i,i} = 1 - \sum_{j \neq i} H_{i,j} \tag{4-55}$$

Therefore, by using Gibbs's theorem, the diagonal elements of the matrix H can be obtained from the off-diagonal elements and the calculation difficulties are avoided.

4.3.7 Self-Equilibrium

Cathodic protection systems do not lose or gain current from their surroundings. In other words, the current is conserved. Therefore, if the flux between the

anode and the pipe is self-equilibrium, the flux at infinity will be zero. To implement this condition, an extra equation, equation (4-56) is added to the system.[31,77]

$$\int_S q dS = 0 \tag{4-56}$$

It indicates the intensity of an equivalent source distributed over S. It also can be written as

$$i_\infty = \sum_k i_{p,k} A_{p,k} + \sum_k i_{a,k} A_{a,k} = 0 \tag{4-57}$$

where

$$A_k = \int_{S_k} dS_k, k \in [0, n_p] \quad or \quad [0, n_a] \tag{4-58}$$

Adding equation (4-57) to equation (4-47) and (4-48), and defining the potential vector $\mathbf{u}$ as

$$\phi = \begin{bmatrix} \phi_p \\ \phi_a \\ \phi_\infty \end{bmatrix}_{(n_p+n_a)\times 1} \tag{4-59}$$

the flux vector $\mathbf{q}$ as

$$\mathbf{n} \cdot \nabla\phi = \begin{bmatrix} n \cdot \nabla\phi_p \\ n \cdot \nabla\phi_a \end{bmatrix}_{(n_p+n_a)\times 1} \tag{4-60}$$

we get

$$\begin{bmatrix} H_{p,p} & H_{p,a} & -1 \\ H_{a,p} & H_{a,a} & -1 \\ 0 & 0 & 0 \end{bmatrix} \begin{Bmatrix} \phi_p \\ \phi_a \\ \phi_\infty \end{Bmatrix} = \begin{bmatrix} G_{p,p} & G_{p,a} \\ G_{a,p} & G_{a,a} \\ A_p & A_a \end{bmatrix} \begin{Bmatrix} -n \cdot \bigtriangledown\phi_p \\ -n \cdot \bigtriangledown\phi_a \end{Bmatrix} \tag{4-61}$$

Here $\boldsymbol{H}$ matrix is singular because there is still a row of zeros in it. However, it will only be the case when Neumann type boundary conditions are specified everywhere. The Neumann problem results in an infinite number of solutions.

Therefore, at least one element in the system must have a Dirichlet boundary condition to make the $\boldsymbol{H}$ matrix nonsingular and result in a unique solution. In addition $-n \cdot \bigtriangledown\phi$ has a minus sign because the normal vector direction is outward of boundary S.

4.4 Forward Model

4.4.1 Constant Steel Potential Assumption

Since the axial variation of potential in pipe steel is trivial for a short section or low resistance pipelines, the potential of pipe steel is assumed to be a constant in this chapter.

Rewriting equation (4-61) by making a variable substitution $\phi = V - \psi$, we get

$$\begin{bmatrix} H_{p,p} & H_{p,a} & -1 \\ H_{a,p} & H_{a,a} & -1 \\ 0 & 0 & 0 \end{bmatrix} \begin{Bmatrix} V-\psi_p \\ V-\psi_a \\ V-\psi_\infty \end{Bmatrix} = \begin{bmatrix} G_{p,p} & G_{p,a} \\ G_{a,p} & G_{a,a} \\ A_p & A_a \end{bmatrix} \begin{Bmatrix} -n \cdot \bigtriangledown(V-\psi_p) \\ -n \cdot \bigtriangledown(V-\psi_a) \end{Bmatrix} \quad (4\text{-}62)$$

where V is the potential of pipe steel. Decomposing the vector $V - \psi$ and $-n \cdot \bigtriangledown(V - \psi)$, equation (4-62) becomes

$$\begin{aligned} &\begin{bmatrix} H_{p,p} & H_{p,a} & -1 \\ H_{a,p} & H_{a,a} & -1 \\ 0 & 0 & 0 \end{bmatrix} \begin{Bmatrix} V \\ V \\ V \end{Bmatrix} - \begin{bmatrix} H_{p,p} & H_{p,a} & -1 \\ H_{a,p} & H_{a,a} & -1 \\ 0 & 0 & 0 \end{bmatrix} \begin{Bmatrix} \psi_p \\ \psi_a \\ \psi_\infty \end{Bmatrix} \\ = &\begin{bmatrix} G_{p,p} & G_{p,a} \\ G_{a,p} & G_{a,a} \\ A_p & A_a \end{bmatrix} \begin{Bmatrix} n \cdot \bigtriangledown\psi_p \\ n \cdot \bigtriangledown\psi_a \end{Bmatrix} \end{aligned} \quad (4\text{-}63)$$

Since the potential of steel V is assumed to be a constant, $-n \cdot \bigtriangledown V = 0$. Moreover,

according to equation (4-55)

$$H_{p,p} + H_{p,a} = 1 \tag{4-64}$$

$$H_{a,p} + H_{a,a} = 1 \tag{4-65}$$

Thus, the first term on the left hand side of equation (4-63) is vanished, and we can readily obtain

$$\begin{bmatrix} H_{p,p} & H_{p,a} & -1 \\ H_{a,p} & H_{a,a} & -1 \\ 0 & 0 & 0 \end{bmatrix} \begin{Bmatrix} \psi_p \\ \psi_a \\ \psi_\infty \end{Bmatrix} = - \begin{bmatrix} G_{p,p} & G_{p,a} \\ G_{a,p} & G_{a,a} \\ A_p & A_a \end{bmatrix} \begin{Bmatrix} n \cdot \bigtriangledown \psi_p \\ n \cdot \bigtriangledown \psi_a \end{Bmatrix} \tag{4-66}$$

Equation (4-11) can be rewrite as

$$n \cdot \bigtriangledown \psi_p = \frac{\rho_{soil}}{\rho_{coat}\delta}(\psi_p - \psi_{corr}) \tag{4-67}$$

Substituting equation(4-67) into equation (4-66), we can get

$$\begin{bmatrix} H_{p,p} & H_{p,a} & -1 \\ H_{a,p} & H_{a,a} & -1 \\ 0 & 0 & 0 \end{bmatrix} \begin{Bmatrix} \psi_p \\ \psi_a \\ \psi_\infty \end{Bmatrix} = - \begin{bmatrix} G_{p,p} & G_{p,a} \\ G_{a,p} & G_{a,a} \\ A_p & A_a \end{bmatrix} \begin{Bmatrix} \frac{\rho_{soil}}{\rho_{coat}\delta}(\psi_p - \psi_{corr}) \\ n \cdot \bigtriangledown \psi_a \end{Bmatrix} \tag{4-68}$$

Equation (4-68) will be applied in the two cases as below.

Sacrificial anode case

For the sacrificial anode protection method, we set the potential of the anode as a constant and the current density of the anode is unknown except that it is zero at the two ends of the anode. The potential of the pipe is unknown. The current density of pipe is also unknown except the zero value is given at the ends of pipe. In addition, the potential and the current density of the pipe satisfy the relation of equation (4-67).

Rearranging the equation (4-68),

$$\begin{bmatrix} H_{p,p} + G_{p,p}\frac{\rho_{soil}}{\rho_{coat}\delta} & G_{p,a} & -1 \\ H_{a,p} + G_{a,p}\frac{\rho_{soil}}{\rho_{coat}\delta} & G_{a,a} & -1 \\ +A_p\frac{\rho_{soil}}{\rho_{coat}\delta} & A_a & 0 \end{bmatrix} \begin{Bmatrix} \psi_p \\ n\cdot\bigtriangledown\psi_a \\ \psi_\infty \end{Bmatrix} = \begin{bmatrix} G_{p,p}\frac{\rho_{soil}}{\rho_{coat}\delta} & -H_{p,a} \\ G_{a,p}\frac{\rho_{soil}}{\rho_{coat}\delta} & -H_{a,a} \\ A_p\frac{\rho_{soil}}{\rho_{coat}\delta} & 0 \end{bmatrix} \begin{Bmatrix} \psi_{corr} \\ \psi_a \end{Bmatrix} \tag{4-69}$$

it can be used to model sacrificial anode CP system.

Impressed current case

To simulate the impressed current protection method, we set the current density of the anode as a constant value, but the potential of the anode is unknown. The conditions of current density and potential of pipe are same as those of the sacrificial anode case. Likewise, the following equation can be obtained.

$$\begin{bmatrix} H_{p,p} + G_{p,p}\frac{\rho_{soil}}{\rho_{coat}\delta} & H_{p,a} & -1 \\ H_{a,p} + G_{a,p}\frac{\rho_{soil}}{\rho_{coat}\delta} & H_{a,a} & -1 \\ +A_p\frac{\rho_{soil}}{\rho_{coat}\delta} & 0 & 0 \end{bmatrix} \begin{Bmatrix} \psi_p \\ \psi_a \\ \psi_\infty \end{Bmatrix} = \begin{bmatrix} G_{p,p}\frac{\rho_{soil}}{\rho_{coat}\delta} & -G_{p,a} \\ G_{a,p}\frac{\rho_{soil}}{\rho_{coat}\delta} & -G_{a,a} \\ A_p\frac{\rho_{soil}}{\rho_{coat}\delta} & -A_a \end{bmatrix} \begin{Bmatrix} \psi_{corr} \\ n\cdot\bigtriangledown\psi_a \end{Bmatrix} \tag{4-70}$$

4.4.2 Simulation Results

Typical simulation results for potentials on soil surface directly above a 10m pipeline with one coating defect are shown in Figure 4-10. The potential change at the position corresponding to the coating defects is evident, but the magnitude of the change is small, in agreement with previous calculations.[35,38]

4.5 Inverse Model

The purpose of the *inverse* model is to construct an objective function and to compare different types of regression methods in order to minimize the objective function. The simulated annealing method was found appropriate in the present study since it can escape from the local minima and thereby avoid the influence of the initial guess.

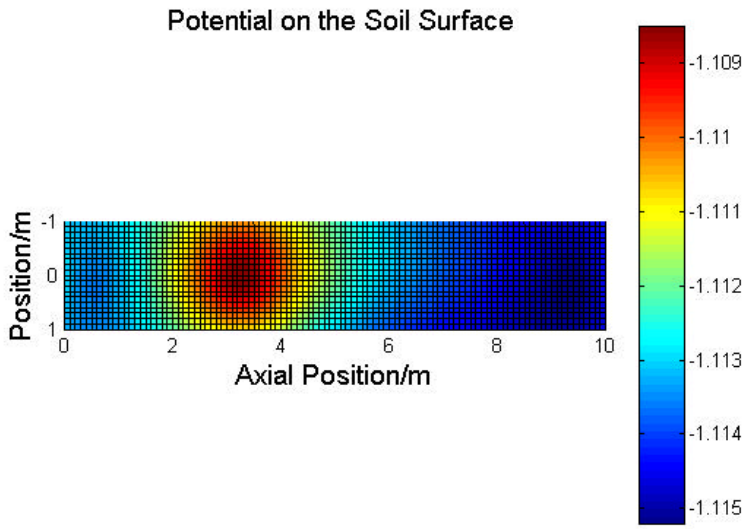

Figure 4-10: False color image of the on-potential on the soil surface that was generated by the *forward* model corresponding to Figure 4-1.

4.5.1 Objective Function

An objective function, which describes the difference between the measured potential and calculated potential on the soil surface, is given as

$$g(x, \rho, \sigma) = \sum_{j=1}^{N} (\psi_j - \widehat{\psi}_j)^2 \tag{4-71}$$

where ψ_j and $\widehat{\psi}_j$ represent measured and calculated soil surface potentials, respectively. The calculated soil surface potential depends on the pipe coating conditions, such as position, resistivity and width of coating defect. Thus, once the minimum of the objective function is reached, the fitted coating parameters will reflect the real physical conditions of pipeline.

4.5.2 Analysis of Regression Methods

Several regression methods were tested, including the conjugate gradient, Levenberg--Marquart, and quasi-Newton methods. A summary of these methods is provided by Press *et al.*[78] These methods, distinguished by the need to evaluate both the function value and the function gradient, were rejected for the pipeline *inverse* model. The extra calculations required for evaluation of the function gradient

added significantly to the computational requirement. In addition, these methods were extremely sensitive to the value of an initial guess and had a tendency to find local rather than global minima.

The downhill simplex method,[78] which requires evaluation of only the objective function and not its gradient, was used successfully for preliminary two--dimensional *inverse* analysis. The downhill simplex method did not work very well for three-dimensional problems because it was strongly affected by the initial guess.

Genetic minimization algorithms, intended to mimic the course of natural selection, have been applied to *inverse* problems for cathodic protection.[42,44,45] Parameters are normally coded as binary strings to reduce the searching population. Procedures of selection, mating and mutation are used repeatedly to create the new generation until the specified stop criterion is satisfied. This method is not very sensitive to the values of initial guesses and can escape from the local minima. However, it has difficulty selecting between close function values.[79]

After trying the alternatives, the simulated annealing optimization approach was selected for the present work. This method is attractive because it is suitable for large-scale problems and can search for a global minimum, which may be hidden among many local minima. Simulated annealing was better than downhill simplex because the simplex method accepts only downhill steps during its searching; whereas, simulated annealing can accept both the downhill and uphill steps. In this way, simulated annealing method can step out of the local optima and successfully locate the global minimum.

4.5.3 Simulated Annealing Method

The term "simulated annealing" comes from a physical process analogy.[78] When a material is heated and then is slowly cooled down, a strong crystalline structure

will be obtained. This crystal is the minimum energy state of the system. In a simulation process, a minimum of the objective function corresponds to the ground state of the substance. The Bolzmann probability distribution, which describes the different energy state in a thermal equilibrium under given temperature, can also be used to mimic the different objective function value at certain searching region. The simulated annealing method starts with a brief view of the searching domain by making large moves and then it focuses on the most possible region. The inherent random fluctuation permits the annealing procedure avoid the local minima. The Metropolis rule

$$p = e^{-(g_2 - g_1)/kT} \tag{4-72}$$

is used to control whether the uphill step is accepted. In equation (4-72), p refers to the probability, g_i is the objective function value and T is an important parameter in the simulated annealing method, which resembles the temperature in the thermal system. For $g_2 < g_1$, the probability p is greater than 1, which means that the downhill steps are always accepted. For $g_2 > g_1$, the probability p is compared with a uniformly distributed random number from $[0, 1]$ to decide whether uphill steps are accepted. Since each parameter has its own limit, once the parameter is out of its limit, the following equation can be used to correct the parameter.

$$x = x_L + \alpha(x_U - x_L) \tag{4-73}$$

where α is a uniformly distributed random number among $[0, 1]$, x_L is the lower limit of x and x_U is the upper limit of x. The parameter x can thus be guaranteed to lie within its bounds.

4.5.4 Simulation Results and Discussions

Examples of the application of the proposed *forward* and *inverse* models are given in this section. In addition, several *inverse* strategies are introduced. The re-

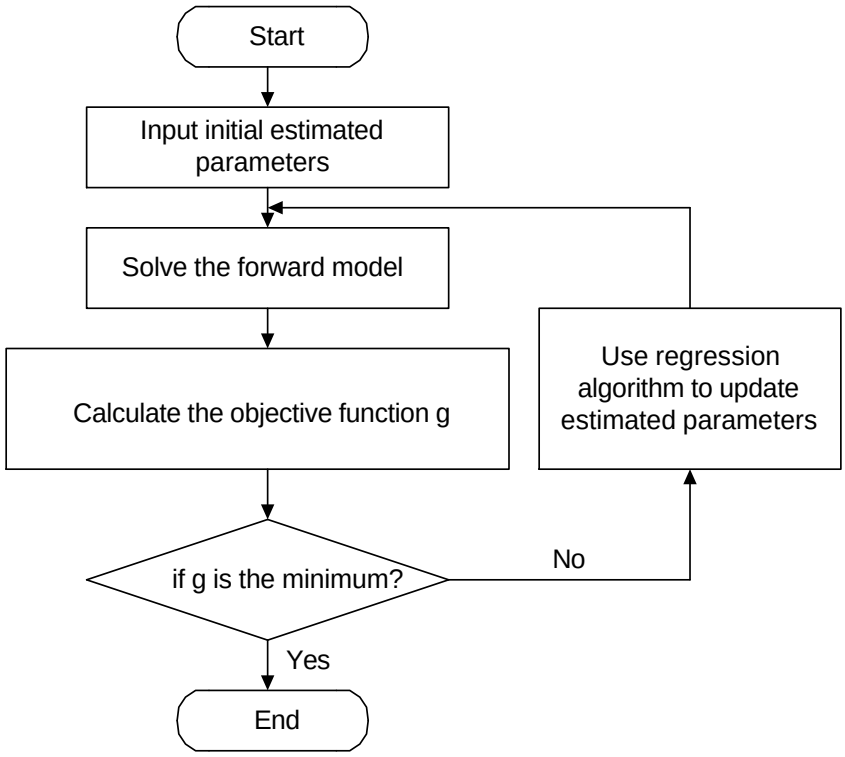

Figure 4-11: Flow chart for the *inverse* model calculations.

gression algorithm employed by the *inverse* model is shown in the Figure 4-11. The set parameters were used as inputs to the *forward* model to get the potential on soil surface. These results were treated as the measured data. These "measured" potentials belong to each point of a 3 x 101-grid area, as shown in Figure 4-12. There are three lines in the grid area: the middle line is right above the pipe centerline, and two other lines of calculated values were placed ± 1 m from the centerline of the pipe. The grid, therefore, comprised 303 data points. Initialize the parameters, the number of defects, each defect's center position, resistivity reduction and the width of the defects, and input them into the *inverse* model. Among all these parameters, the number of defects has the most significant impact on the regression results. In this study, we purpose a method to decide the number of defects which can be obtained from the measurements. The *inverse* analysis result by using simulated annealing method is shown in Table 4.1 for a 10-meter long pipe segment

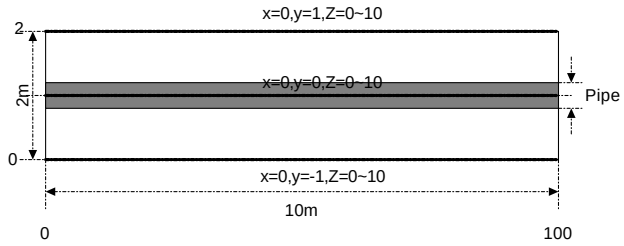

Figure 4-12: Grid showing the location of 303 surface on-potentials calculated using the three-dimensional *forward* model developed in the present work. The grid shown is for a 10m pipe segment. A scaled version of the grid was used for a 100m pipe segment.

with two coating defects. The calculated data were for defects located at the 3.2 and 6.0 m positions with characteristic dimensions of 0.05 and 0.5 m, respectively. The intact coating resistivity had a value of 5.0×10^7 / Ωm, which was fixed for the regression procedure. The input values for surface potentials were calculated at the limits of the precision of the *forward* model, *i.e.*, no noise was added. The regression yielded the correct locations, characteristic defect dimensions, and resistivity changes associated with the coating defects.

The process of finding the minimum of the object function is shown in Figure 4-13. For this test problem, with the *forward* model and no noise added to the synthetic data, the minimum value of the cost function was 10^{-15}. Of the techniques used, only the simulated annealing method could find this global minimum. The best of the other techniques were able to identify local minima with values on the order of 10^{-4} to 10^{-8} preceding the plateau.

A comparison of the set and fitted results for pipe coating resistivity, potential and current density, respectively, is shown in Figures 4-14. Corresponding to the coating resistivity decay, the potential and current density distributions have significant changes. A good agreement between the synthetic data and regression results can be observed.

Table 4.1: Parameter values obtained using the three-dimensional *inverse* model developed in the present work for a 10m pipe segment with two coating defects.

	Coating Defect	Position x_k / m	Resistivity ρ_k / Ω m	Characteristic dimension σ_k / m
Set Values	1	3.2	-4.0×10^7	0.22
	2	6.0	-3.5×10^7	0.71
Initial Values	1	2.5	-3.0×10^7	0.1
	2	5.0	-3.0×10^7	0.1
Regression Result	1	3.206	-3.81×10^7	0.26
	2	6.004	-3.51×10^7	0.70

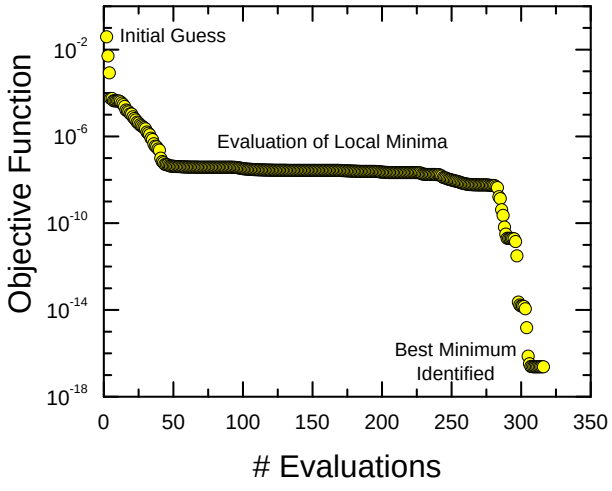

Figure 4-13: The regression objective function as a function of the number of evaluations for a pipe coating with one defect region. The simulated annealing method was used for this regression.

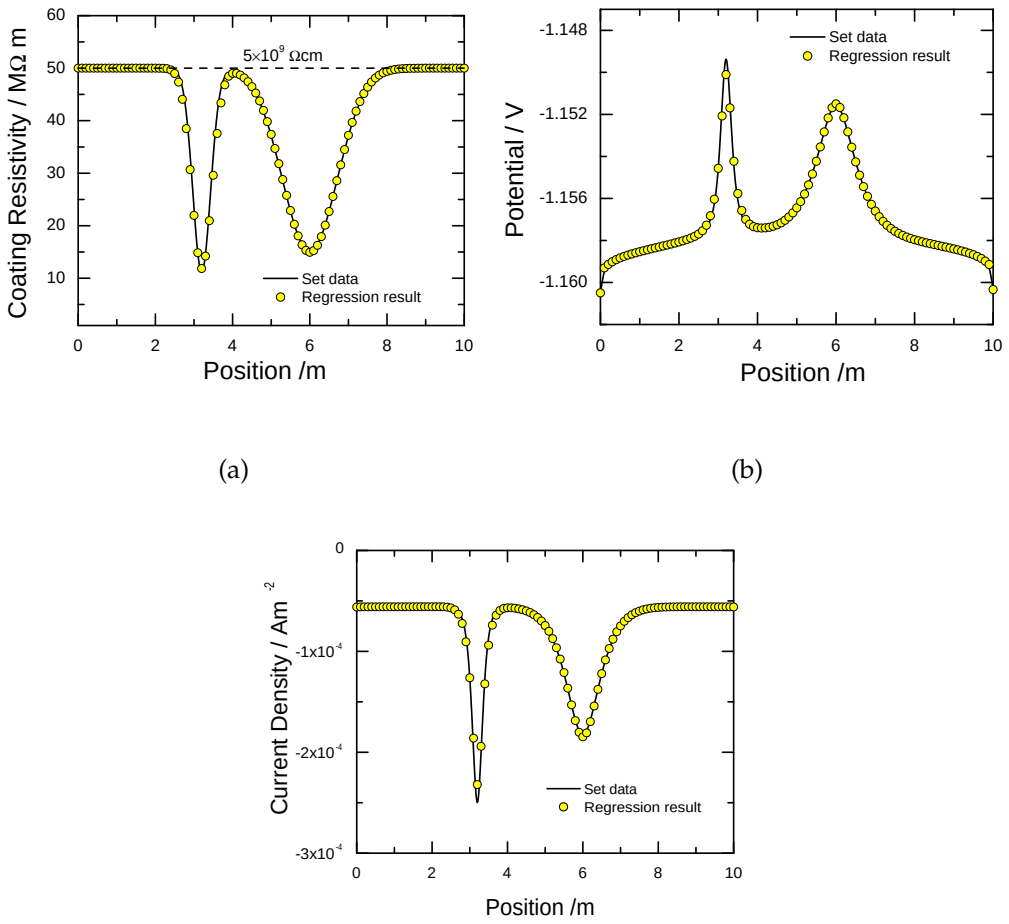

Figure 4-14: Comparison of the set and fitted results for pipe coating with two coating defects: a) coating resistivity; b) potentials; and c) current density.

Table 4.2: Test case parameters with five coating defects on the pipe used to demonstrate the method for determination of the number of statistically significant parameters (see Figure 4-15). The intact coating resistivity had a value of 5.0×10^7 / Ωm.

	Coating Defect	Position x_k / m	Resistivity ρ_k / Ω m	Characteristic dimension σ_k / m
Set Values	1	10	-3.5×10^7	0.45
	2	30	-4.5×10^7	0.32
	3	40	-3.0×10^6	0.55
	4	70	-2.0×10^7	0.45
	5	85	-4.0×10^7	0.63

4.5.5 Inverse Strategies

The strategies, including the determination of the number of significant parameters, the procedures used to reduce the influence of initial guess and the evaluation of the role of noise in the measured data, were explored to assess the confidence level of the *inverse* model results.

Determination of the Number of Statistically Significant Parameters

When the collected data are scattered, it is difficult to decide how many possible defects or coating anomalies should be included in the regression. The approach taken to address this issue was to increase sequentially the number of defects, using the regression statistics to determine when the number of statistically significant parameters was exceeded. This approach is similar to that used to assess the number of statistically significant measurement model parameters can be obtained by regression to impedance spectroscopy data.[80,81]

An example with five defects, shown in Table 4.2, was used to illustrate the approach taken to assess the correct number of statistically significant parameters. The relation between the regression statistic $log(\chi^2/\nu)$ and the number of coating defects assumed in the regression is presented in Figure 4-15. Here, $\nu = N - M$ represents the degree of freedom of the problem which is reduced as the number of

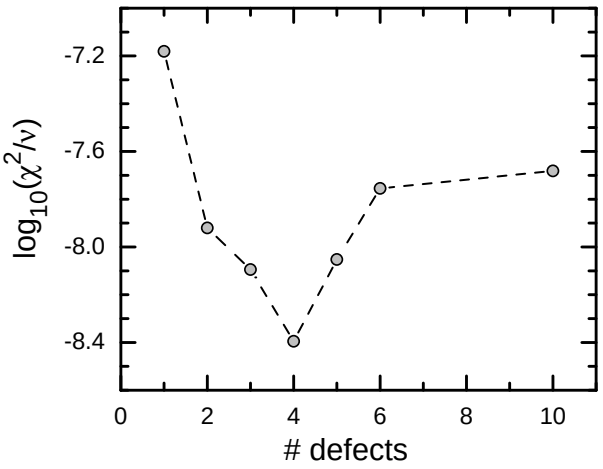

Figure 4-15: The regression statistic as a function of the number of coating defects assumed for the model. The minimum in this value is used to identify the maximum number of coating defects that can be justified on statistical grounds.

parameters is increased. N represents the number of data point, and M represents the number of parameters. χ^2 is the weighted objective function. The lowest point of the curve denotes the number of statistically significant coating defects obtainable by regression. Here, it is four. The fifth coating anomaly, identified in Table 4.2 as defect 3, could not be identified by the regression procedure. The number of coating anomalies identified by this procedure will depend on the amount and quality of data and on the sensitivity of the data to coating condition.

Testing the Robustness of the Inverse Model

To assess the influence of uncertainty in the measured data, normally distributed stochastic errors were added to the soil surface potential generated by the *forward* model. The noise added had standard deviations σ_{noise} of 0.1, 1.0, and 2.0 mV respectively.

The set values, initial guesses, and regression results are presented in Table 4.3. Three coating defects placed at 30, 40, and 70 m positions were used to generate synthetic data. For the lowest noise level, $\sigma_{\text{noise}} = 0.1$ mV, the sequential procedure described in the previous section allowed only two statistically significant defects.

Table 4.3: Regression results from the three-dimensional *inverse* model for a 100m pipe segment with three coating defects. The sequential regression procedure was used to identify the number of defects that were statistically significant. The intact coating resistivity had a value of 5.0×10^7 / Ωm.

	Coating Defect	Position x_k / m	Resistivity ρ_k / Ω m	Characteristic dimension σ_k / m
Set Values	1	30	-4.5×10^7	0.32
	2	40	-3.0×10^6	0.55
	3	70	-2.0×10^7	0.45
Initial Guess	1	50	-3.5×10^7	0.92
	2	50	-3.5×10^6	0.92
	3	50	-3.5×10^6	0.92
Regression Results				
$\sigma_{\text{noise}} = 0.1$ mV	1	29.85	-4.25×10^7	0.66
	2	69.83	-7.57×10^6	1.30
$\sigma_{\text{noise}} = 1.0$ mV	1	32.01	-4.67×10^7	0.087
$\sigma_{\text{noise}} = 1.0$ mV	1	32.01	-4.68×10^7	0.057
	2	90.29	-1.22×10^6	0.86
$\sigma_{\text{noise}} = 2.0$ mV	1	29.95	-3.33×10^7	1.50

The initial guesses placed the defects at the midpoint of the pipe segment. The regression results suggested that the defects exist near the 30 and 70 m locations. The missing defect is the one with the smallest deviation in coating resistivity. Thus, the regression procedure identified the correct location of the two most significant reductions in coating resistivity.

For $\sigma_{\text{noise}} = 1.0$ mV, the sequential procedure using the minimization of the $\sum \chi^2/\nu$ criterion allowed two coating defects. The defect located at 32.01 m was consistent with the most significant defect located at 30 m, but the defect identified at 90 m did not conform to the input data. In addition, the regression failed to identify the second most significant reduction in coating resistivity at 70 m.

The problem here may be an inadequate sensitivity of the χ^2/ν statistic for identifying overfitting of data. Other criteria, such as the Akaiki information criteria,[82,83,84] provide additional penalties for adding parameters to a model. For

$\sigma_{\text{noise}} = 1.0$ mV, the Akaiki performance index

$$A_{\text{PI}} = \sum \chi^2 \frac{1 + n_p/n_{\text{ob}}}{1 - n_p/n_{\text{ob}}} \tag{4-74}$$

suggested that only one defect could be identified; whereas, the Akaiki information criterion

$$A_{\text{IC}} = \log\left(\sum \chi^2 \left(1 + 2n_p/n_{\text{ob}}\right)\right) \tag{4-75}$$

suggests that two defects could be identified. Regression for a single coating defect identified a defect in the close vicinity of the most significant coating reduction. By any of the statistical measures tested, only the largest defect could be identified for $\sigma_{\text{noise}} = 2.0$ mV. The location of the defect was correctly identified; however, the width of the defect was incorrectly determined.

These results can be explained by examination of the synthetic surface potential data used for the *inverse* model analysis. The corresponding results of the *inverse* analysis for $\sigma_{\text{noise}} = 0.1$ mV are shown in Figure 4-16 As is shown in Figure 4.16(a), the level of added noise did not obscure the surface-potential features introduced by the presence of the major coating defects. The regressed and noise-free target values for potential cannot be distinguished; thus, the absence of the minor coating defect did not influence the fit of the model to the synthetic data. As seen in Figure 4.16(b), the regression procedure identified the the two most significant reductions in coating resistivity at 30 and 70 m locations.

In contrast, the random noise added with $\sigma_{\text{noise}} = 1.0$ mV, shown in Figure 4.17(a), almost completely obscures the influence of the coating defects. Nevertheless, a major defect can be resolved by the regression procedure in the vicinity of the largest defect, as shown in Figure 4.17(b). The anomalous defect introduced by the regression procedure at 90 m has associated with it a small reduction on coating resistivity. There is a question as to whether this defect can be considered to

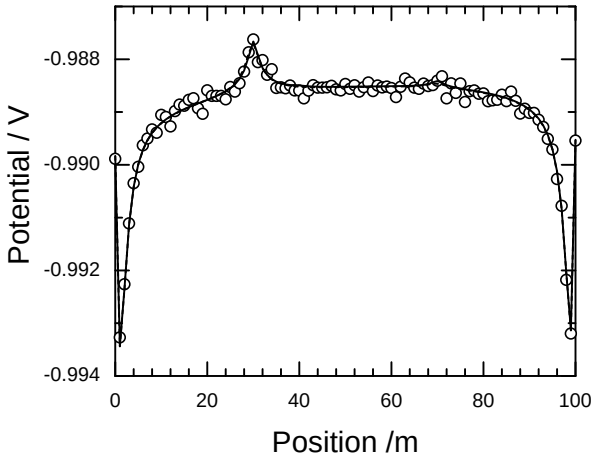

(a)

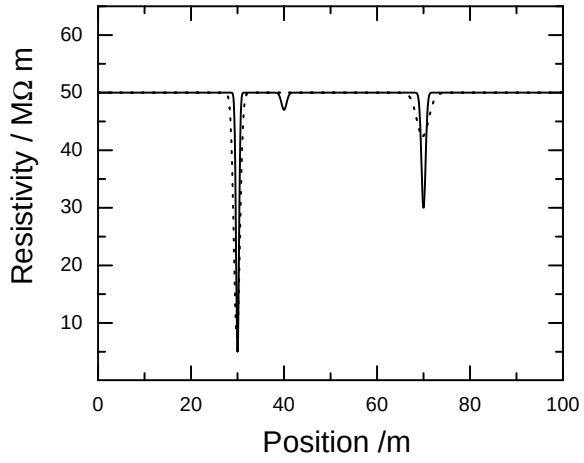

(b)

Figure 4-16: Comparison between the input values and regression results for $\sigma_{\text{noise}} = 0.1$ mV: a) soil-surface potential (at the centerline of the pipe); b) coating resistivity.

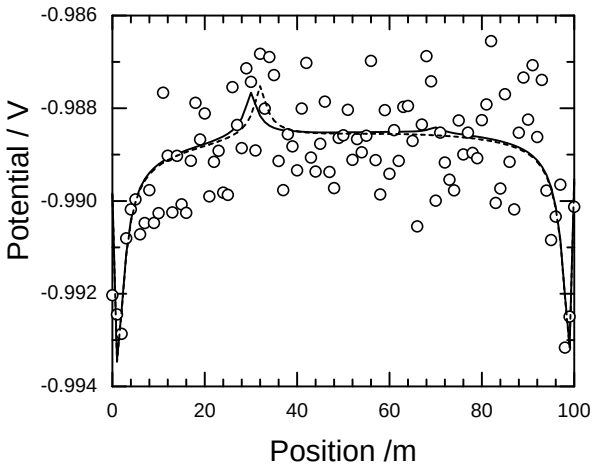

(a)

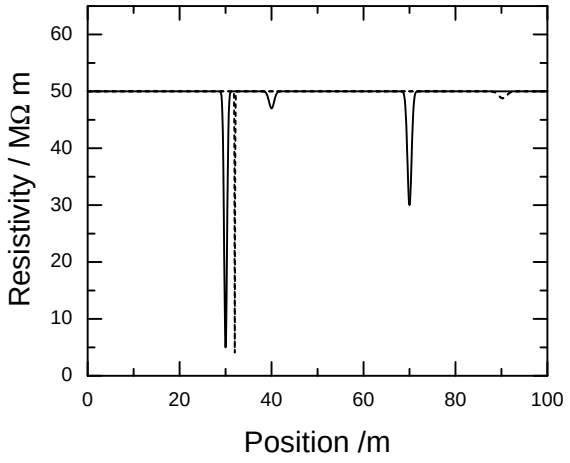

(b)

Figure 4-17: Comparison between the input values and regression results for $\sigma_{\text{noise}} = 1.0$ mV: a) soil-surface potential (at the centerline of the pipe); b) coating resistivity.

be statistically significant, but, nevertheless, the regression procedure would have given adequate guidance for excavation of the pipe.

By visual inspection, the random noise added with $\sigma_{\text{noise}} = 2.0$ mV, shown in Figure 4.18(a), would appear to obscure the influence of even the major coating defect. The regression procedure identified a single statistically significant coating defect located near the 30 m defect. The agreement between the regressed potential profile and the noise-free target values was surprisingly good. As shown in Figure 4.17(b), the correct location for the principal defect was correctly identified, even though the breadth of the defect was not correctly determined.

The results suggest that, while it is difficult to extract coating conditions from the data when the influence of the coating defect on the surface potential is comparable with noise, the regression procedure showed a surprising ability to identify the location of the most significant coating defects from noisy data. This result suggests that an *inverse* model is feasible, in particular when other types of data are included.

Sensitivity to Initial Guess

The values used for an initial guess have a significant influence on most of the conventional nonlinear regression methods. To reduce this effect and to test the robustness of the present *inverse* model, identical parameters for each defect were used. For example, as the *initial guess* in Table 4.3, the positions of the defects were all set to the middle of the pipeline. This kind of initial guess created significant difficulties for conventional regression methods, but posed no problems for the simulated annealing method used in the present *inverse* model.

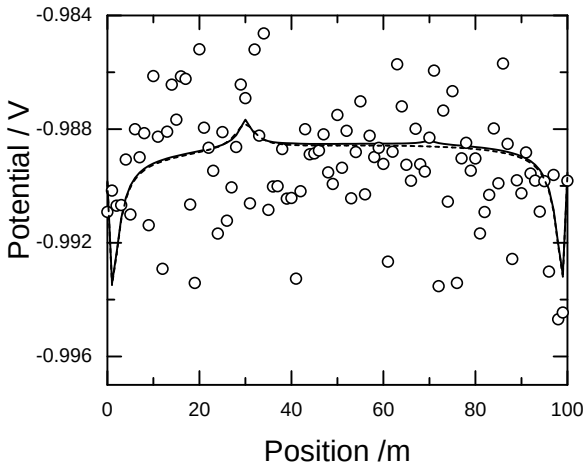

(a)

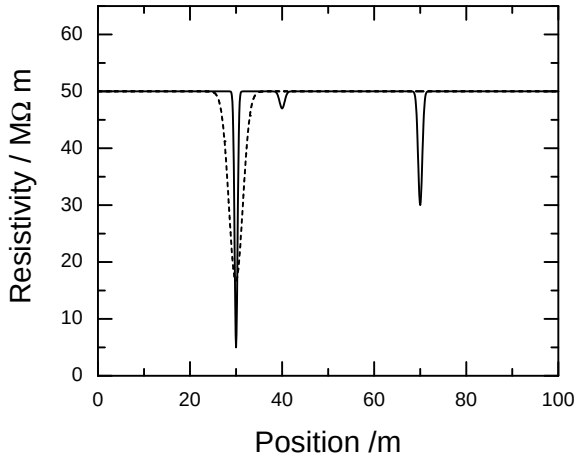

(b)

Figure 4-18: Comparison between the input values and regression results for $\sigma_{\text{noise}} = 2.0$ mV: a) soil-surface potential (at the centerline of the pipe); b) coating resistivity.

4.6 Conclusions

In this chapter, both the *forward* model and the *inverse* model for the three--dimensional CP system was introduced. The simplified *forward* model has the following advantages.

1. The Laplace's equation with the simplified linear boundary condition was applied. This approach not only simplifies the *forward* calculation, but also reduces the computational effort to the *inverse* calculation.

2. The line shape approximation for the pipe coating resistivity makes it possible to limit the number of parameters needed to describe the coating conditions along the whole pipe. It dramatically increases the degree of freedom of the problem as compared to the method that represents the coating conditions element by element.

3. The BEM method with cylindrical element was developed. The basic theory of BEM, such as use of the mirror reflection technique for the half-infinity domain, row sum elimination, and self-equilibrium, were introduced. In addition, the implementation techniques, for example, the coordinates transformation, element discritization, were also included.

4. The simplified *forward* model was used to obtain the potentials of the pipe on the soil surface. The potential and the current density of the pipe and the anode could also be calculated.

The *inverse* part of work represents an ambitious research effort with a potentially large payoff for the oil and gas transmission industry. The central question is whether a regression approach could be used to assess pipeline coating conditions from field data in a way that is consistent with the laws of physics. The rationale,

methodology, and results are presented, which demonstrate the feasibility of the *inverse* model for pipelines.

1. This work has demonstrated that it is possible to couple a boundary element *forward* model with a nonlinear regression algorithm to obtain pipe surface properties from measured soil-surface potentials. The resulting model is called an *inverse* model.

2. The technique identifies the location of coating anomalies as well as the breadth of the anomaly and the amount that the local resistivity has changed.

3. The performance of the *inverse* model is sensitive to the regression procedure used. The simulated annealing algorithm proved to be the most robust and had greatest capability to seek the global minimum for this problem.

4. An algorithm was developed that could be used to identify the maximum number of coating anomalies that can be detected. This number is sensitive to the quality of data as well as to the actual coating condition.

5. If the number of coating anomalies detected is smaller than the actual number of coating defects, the technique will identify the most serious anomalies.

The results of this effort, limited to a single pipe in a right-of-way, demonstrate the feasibility of a program to interpret survey data in terms of the state of protection of the pipe.

CHAPTER 5
DEVELOPMENT OF THREE-DIMENSIONAL FORWARD AND INVERSE MODELS FOR PIPELINE WITH BOTH POTENTIAL AND CURRENT DENSITY SURVEY DATA

5.1 Forward Model

5.1.1 Introduction

In Riemer's work, there were two separate domains for the flow of current. The first was the soil domain up to the surfaces of the pipes and anodes. The boundary conditions for the soil domain were the kinetics of the corrosion reactions. The second domain was the internal pipe metal, anode metal and connecting wires for the return path of the cathodic protection current.[38] The BEM method was used for the first domain. The FEM method was applied to the second domain. Brichau also coupled the BEM and FEM to solve the two domains.[72] In this chapter, to simplify the calculations, not only the potential but also the current density along the pipe steel will be obtained by using the BEM method.

5.1.2 Pipeline with Varying Steel Potential

In chapter 4, the potential V on the pipe steel was assumed to be a constant. Actually, the potential on the pipe steel varies along the pipe since the pipeline has its own internal resistance. For a short section of pipe, since the potential drop due to the pipe resistance is very small, it is reasonable to assumed it to be constant. However, for a long pipeline or a high resistance pipe, the potential drop along the pipe steel is significant and cannot be ignored. The model in chapter 4 was extended to account for the electrical potential of the pipeline steel.

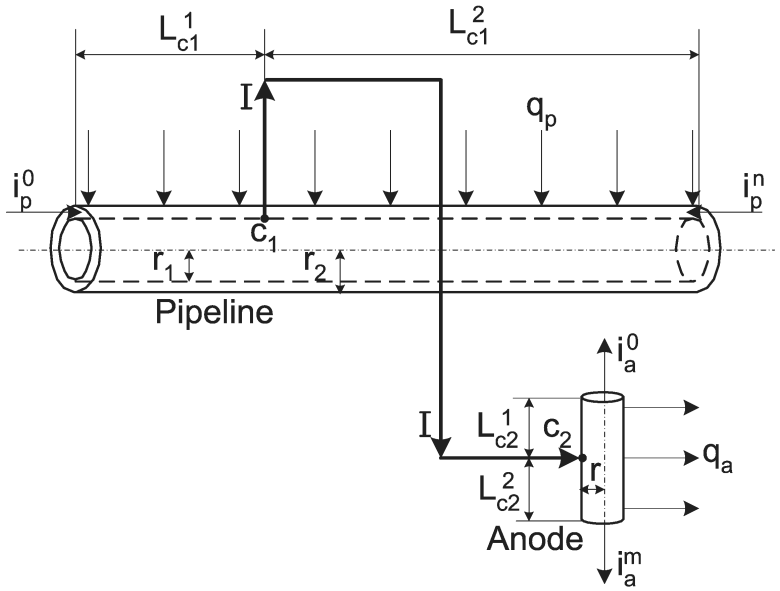

Figure 5-1: Cathodic protection system with variant potential along the pipe and anode.

The method of calculation is illustrated schematically in Figure 5-1, where a horizontally placed pipeline is connected by a wire to a vertically placed sacrifice anode. The connection points are c_1 on the pipe and c_2 on the anode. In Figure 5-1, i represents the current density along the axial direction of pipeline or anode, and subscripts p and a designate pipeline and anode, respectively. The current density entering the pipe at the ends is designated by i_p^0 and i_p^n, and the current density entering the anode at the ends is designated by i_a^0 and i_a^n. The current density entering the pipe coating in the radial direction is given by q. As shown in Figure 5-1, the protecting current flows away from the anode to the soil, then flows to the pipeline. On the pipeline, the currents flow from the two opposite directions to the connection point c_1 and they are concurrent as current I. The current I flows back to the anode through the wire.

The current density in the pipeline steel along axial direction is given by

$$i = \frac{1}{\rho_{steel}}(-n \cdot \nabla V) = -\frac{1}{\rho_{steel}}\frac{dV}{dz} \tag{5-1}$$

where V represents the potential of the steel in the pipe. Equation (5-1) can be

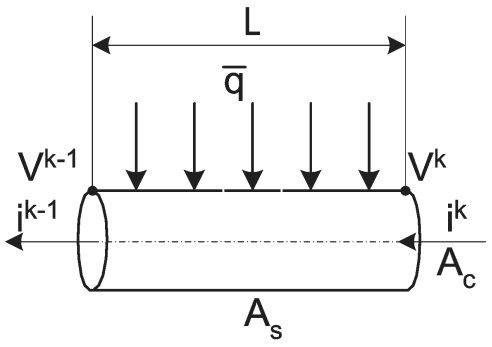

Figure 5-2: Relation of potential V and current density.

integrated in the axial direction along a segment with length dz, shown in Figure 5-2, such that

$$\int_{V_{k-1}}^{V_k} dV = -\rho_{steel} \int_{z_{k-1}}^{z_k} i dz \tag{5-2}$$

The potential change across the segment is given by

$$V_k - V_{k-1} = -\rho_{steel} \int_{z_{k-1}}^{z_k} \left(\frac{z - z_{k-1}}{z_k - z_{k-1}} i^{k-1} + \frac{z_k - z}{z_k - z_{k-1}} i^k\right) dz \tag{5-3}$$

or

$$V_k - V_{k-1} = \rho_{steel}(z_k - z_{k-1}) \frac{(i^{k-1} + i^k)}{2} \tag{5-4}$$

where the potential difference between two points is found as the product of the average current density $(i^{k-1} + i^k)/2$ and the resistance $\rho_{steel}(z_k - z_{k-1})$.

Conservation of charge requires that the current flowing into the pipe segment is equal to the current flowing out. Thus,

$$i^{k-1} = i^k + \frac{A_s}{A_c} \bar{q} \tag{5-5}$$

where $\bar{q}$ is the average current density entering the coated surface of the element in the radial direction. A_c and A_s represent the areas of the steel cross-section and side walls, respectively. For the cathodic protected system, the protecting current flow away from the anode to the soil, and then flow to the pipeline. On the pipeline, the currents from the two sides of the connection point c_1 flow head

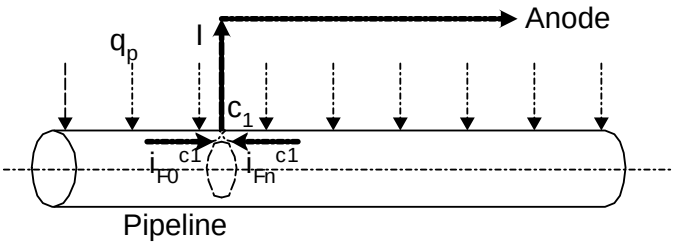

Figure 5-3: Axial direction current flow along the pipeline.

to head and are concurrent as current I flows back to the anode through the wire which is connecting the pipe and the anode. Therefore, for each segment of the pipe before connection point c_1, the potential difference is,

$$\begin{aligned}
V_0 - V_1 &= (i^0 + i^1)R = [2i^0 - \left(\frac{A_s^p}{A_c^p}\right) \cdot \frac{(q^0 + q^1)}{2}]R \\
V_1 - V_2 &= (i^1 + i^2)R = [2i^0 - \left(\frac{A_s^p}{A_c^p}\right) \cdot \frac{(q^0 + 2q^1 + q^2)}{2}]R \\
&\vdots \\
V_{c_1-1} - V_{c_1} &= (i^{c_1} + i^{c_1-1})R = [2i^0 - \left(\frac{A_s^p}{A_c^p}\right) \cdot \frac{(q^0 + 2q^1 + \cdots + 2q^{c_1-1} + q^{c_1})}{2}]R
\end{aligned}$$

For each segment of the pipe after the connection point c_1

$$\begin{aligned}
-V_{c_1+1} + V_{c_1} &= (i^{c_1+1} + i^{c_1})R = [2i^n + \left(\frac{A_s^p}{A_c^p}\right) \cdot \frac{(q^n + 2q^{n-1} + \cdots + 2q^{c_1+1} + q^{c_1})}{2}]R \\
&\vdots \\
-V_n + V_{n-1} &= (i^n + i^{n-1})R = [2i^n + \left(\frac{A_s^p}{A_c^p}\right) \cdot \frac{(q^n + q^{n-1})}{2}]R
\end{aligned}$$

There are n equations if the pipeline is discritized as n segments, while there are $n+1$ the unknown variables $V_0, V_1, \cdots V_n$. One more equation is needed in order to get a unique solution. The potential $V = 0$ can be set at any position along the pipe. In this study, zero potential was set at the pipe and anode connection point c_1, that is, $V_{c_1} = 0$. The current flow in the anode through the wire will flow to the different direction along the anode. Likewise, for each segment of the anode

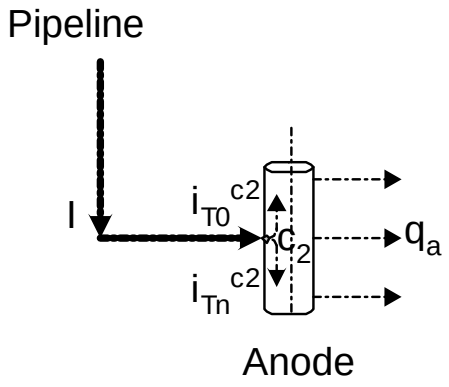

Figure 5-4: Axial direction current flow along the anode.

before the connection point c_2,

$$\begin{aligned} V_0 - V_1 &= [2i^0 - \left(\frac{A_s^a}{A_c^a}\right) \cdot \frac{(q^0 + q^1)}{2}]R \\ V_1 - V_2 &= [2i^0 - \left(\frac{A_s^a}{A_c^a}\right) \cdot \frac{(q^0 + 2q^1 + q^2)}{2}]R \\ &\vdots \\ V_{c_2-1} - V_{c_2} &= [2i^0 - \left(\frac{A_s^a}{A_c^a}\right) \cdot \frac{(q^0 + 2q^1 + \cdots + 2q^{c_2-1} + q^{c_2})}{2}]R \end{aligned}$$

For each segment of the anode after connection point c_2

$$\begin{aligned} -V_{c_2+1} + V_{c_2} &= [2i^m + \left(\frac{A_s^a}{A_c^a}\right) \cdot \frac{(q^m + 2q^{m-1} + \cdots + 2q^{c_2+1} + q^{c_2})}{2}]R \\ &\vdots \\ -V_m + V_{m-1} &= [2i^m + \left(\frac{A_s^a}{A_c^a}\right) \cdot \frac{(q^m + q^{m-1})}{2}]R \end{aligned}$$

Corresponding to the m segments of the anode, there will be $m+1$ unknown variables $V_0, V_1, \cdots V_m$. Another equation is needed. If the wire connecting the pipe and the anode has resistance R_{wire}, and the current flow through the wire is I, then

$$V_{c_1} = V_{c_2} - IR_{wire} = 0 \tag{5-6}$$

In order to satisfy the self-equilibrium limitation, the current I needs to obey the relations as below.

For the pipeline, as shown in Figure 5-3,

$$i_{F0}^{c_1} = i^0 - \left(\frac{A_s^p}{A_c^p}\right) \cdot \frac{(q^0 + 2q^1 + \cdots + 2q^{c_1-1} + q^{c_1})}{2} \tag{5-7}$$

$$i_{Fn}^{c_1} = i^n + \left(\frac{A_s^p}{A_c^p}\right) \cdot \frac{(q^{c_1} + 2q^{c_1+1} + \cdots + 2q^{n-1} + q^n)}{2} \tag{5-8}$$

where $i_{F0}^{c_1}$ is the current density coming from left end of pipe to the point c_1, and $i_{Fn}^{c_1}$ is the current density coming from right end of pipe to the point c_1. By combining these two equations,

$$(i_{F0}^{c_1} - i_{Fn}^{c_1})A_c^p = I \tag{5-9}$$

We have

$$(i^0 - i^n)A_c^p - \frac{(q^0 + 2q^1 + \cdots + 2q^{n-1} + q^n)}{2} A_s^p = I \tag{5-10}$$

For the anode, as shown in Figure 5-4,

$$i_{T0}^{c_2} = i^0 - \left(\frac{A_s^a}{A_c^a}\right) \cdot \frac{(q^0 + 2q^1 + \cdots + 2q^{c_2-1} + q^{c_2})}{2} \tag{5-11}$$

$$i_{Tm}^{c_2} = i^m + \left(\frac{A_s^a}{A_c^a}\right) \cdot \frac{(q^{c_2} + 2q^{c_2+1} + \cdots + 2q^{m-1} + q^m)}{2} \tag{5-12}$$

where $i_{T0}^{c_2}$ is the current density enter at c_2 and flow to the upper end of anode, and $i_{Tm}^{c_2}$ is the current density enter at c_2 and flow to the lower end of anode. Again, by combining these two equations,

$$(i_{T0}^{c_2} - i_{Tm}^{c_2})A_c^a = I \tag{5-13}$$

We have

$$(-i^0 + i^m)A_c^a - \frac{(q^0 + 2q^1 + \cdots + 2q^{m-1} + q^m)}{2} A_s^a = I \tag{5-14}$$

Summarizing the $n+1$ equations for pipeline in matrix form, and defining K_p, F_p,

V_p, q_p and i_p^{end} as

$$\mathbf{K_p} = \begin{bmatrix} 1 & -1 & 0 & \cdots & & \cdots & & \cdots & & \cdots & 0 \\ 0 & 1 & -1 & 0 & \cdots & & \cdots & & \cdots & & 0 \\ \cdots & & \cdots & & \cdots & & \cdots & & \cdots & & \cdots \\ 0 & \cdots & & 0 & 1 & -1 & 0 & \cdots & & \cdots & 0 \\ 0 & \cdots & & \cdots & 0 & 1 & -1 & 0 & \cdots & & 0 \\ \cdots & & \cdots & & \cdots & \cdots & & \cdots & & \cdots & \\ 0 & \cdots & & \cdots & & \cdots & & \cdots & 0 & 1 & -1 \\ 0 & \cdots & & 0 & 1 & 0 & \cdots & & \cdots & & 0 \end{bmatrix}$$

$$\mathbf{T_p} = 2R \begin{bmatrix} 1 & 0 \\ 1 & 0 \\ \cdots & \\ 1 & 0 \\ 0 & 1 \\ 0 & 1 \\ \cdots & \\ 0 & 1 \\ 0 & 0 \end{bmatrix}$$

$$\mathbf{F_p} = -\left(\frac{A_s^p}{A_c^p}\cdot\frac{R}{2}\right)\begin{bmatrix} 1 & 1 & 0 & \cdots & & \cdots & & \cdots & & \cdots & 0 \\ 1 & 2 & 1 & 0 & \cdots & & \cdots & & \cdots & & 0 \\ \cdots & & \cdots & & \cdots & & \cdots & & \cdots & \cdots & \\ 1 & 2 & \cdots & & 2 & 1 & 0 & \cdots & & \cdots & 0 \\ 0 & \cdots & & \cdots & 0 & -1 & -2 & \cdots & & -2 & -1 \\ \cdots & & \cdots & & \cdots & & \cdots & & \cdots & & \cdots \\ 0 & \cdots & & \cdots & & \cdots & & \cdots & 0 & -1 & -1 \\ 0 & \cdots & & \cdots & & \cdots & & \cdots & & \cdots & 0 \end{bmatrix}$$

$$\mathbf{V_p} = \begin{bmatrix} V_0 \\ V_1 \\ \vdots \\ V_{c_1} \\ V_{c_1+1} \\ \vdots \\ V_{n-1} \\ V_n \end{bmatrix}, \mathbf{q_p} = \begin{bmatrix} q^0 \\ q^1 \\ \vdots \\ q^{c_1} \\ q^{c_1+1} \\ \vdots \\ q^n \end{bmatrix}, \mathbf{i_p^{ends}} = \begin{bmatrix} i^0 \\ i^n \end{bmatrix}$$

We get

$$\mathbf{K_p V_p} = \mathbf{T_p i_p^{ends}} + \mathbf{F_p q_p} \tag{5-15}$$

Likewise, define K_a, F_a, V_a, q_a and i_a^{end} as

$$\mathbf{K_a} = \begin{bmatrix} 1 & -1 & 0 & \cdots & & \cdots & & \cdots & & \cdots & 0 \\ 0 & 1 & -1 & 0 & \cdots & & \cdots & & \cdots & & 0 \\ \cdots & & \cdots & & \cdots & & \cdots & & \cdots & & \cdots \\ 0 & \cdots & & 0 & 1 & -1 & 0 & \cdots & & \cdots & 0 \\ 0 & \cdots & & \cdots & 0 & 1 & -1 & 0 & \cdots & & 0 \\ \cdots & & \cdots & & \cdots & \cdots & & \cdots & & \cdots & \\ 0 & \cdots & & \cdots & & \cdots & & \cdots & 0 & 1 & -1 \\ 0 & \cdots & & 0 & 1 & 0 & \cdots & & \cdots & & 0 \end{bmatrix}$$

$$\mathbf{T_a} = 2R \begin{bmatrix} 1 & 0 \\ 1 & 0 \\ \cdots & \\ 1 & 0 \\ 0 & 1 \\ 0 & 1 \\ \cdots & \\ 0 & 1 \\ -\frac{A_c}{2R} R_{wire} & -\frac{A_c}{2R} R_{wire} \end{bmatrix}$$

$$\mathbf{F_a} = -\left(\frac{A_s^a}{A_c^a}\cdot\frac{R}{2}\right)\begin{bmatrix} 1 & 1 & 0 & \cdots & & \cdots & & \cdots & & \cdots & 0 \\ 1 & 2 & 1 & 0 & \cdots & & \cdots & & \cdots & & 0 \\ \cdots & & \cdots & & \cdots & & \cdots & & \cdots & \cdots & \\ 1 & 2 & \cdots & & 2 & 1 & 0 & \cdots & & \cdots & 0 \\ 0 & \cdots & & \cdots & 0 & -1 & -2 & \cdots & & -2 & -1 \\ \cdots & & \cdots & & \cdots & & \cdots & & \cdots & & \cdots \\ 0 & \cdots & & \cdots & & \cdots & & \cdots & 0 & -1 & -1 \\ -\frac{A_s}{R}R_{wire} & \cdots & & \cdots & & \cdots & & \cdots & & \cdots & -\frac{A_s}{R}R_{wire} \end{bmatrix}$$

$$\mathbf{V_a} = \begin{bmatrix} V_0 \\ V_1 \\ \vdots \\ V_{c_2} \\ V_{c_2+1} \\ \vdots \\ V_{m-1} \\ V_m \end{bmatrix}, \mathbf{q_a} = \begin{bmatrix} q^0 \\ q^1 \\ \vdots \\ q^{c_2} \\ q^{c_2+1} \\ \vdots \\ q^m \end{bmatrix}, \mathbf{i_a^{ends}} = \begin{bmatrix} i^0 \\ i^m \end{bmatrix}$$

The $m+1$ equations of the anode in matrix form are,

$$\mathbf{K_a V_a} = \mathbf{T_a i_a^{ends}} + \mathbf{F_a q_a} \tag{5-16}$$

Introducing the equations (5-15), (5-16) into equation (4-61) in the previous chap-

ter, we obtain

$$\begin{bmatrix} K_p & 0 & 0 & 0 & 0 \\ 0 & K_a & 0 & 0 & 0 \\ 0 & 0 & H_{pp} & H_{pa} & -1 \\ 0 & 0 & H_{ap} & H_{aa} & -1 \\ 0 & 0 & 0 & 0 & 0 \end{bmatrix} \begin{Bmatrix} V_p \\ V_a \\ \phi_p \\ \phi_a \\ \phi_\infty \end{Bmatrix} = \begin{bmatrix} F_p & T_p & 0 & 0 \\ 0 & 0 & F_a & T_a \\ G_{pp} & 0 & G_{pa} & 0 \\ G_{ap} & 0 & G_{aa} & 0 \\ A_p & & A_a & \end{bmatrix} \begin{Bmatrix} (-n \cdot \nabla\phi)_p \\ i_p^0 \\ i_p^n \\ (-n \cdot \nabla\phi)_a \\ i_a^0 \\ i_a^m \end{Bmatrix} \tag{5-17}$$

The *forward* model, equation (5-17), can be used to calculate both the potential on the soil surface, and pipe steel potentials. Furthermore, pipe steel potentials allows calculation of the current flowing in the pipe, which can be compared with the field measurements.

5.1.3 Simulation Results

In order to show the simulation results with variant pipe steel potentials, a test case of CP system was studied. A 500 m long pipe is assumed to be buried 1.45 m (4.75 feet) below the soil surface. Its diameter is 0.457 m (1.5 feet). A anode is placed 50 m away from the center of the pipe. The diameter of the anode is 0.152 m and its length is 1.22 m (4 feet). The soil resistivity is 100 Ωm. The boundary conditions are shown in Figure 4-1. A 0.5 mm-thick coating is assumed to cover the side area of the pipe, with the exception at the two end, which are assumed to be insulated. A wire connected the pipeline to the anode at 50 m position and 0.5 m position, respectively. The potential of the pipe steel varies along the pipe. A coating defect is set on the middle of the length of pipeline.

The simulation results of anode and pipeline are shown in Figure 5-5 and Figure 5-6 respectively.

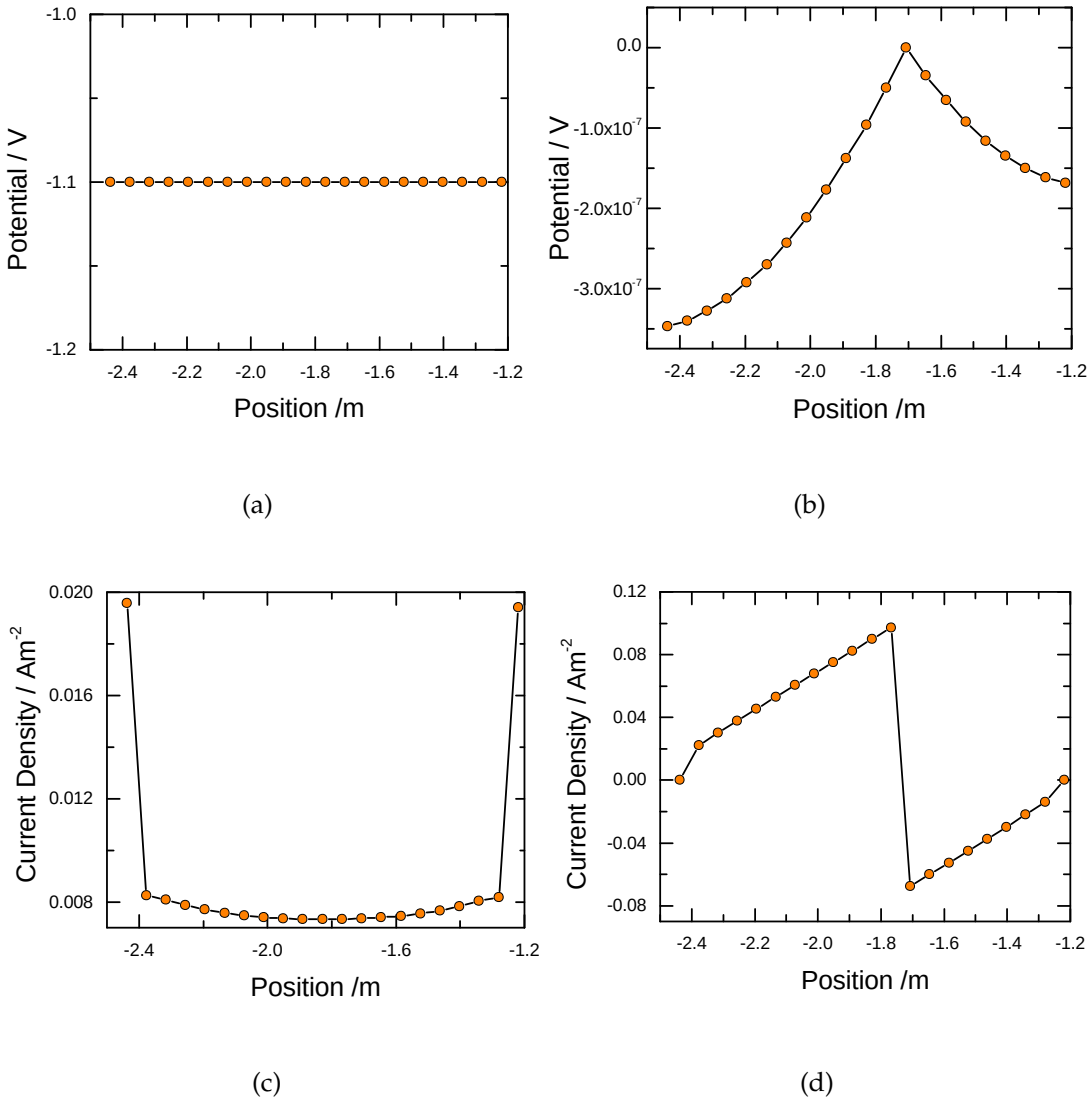

Figure 5-5: Potential and current density along the anode: a) potential Ψ along the anode (given value); b) potential V along the anode; c) radical direction of current density along the anode; d) axial direction of current density along the anode.

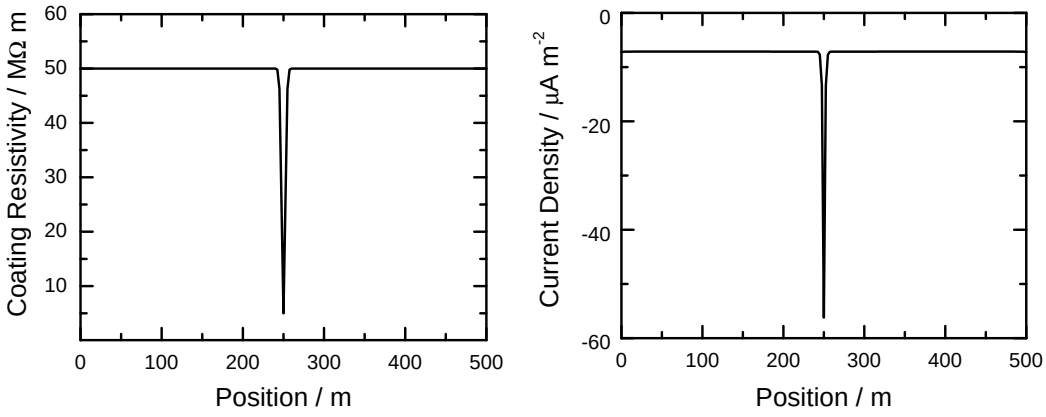
Coating Resistivity / MΩ m
60
50
40
30
20
10
0
100
200
300
400
500
Position / m
Current Density / μA m-2
0
-20
-40
-60
0
100
200
300
400
500
Position / m

(a) (b)

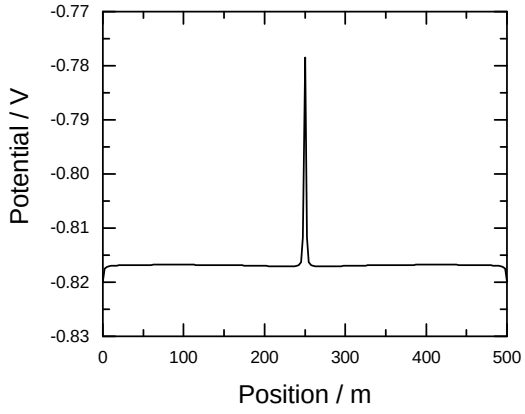
Potential / V
-0.77
-0.78
-0.79
-0.80
-0.81
-0.82
-0.83
0
100
200
300
400
500
Position / m

(c)

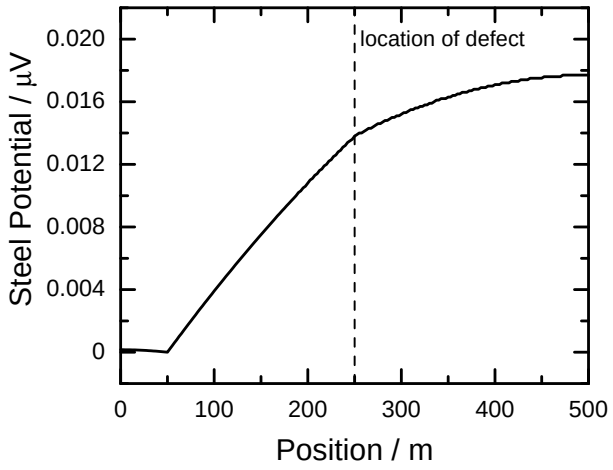

(d)

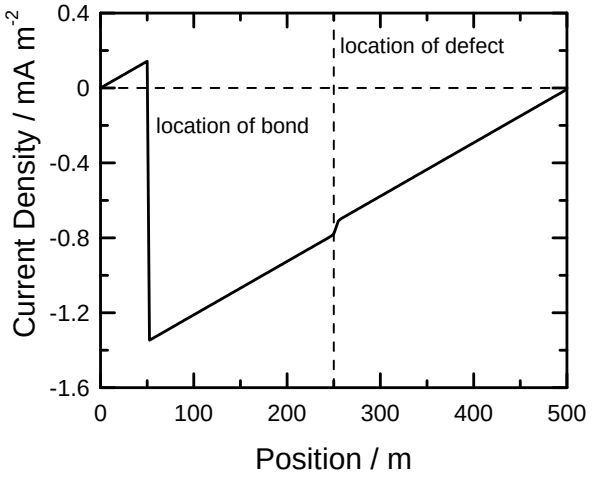

(e)

Figure 5-6: Simulated axial distributions along the pipeline: a) input value for coating resistivity; b) radial component of current density; c) calculated value for potential ψ; d) calculated value for steel potential V; and e) axial component of current density in the pipe.

5.1.4 Analysis of the Simulation Results

Figure 5.5(a) shows that $\psi_a = -1.1$V, because the anode is a sacrificial anode and its potential is a given boundary condition. Figure 5.5(b) indicates the potentials along the anode steel are variant. At the position where the potential equals zero, a wire connects the anode to the pipeline. In order to protect the pipeline, the current of the anode flows away from the anode, and flows back to the anode through the wire. Therefore, the farther the position is from the wire connected position, the lower the anode steel potential than that of the potential at the wire connection point. Figure 5.5(c) exhibits the radial direction of current density. Figure 5.5(d) shows that the axial direction of current density is equal to zero at the two ends of the anode. This is a given boundary condition. The current densities at the two sides of the wire connection point have different signs, which means that the current flows away from the wire connecting position to two opposite directions.

The coating resistivity of the pipeline is shown in Figure 5.6(a) where the nominal resistivity of defect-free coating is seen to be $5.0 \times 10^7 \Omega$m. The resistivity was assumed to decrease abruptly at a position of 250 m, corresponding to the position of a significant coating defect. The cathodic radial current density increased dramatically at the position of the coating defect, as shown in Figure 5.6(b). Figure 5.6(c) shows that the potential is less negative at the coating defect position than other places. It means that pipe is less protected at the coating defect.

The variation of potential within the pipe steel is presented in Figure 5.6(d). Since the length of the 500 m pipe was not large, the potential drop over the pipe was very small, on the order of $10^{-3} \sim 10^{-2}$ μV. The calculation of steel potential was primarily useful for allowing calculation of the current flow in the pipe. The steel potential was set to a value of zero at the 50 m position where the anode and

pipe were connected. This represents the minimum value for steel potential. The current coming from soil enters the pipeline and flows along the pipe from two opposite directions to the wire connecting point on the pipe. Hence, the potentials on either side of the connection position have higher values. A sharp change in the slope of the potential is seen at the position of the coating defect.

The axial direction current distribution shown in Figure 5.6(e) reveals that the current density at the two ends of pipe was set to zero values. The current density changed sign at the bond location where the wire was connected to the pipe. A significant step increase in current is observed at the coating defect due to the contribution of the enhanced axial direction current density.

5.1.5 Validation with *CP3D*

The *forward* model used in the present work is a simplification as compared with CP3D. There are some common features between the two models, such as

- The same governing equation, *i.e.*, Laplace's equation, was applied to the three-dimensional cathodic protection pipeline system.
- The system geometry and position can be the same.

However, there are also some major differences between the two models:

- Coating conditions for the pipe were different. *CP3D* allowed modeling a coating, that exposes bare steel; whereas, using the present model, defective coating was modeled as a section of low coating resistivity.
- The boundary conditions for the pipe were different as the consequence of the different coating conditions. *CP3D* applied a nonlinear polarization curve, whereas the present work used linear boundary conditions.

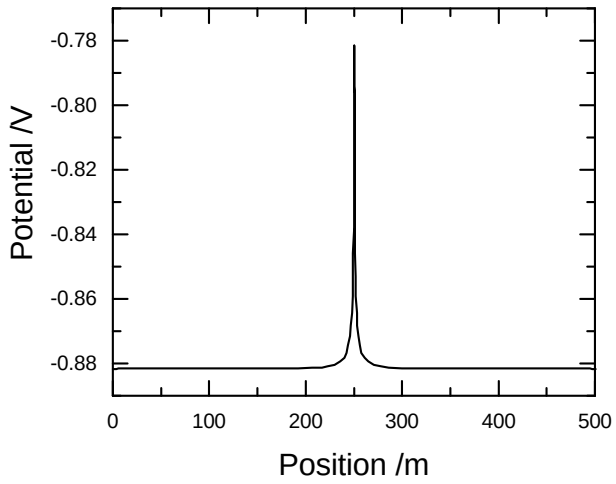

Figure 5-7: Potential of pipe calculated by using *CP3D* .

- More elements of higher order were used in *CP3D* . The present model applied linear cylindrical element to reduce the number of segments and computational task.

- *CP3D* combined the BEM and FEM to solve the system. The current work applied only the BEM to simplify the calculation.

To compare the results obtain from these two models, the same conditions, such as soil resistivity, the dimensions of the pipe and anode system, the applied potential and the defect-free coating resistivity, as those used in the example of section 5.1.3, were applied to the *CP3D* .

The results are shown in Figures 5-7, which could be compared with the Figure 5.6(c). At the position of the defect, 250 m, the potential has a peak value. The peak value in the two figures are both around -0.78V. At the other position on the pipe, the curve tends to be horizontal. The value for the former figure is about -0.88V, which for the latter one is about -0.82V. In addition, in Figure 5.6(c), the potentials at the two ends of the pipe dropped a little. This phenomena is less pronounced in Figure 5-7. Figure 5-8 and Figure 5.6(d) has similar tendency, that is, at the 50 m position, where the wire connects the pipe and the anode, the potential of the pipe

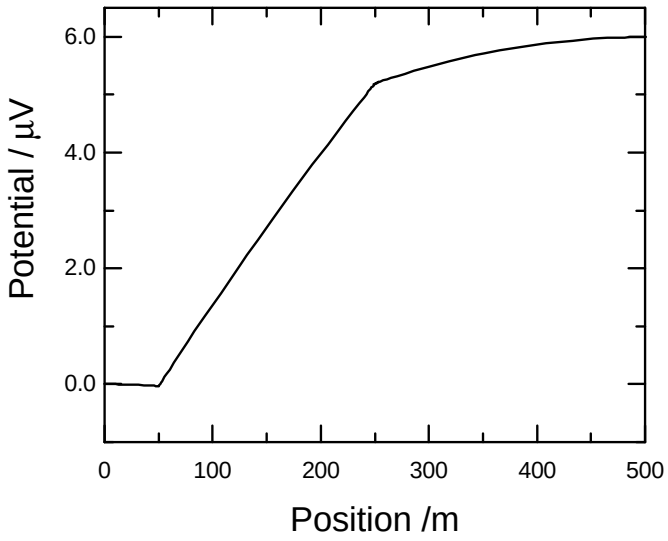

Figure 5-8: Potential of pipe steel calculated by using *CP3D* .

steel is zero. Moreover, at the 250 m position, which is the position of the coating defect, the potential of the pipe steel has a slope change. The difference of these two figures is that the potential value is around 6.0×10^{-6}V vs. CSE reference electrode for the former, and it is around 1.6×10^{-8}V for the latter.

CP3D does not provide the current density of the pipe at the axial direction, but it can be calculated from the data of the potential of the pipe steel and the pipe resistivity. Figure 5-9 was obtained using this method. The current along the pipe (see Figure 5-9 and Figure 5.6(e)) shows qualitatively the same behavior, which gives support to the idea that the simplified model may be sufficient to identify regions of defective coating.

The comparison between Figure 5-10 and Figure 5.5(c) shows that both the curve shape and the order of value are approximately the same. However, the figure from *CP3D* has smoother curve than that from current work at the two ends of the anode. The reason is that *CP3D* used two half spheres as the end and the profile of the anode is continuous. On the contrast, the circles are applied as the two ends in present study. It clearly shows that, from all the comparisons

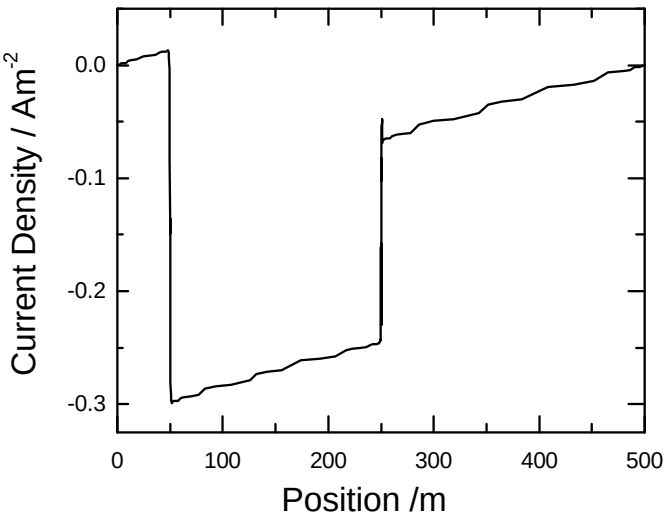

Figure 5-9: Axial direction current density of pipe calculated by using *CP3D* .

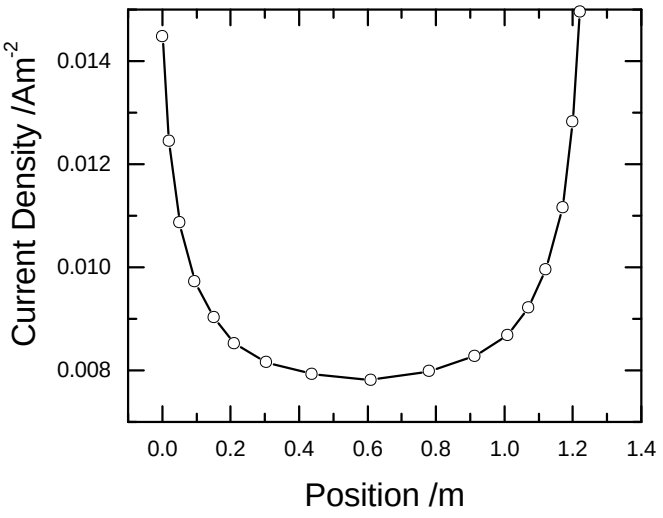

Figure 5-10: Radial direction current density of anode calculated by using *CP3D* .

above, the two models can describe the similar tendency. But the different coating conditions and correspondingly different boundary conditions may result in the value differences. In addition, the total current flows to the pipe in *CP3D* model is about 0.056618Amps, while it is about 0.05489Amps in present model due to the difference of coating defect. The defect set in *CP3D* is a section of bare pipe steel. It needed more current to protect the pipeline than a section of low resistivity coating. Moreover, the present model does not account the deposition of scales on the pipe steel, which may reduce the current necessary for cathodic protection.

5.2 Inverse Model

5.2.1 Introduction

All the *inverse* models developed to date rely on a single type of data, *i.e.,* potential readings from soil surface surveys or from individual sensor electrodes. As indicated by Wrobel and Miltiadou,[45] for successful identification of coating defects, potential readings should be in close proximity to the coating defects. Even one meter of top cover may be sufficient to obscure the effects of localized underprotected regions.[35,38] Thus, in some cases, a serious coating defect may lead to insignificant changes in potential at the soil surface. The low sensitivity of potential measurements to coating failures can be mitigated by including other types of data, for example, current densities in the pipeline metal. A schematic representation of the incorporation of potential survey and current data is given as Figure 5-11.

Masilela and Pereira describe the use of soil surface potential gradient surveys to assess the condition of pipeline coatings.[85] Fischer *et al.* discuss the difficulties of obtaining IR-free measurements of soil potential.[86] Gummow and Eng describe use of four-electrode methods to measure currents in pipelines.[87] Aerial surveys with magnetometers can be used to assess the flow of current in pipelines.

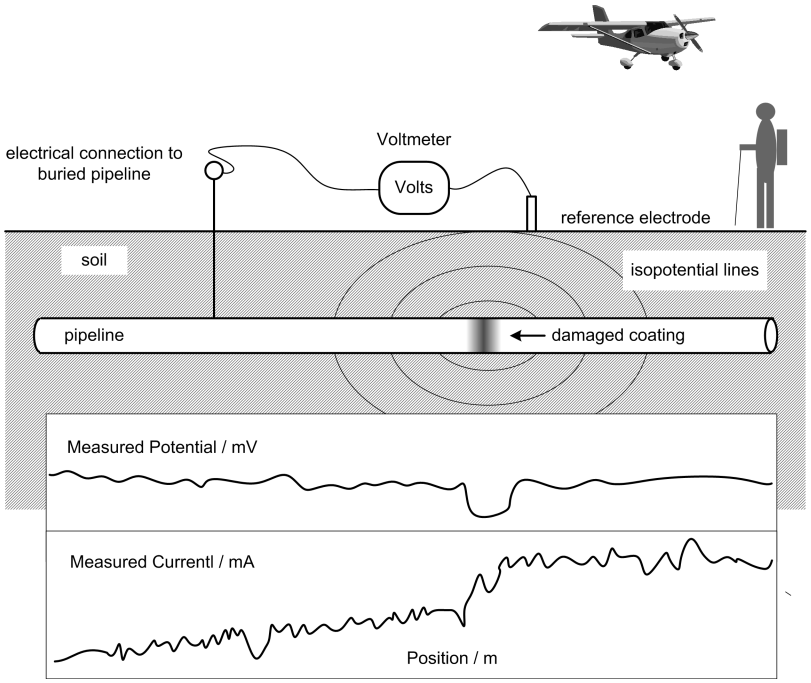

Figure 5-11: Schematic illustration of the coupling of a soil-surface-level potential survey method to an aerial magnetometer current survey to assess the condition of a buried pipeline.

Conversely, the presence of pipelines under cathodic protection confounds interpretation of high-resolution aeromagnetic data.[88] Campbell and Zimmerman describe the use of remote sensing of current in the Trans-Alaska Pipeline.[89] Murphy *et al.* coupled impedance spectroscopy with use of SQUID magnetometer for remote sensing of current to assess localized corrosion rates on buried metallic structures.[90]

To create the *inverse* model, the BEM code described in the previous section was used as part of the objective function in a nonlinear regression algorithm. The simulated annealing optimization approach was selected for the present work according to chapter 4.

The *inverse* model acts to minimize the value of an objective function which represents the difference between measured and calculated values. The parameter set which results in the smallest value of the objective function can be assumed to reflect the condition of the coated pipe. The *inverse* results are strongly dependent

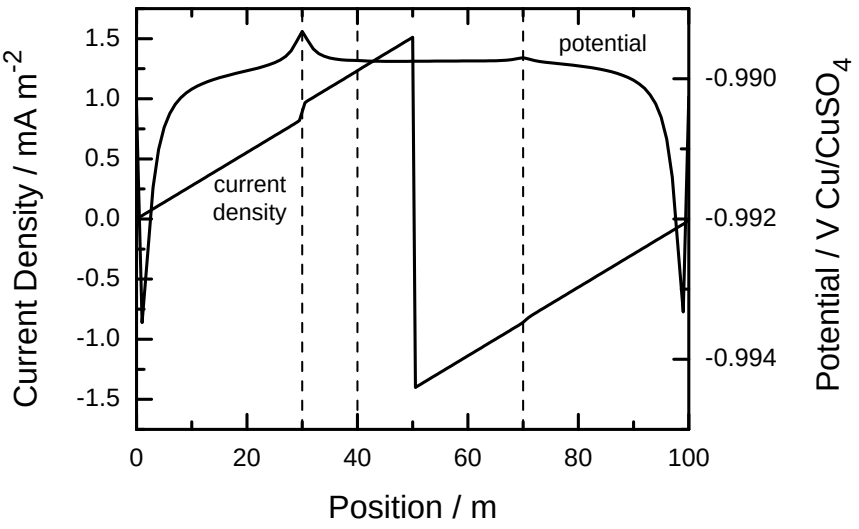

Figure 5-12: Synthetic pipe current and surface potential data corresponding to Table 5.1. Dashed lines indicate the location of coating defects.

on the form of the objective function chosen.

5.2.2 Regression to Noise-Free Data

Preliminary regression results were obtained using synthetic data generated with machine precision. The physical situation consisted of a single pipe connected to a single anode, as presented schematically in Figure 4-1. The pipeline was 100 m long. Three coating defects were assumed to exist on the pipe coating with parameters presented in Table 5.1. The *forward* model was used to obtain synthetic surface potential and current density data which were then used as the field data for the *inverse* model. The synthetic data are shown in Figure 5-12. Dashed lines indicate the location of coating defects. The presence of defects at 30 and 70 m positions can be inferred from subtle changes in the current and surface potential distributions shown in Figure 5-12; however, it is difficult to discern the defect located at 40 m.

The potential data set comprised 303 values corresponding to three lines of 101 points each located directly above the pipe segment and one meter to either side. There were 99 current density data points. Regression was performed to homoge-

neous data sets which comprised either the current or potential data. Regression was also performed to heterogeneous data sets which included both current and potential data.

Regression to Homogeneous Data Sets

An objective function, which describes the difference between the measured potential and the calculated potential on the soil surface, or difference between the measured current density along the pipe and the calculated current density data, is given as

$$g(x,\rho,\sigma) = \sum_{k=1}^{N_c} \left(i_k - \widehat{i}_k\right)^2 \tag{5-18}$$

for current survey data and

$$g(x,\rho,\sigma) = \sum_{j=1}^{N_p} \left(\psi_j - \widehat{\psi}_j\right)^2 \tag{5-19}$$

for potential survey data. The objective function value g is a function of the coating defect parameter vectors x, ρ and σ, shown in equation (4-12). In equations (5-18) and (5-19), i_k and ψ_j represent the measured current density along the pipeline and soil surface potentials, and $\widehat{i}_k$ and $\widehat{\psi}_j$ represent the corresponding values obtained by the mathematical model. The number of current density data points is given by N_c, and the number of potential data points is given by N_p. Both types of data are influenced by the pipe coating condition; therefore the minimum of the objective function is obtained when the coating parameter space reflects the condition of the pipeline coating.

An exploration of the regression strategy is presented in Table 5.1 regression using either equation (5-19) or (5-18) for homogeneous synthetic data without added noise. The influence of initial guesses for the nonlinear regression was minimized by assigning initial values of $x_k = 50$ m, $\rho_k = -3.5 \times 10^7$ Ωm, and $\sigma_k = 0.92$ m for each defect.

Table 5.1: Regression results using either equation (5-19) or (5-18) for homogeneous synthetic data without added noise or equation (5-20) for heterogeneous synthetic data without added noise. The initial values for each defect was $x_k = 50$ m, $\rho_k = -3.5 \times 10^7$ Ωm, and $\sigma_k = 0.92$ m.

Data Type	Equation	Coating Defect	Position x_k / m	Resistivity ρ_k / Ω m	Dimension σ_k / m	χ^2/ν
Set Defect Values						
		1	30	-4.5×10^7	0.316	
		2	40	-3.0×10^6	0.548	
		3	70	-2.0×10^7	0.447	
Regression Result						
Current	(5-18)	1	29.91	-4.94×10^7	0.217	6.7×10^{-11}
		2	70.00	-1.95×10^7	0.460	
Potential	(5-19)	1	30.02	-3.90×10^7	0.999	9.7×10^{-8}
Potential	(5-19)	1	30.03	-2.62×10^7	2.37	1.2×10^{-7}
		2	70.06	-3.04×10^7	1.07	
Potential	(5-19)	1	29.95	-1.60×10^7	2.10	8.0×10^{-8}
		2	30.01	-2.66×10^7	0.31	
		3	43.03	-0.17×10^7	2.32	
Both	(5-20)	1	30.03	-3.12×10^7	1.54	3.7×10^{-8}
		2	70.00	-2.99×10^7	0.012	
Both	(5-21)	1	29.98	-4.51×10^7	0.30	3.0×10^{-4}
		2	38.96	-0.14×10^7	1.41	
		3	69.75	-0.50×10^7	2.46	

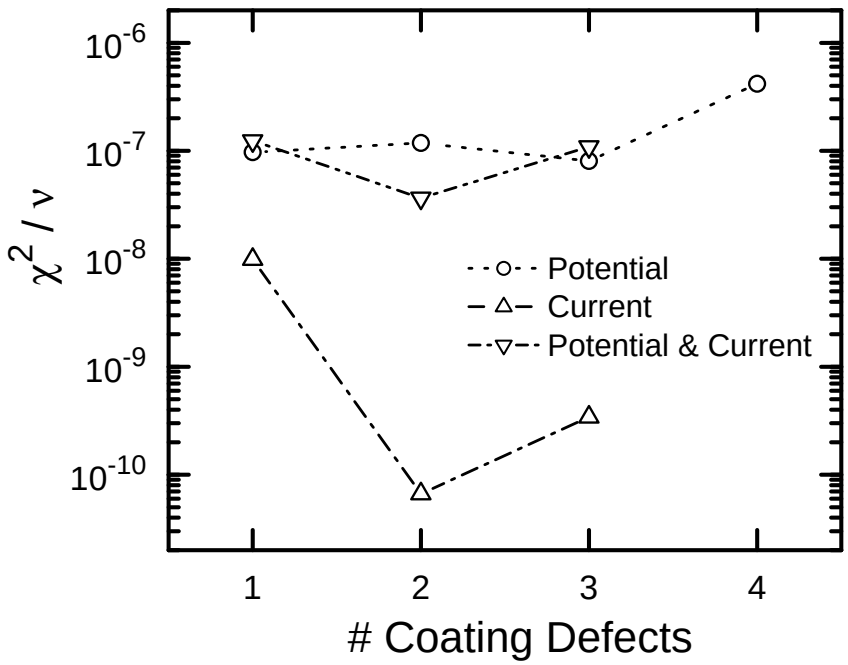

Figure 5-13: The χ^2/ν statistic corresponding to Table 5.1 as a function of the number of coating defects assumed in the regression.

The χ^2/ν statistic is presented in Figure 5-13 as a function of the number of coating defects assumed in the regression. The method proposed by Qiu and Orazem[91] for determination of the maximum number of defects revealed a clear minimum at 2 coating defects when regression was made to current data alone. One defect was located at the 30 m position and the other was at the 70 m position. Since the resistivity reduction of the set defect at the 40 m position was relatively small, it was difficult to find this defect by regression.

The method for selecting the statistically significant coating defects yielded more equivocal results when regression was made to surface potential data only. No clear minimum could be found. When regression was made to a model with one coating defect, the defect found was that at the 30 m position. A small improvement in the χ^2/ν statistic was found by regressing to two coating defects. The second coating discovered was located at the 43 m position, which was close to the defect set at the 40 m position. The smallest value of the χ^2/ν statistic was

found for three coating defects, but the results, showing two defects located at the same position, were not statistically significant. Use of the Akaike information criteria[82,83,84] did not yield a clearer definition of the maximum number of resolvable parameters. The difficulty of obtaining the statistically significant number coating defects for regression to potential data indicates that work is needed to establish refined methods for evaluating the regression results.

Better *inverse* results were obtained by using current density data, even though there were fewer current data than potential data.

Unweighted Regression to Heterogeneous Data Sets

In order to take advantages of the information from both the potential and the current density data, an objective function was obtained as the summation of the least square differences of the two sets of data, *i.e.*,

$$g(x,\rho,\sigma) \quad = \quad \sum_{j=1}^{N_p}(\psi_j - \widehat{\psi}_j)^2 + \sum_{k=1}^{N_c}(i_k - \widehat{i}_k)^2 \tag{5-20}$$

The *inverse* results of applying potential and current density data to equation (5-20) are shown in Table 5.1. As shown in Figure 5-13, the χ^2/ν statistic indicated that two defects could be identified, and these were located near the 30 and 70 m positions. The results obtained using equation (5-20) are comparable to those obtained using the current data alone. Use of equation (5-20) for regression to heterogeneous data did not improve the resolution of pipe coating condition.

Weighted Regression to Heterogeneous Data Sets

The regression strategy used for equation (5-20) failed because the magnitude of the two types of data was vastly different. A weighting strategy was employed in which the regression was scaled by the magnitude of the data, *i.e.*,

$$g(x,\rho,\sigma) = \sum_{j=1}^{N_p}\frac{(\psi_j - \widehat{\psi}_j)^2}{\psi_j^2} + \sum_{k=1}^{N_c}\frac{(i_k - \widehat{i}_k)^2}{i_k^2} \tag{5-21}$$

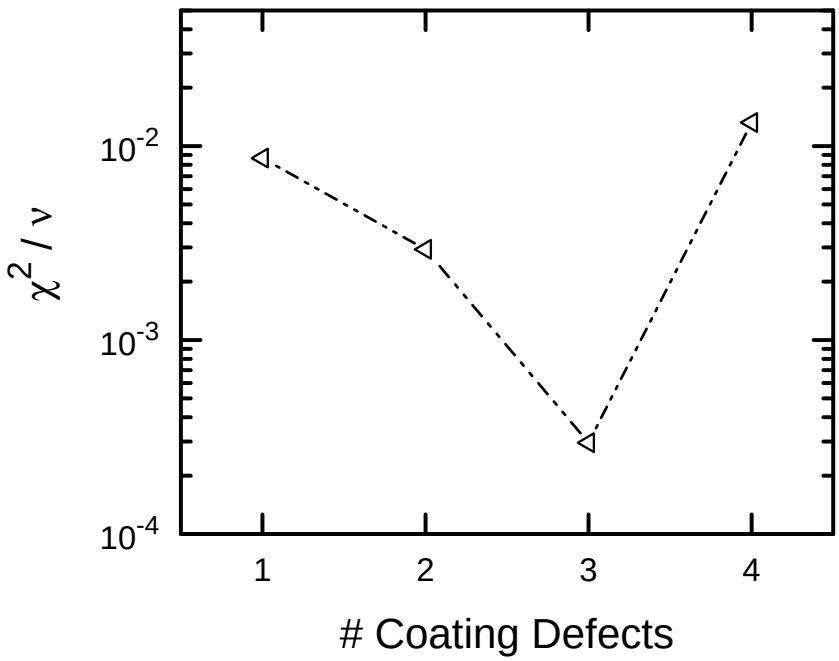

Figure 5-14: The χ^2/ν statistic corresponding to regression of equation (5-21) (see Table 5.1) as a function of the number of coating defects assumed in the regression.

Under the assumption that the weighting strategy should be based on the variance of the data,[92,93] use of equation (5-21) is consistent with the assumption of a proportional error structure.

The χ^2/ν statistic is presented in Figure 5-14 as a function of the number of coating defects assumed in the regression. Each of the three coating defects could be found. The defect 1 approximately has the same coating parameters as those of the defect at the 30 m position. The position of defect 2 is close to the defect at the 40 m position, and the relative error for the position is about 3 percent. The defect 3 refers to the defect at the 70 m position. For the defects 2 and 3, the coating resistivity reduction and the defect width differ from the set values due to the correlation among defect parameters evident in equation (4-12).

The importance of weighting for regression strategies is particularly evident for heterogeneous data sets. Proportional weighting is generally recommended for synthetic data for which the uncertainty is governed by the accuracy of the

calculation. For experimental data, a weighting strategy should be guided by the perceived or measured variance of the experimental data.

5.2.3 Regression to Noisy Data

For the purpose of testing the robustness of the *inverse* model, noise was added to the data set. Noise was added to the potential data according to

$$\psi = \psi + \sigma_\psi * \mathbf{P}(0,1) \tag{5-22}$$

where $\mathbf{P}(0,1)$ represents a normally distributed random number with mean value equal to zero and standard deviation equal to unity. The randomly generated number was scaled by a standard deviation, which was assigned a value $\sigma_\psi =$ 0.4 mV. The noise in the current signal was assumed to be proportional to the current such that

$$i = i * (1 + \alpha_i * \mathbf{P}(0,1)) \tag{5-23}$$

The value of α_i was 0.02; thus, the noise level for the current measurement represented 2 percent of the measured value. The comparison between the base value and the noise-added value for the potential data and the current density data is shown in Figures 5.15(a) and 5.15(b), respectively. While the objective function (5-21) was very well suited for regression to noise-free synthetic data, only the largest coating defect at the 30 m position could be found when it was used to regress to the synthetic data with added noise. The situation was not improved by replacing the proportional weighting shown in equation (5-21) with weighting based on the assumed error structure.

Weighted and Scaled Regression to Heterogeneous Data Sets

The reason for the poor results obtained by regression of equation (5-21) could be related to the large number of potential measurements which are relatively in-

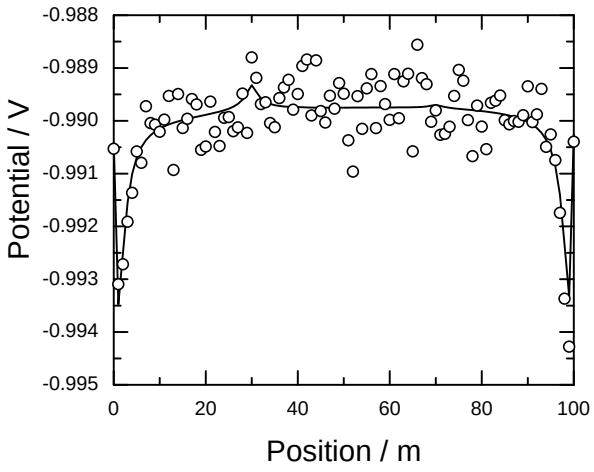

(a)

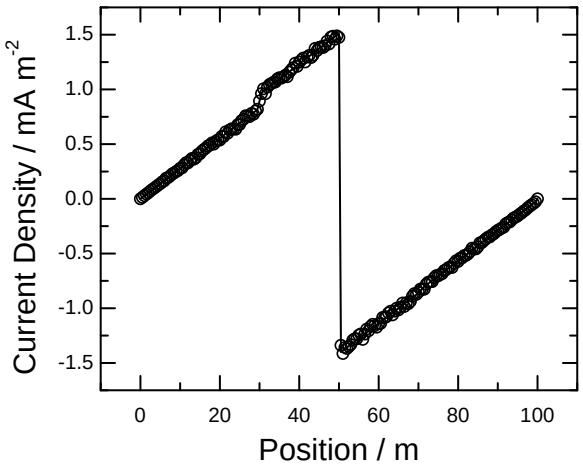

(b)

Figure 5-15: Synthetic data with added noise. The line represents the noise-free values and the symbols represent synthetic data with added noise. a) surface on-potential value with $\sigma_\psi = 0.4$ mV; b) axial current density value with proportional noise corresponding to 2 percent of the value.

Table 5.2: Regression results using equation (5-24) for heterogeneous synthetic data with added noise. The initial values for each defect was $x_k = 50$ m, $\rho_k = -3.5 \times 10^7$ Ωm, and $\sigma_k = 0.92$ m.

Data Type	Equation	Coating Defect	Position x_k / m	Resistivity ρ_k / Ω m	Dimension σ_k / m	χ^2/ν
Set Defect Values						
		1	30	-4.5×10^7	0.316	
		2	40	-3.0×10^6	0.548	
		3	70	-2.0×10^7	0.447	
Regression Result						
Both	(5-24)	1	30.1	-4.59×10^7	0.50	3.02
Both	(5-24)	1	30.1	-4.99×10^7	0.31	2.71
		2	69.4	-0.77×10^7	1.27	
Both	(5-24)	1	38.8	-2.05×10^7	0.88	10.8
		2	46.4	-0.66×10^7	2.07	
		3	46.8	-2.13×10^7	1.50	

sensitive to coating condition. A re-scaled objective function was proposed as

$$g(x,\rho,\sigma) = \frac{1}{N_p}\sum_{j=1}^{N_p}\frac{(\psi_j - \widehat{\psi}_j)^2}{\sigma_\psi^2} + \frac{1}{N_c}\sum_{k=1}^{N_c}\frac{(i_k - \widehat{i}_k)^2}{(\sigma_i)^2} \tag{5-24}$$

where σ_ψ^2 and $(\sigma_i)^2 = (\alpha_i i_k)^2$ provide a weighting based on the error structure of the data. Equation (5-24) provides an objection function in which the contributions of potential and current data are scaled such that they provide equal weight to the regression.

The regression results are shown in Table 5.2. The weighted χ^2/ν statistic reached a minimum value for two coating defects, indicating that two defects could be identified. The scaled objective function (5-24) has the advantages that, for each data type, the weighting strategy is based on the error structure of that data and that it decreases the influence of superfluous input information.

Generalization of the Objective Function

The proper scaling of the objective function will be determined by the relative sensitivity of a particular type of data to the coating condition. A form of equation

(5-24) that is readily generalizable to multiple types of data can be expressed as

$$g(x, \rho, \sigma) = \sum_{k=1}^{M} \lambda_k g_k \tag{5-25}$$

where g_k is the objective function for a given type of field data scaled by the number of data, *i.e.*,

$$g_k(x, \rho, \sigma) = \frac{1}{N_k} \sum_{j=1}^{N_k} \frac{(x_{k,j} - \widehat{x}_{k,j})^2}{(\sigma_{k,j})^2} \tag{5-26}$$

and λ_k is a scaling factor that accounts for the relative sensitivity of the data type to coating condition. According to the error structure of the data, $\sigma_{k,j}^2$ can be a value or equal to $(\alpha_k x_{k,j})^2$. To facilitate interpretation of the χ^2/ν statistic, it is appropriate to constrain λ_k such that

$$\sum_{k=1}^{M} \lambda_k = 1 \tag{5-27}$$

In equation (5-26), $x_{k,j}$ and $\widehat{x}_{k,j}$ represent the measured and calculated values respectively for data type k, and $\sigma_{k,j}$ represents the corresponding standard deviation for the measured values. The data sets may comprise, among others, surface on-potential, surface off-potential, current density data, or readings from buried reference electrodes or coupons.

5.3 Conclusions

In this chapter, the potential of the pipe steel was assumed to vary along the pipe. The current density of the pipe in axial direction was calculated in the *forward* model without using the finite element method (FEM), which simplified the calculation process.

In addition, as the current density data were available from the *forward* model, there were two kinds of data sets, potential data and current density data, that could be used as measured data for the *inverse* model.

A strategy was developed that can be used to identify the maximum number of coating defects that can be detected. This number is sensitive to the quality of data as well as to the actual coating condition.

If the number of coating defects detected is smaller than the actual number of coating defects, the technique will identify the most serious ones.

During the procedure to build the four objective functions, adding different weight for each data point and including the number of the data points have been proved effective to form the objective function.

The present work proves the feasibility of coupling a boundary element *forward* model with a nonlinear regression algorithm to obtain pipe surface properties from pipeline survey data.

CHAPTER 6
APPLICATION OF OFF-POTENTIAL DATA TO THE INVERSE MODEL

In Chapter 4, the potential calculated in the *forward* model is the on-potential, or the potential measured when the anode is connected to the pipeline. In this chapter, the *forward* model is extended to calculate the potential on the soil surface immediately after the anode is disconnected with the pipeline. This kind of potential is called off-potential.

Three kinds of data sets, *i.e.*, on-potential, off-potential and current density data could be obtained from the *forward* model. They were then applied to the *inverse* model to prove the validity of the general form of the objective function built in Chapter 5.

6.1 Forward Model-Calculation of the Soil Surface Off-Potential

6.1.1 Physical Process

When the anode is disconnected with the pipe, no current will flow to the pipe. Likewise no current will flow back to the anode through the wire. The potential measured on the soil surface at this moment is called the off-potential. The technique is established on the principle that the IR component in the potential measurement decays almost instantaneously, while the pipe-to-soil interface polarization decays relatively slowly. Thus the correct pipe-to-soil potential free of the IR drop can be measured. There is no general standard to identify the time required to measure the potential after switch off the protection current. The time can range from 100 microseconds to seconds, or even days.[13]

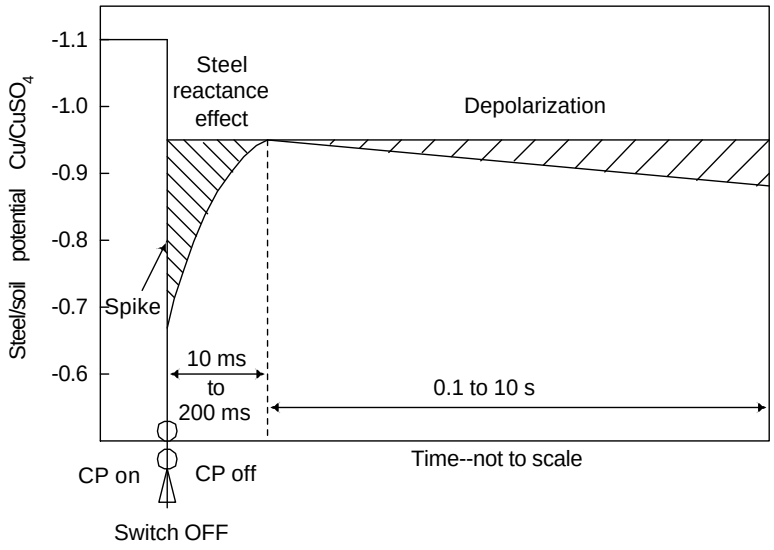

Figure 6-1: Switch off CP power source to determine instant off-potential.

6.1.2 Assumptions

According to Cox's study,[94] a sharp peak is observed in the pipe-to-soil potential as the potential is interrupted (Figure 6-1).

The spike lasts about 10 microseconds to 200 microseconds, then depolarization will take place. In present study, after the current is shut off, the condition right after the development of the spike and just before the depolarization occurrence is studied. At that moment, the potential in the soil ϕ will not change since the depolarization has not yet begun. However, the potential of the pipe steel V will be redistributed to keep the potential uniform along the pipe, which makes current flow along the pipe from region of high potential to region of low potential. The result is that the potential of the pipe steel becomes zero along the pipeline. Since the potential of the voltmeter reading ψ depends on the potentials ϕ and V as $\psi = V - \phi$, ψ will be changed after the sacrificial current is switched off.

6.1.3 Model Implementation

The system satisfies the Laplace's equation. The pipeline is the only object of the system. Applying the same techniques mentioned in Chapter 4, such as the

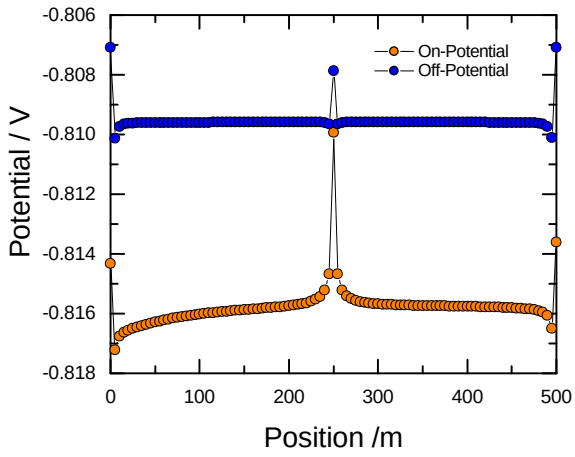

Figure 6-2: On-potential and off-potential on soil surface.

BEM for half-infinity domain, and the self-equilibrium limitation, we can obtain

$$\begin{bmatrix} -G_{pp} & -1 \\ -A_p & 0 \end{bmatrix} \begin{Bmatrix} n \cdot \nabla \phi_p \\ \phi_\infty \end{Bmatrix} = \begin{bmatrix} -H_{pp} \\ 0 \end{bmatrix} \{ \phi_p \} \tag{6-1}$$

The last equation in the above matrix form means that the current flowing away from pipe, for example, at the coating defect position, will not be lost in the soil domain. The current will flow back to the pipe. Therefore, no current will be gained or lost at the infinity boundary. Because ϕ will remain the same as that when the anode is connected to the pipe, it is a known boundary condition in equation (6-1). The unknowns are the current density of the pipeline and the potential at infinity.

6.1.4 Simulation Results and Analysis

The test example with 500m long pipe shown in Chapter 5 is solved to get the off-potential on the soil surface. The comparison of the on-potential and off-potential is shown in Figure 6-2, which agrees well with the expected trend (Figure 6-3).[95] The on-potential is more negative than the off-potential. In addition, the on-potential on the soil surface shows observable differences right above the pipe and at certain distances away from the center line of the pipe (as Figure 4-10). However, the variation for the off-potential on the soil surface surrounding the

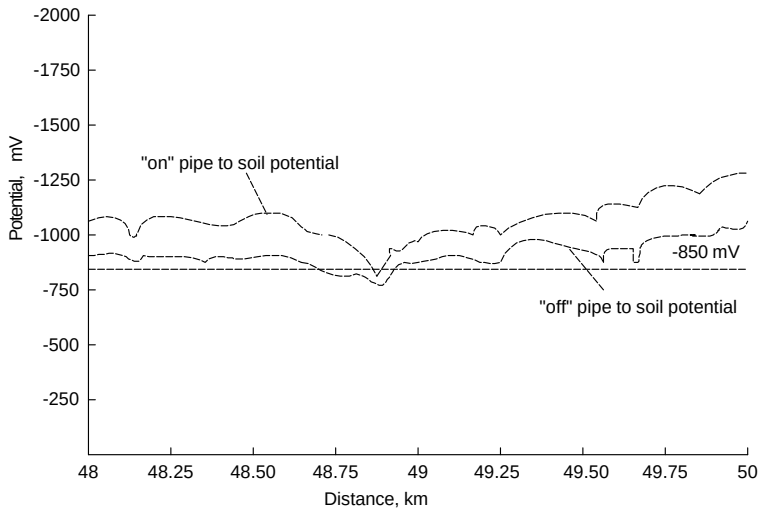

Figure 6-3: Typical close-interval potential graph.

pipe area is small. Therefore, the number of the off-potential data can be reduced.

6.2 Inverse Model-Using Three Kinds of Heterogeneous Data Sets

The heterogeneous data sets, such as the soil surface on-potential, off-potential and the current density in the axial direction along the pipe, was used in the *inverse* model to test the effectiveness of the general form of objective function, equations (5-25), (5-26) and (5-27). The testing process involved two different cases, *i.e.*, the data without added noise and data with added noise.

6.2.1 Data without Noise

Three sets of data without noise are applied to the general form of objective function. Since the data were independent of the noise, the $\sigma_{k,j} = x_{k,j}$. The regression results obtained by setting the initial guess as one, two and three defects with the same coating parameters are shown in Table 6.1. When there was only one defect, the most serious defect at 30 m position was found. Assuming two defects at the beginning, the two most serious defects were found. These are the defects at the 30 m and the 70 m positions. All the three parameters for holiday 1 were close to the set values. When three defects were assumed, the positions

Table 6.1: Regression results from the data without added noise obtained by using the general form of the objective function (5-25), (5-26) and (5-27). The initial values for each defect was $x_k = 50$ m, $\rho_k = -3.5 \times 10^7$ Ωm, and $\sigma_k = 0.92$ m.

Data Type	Coating Defect	Position x_k / m	Resistivity ρ_k / Ω m	Dimension σ_k / m	χ^2/ν
Set Defect Values					
	1	30	-4.5×10^7	0.316	
	2	40	-3.0×10^6	0.548	
	3	70	-2.0×10^7	0.447	
Regression Result					
Three	1	30.0	-4.53×10^7	0.09	4.35×10^{-5}
Three	1	30.0	-4.50×10^7	0.34	2.24×10^{-6}
	2	69.6	-4.04×10^7	3.14	
Three	1	30.0	-4.50×10^7	0.316	2.23×10^{-8}
	2	40.0	-1.06×10^6	1.70	
	3	70.0	-1.66×10^7	0.58	
Three	1	30.0	-2.18×10^7	0.24	5.97×10^{-7}
	2	30.0	-2.31×10^7	0.45	
	3	40.5	-3.63×10^5	3.02	
	4	69.9	-8.06×10^6	1.43	

of all the three preset coating defects could be found. The two parameters, *i.e.*, the resistivity reduction and the width, of defect 1 were approximately same as those of set values. However, those parameters for defect 2 and defect 3 were different from set values, indicating further that the existence of the coupling effect between the parameters as in equation (4-12). When four defects were assumed, both defect 1 and 2 referred to the defect at 30 m position. The defects at 40 m and 70 m positions could also be found. The strategy used in chapter 5 was applied to determined the appropriate number of defects. χ^2/ν as a function of the number of defects is shown in Figure 6-4. The appropriate number of defects is three in the current example. Comparing the last two rows of Table 5.1 and Table 6.1, it is found that the optimal number of detectable defects is two for the former case, while it is three for the latter case. It can also be concluded that adding more data sets, *e.g.*, adding the off-potential data as input information, yielded regression re-

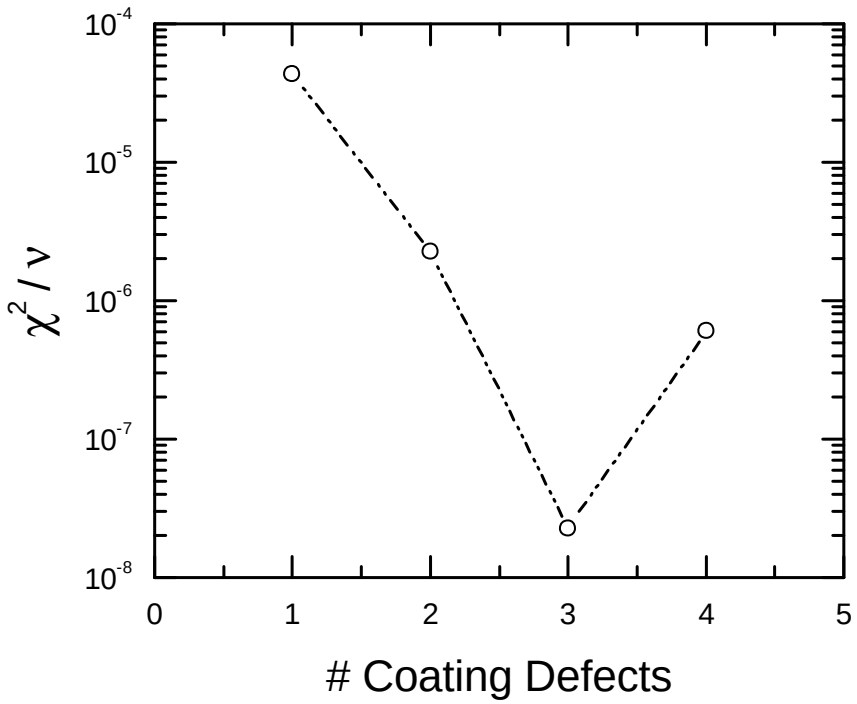

Figure 6-4: Decide the number of defects using noise free soil surface on and off-potential and current density data.

sults that were closer to the set values. The general form of the objective function is effective for data sets without added noise.

6.2.2 Data with Added Noise

The data sets with added noise were used to test the correctness of the equations (5-25), (5-26) and (5-27). The noise on-potential and current density data were the same as shown in Figures 5.15(a) and 5.15(b). The noise with $\sigma_\psi = 0.2$mV standard deviation was added to the off-potential on the soil surface, as shown in equation (5-22). The resulting soil surface off-potential were shown in Figure 6-5. The three sets of noisy data were used as the measured data. Thus, $\sigma_{\psi_{on}} = 0.4$mV is for the on-potential data set, $\sigma_{\psi_{off}} = 0.2$mV is for the off-potential data set and $\sigma_i = 2\% i_k$ is for the current density data set. All the initial guesses of the defect parameters were the same as the previous case. If there was only one defect, the largest coating defect at the 30 m position was found. Assuming two defects, the

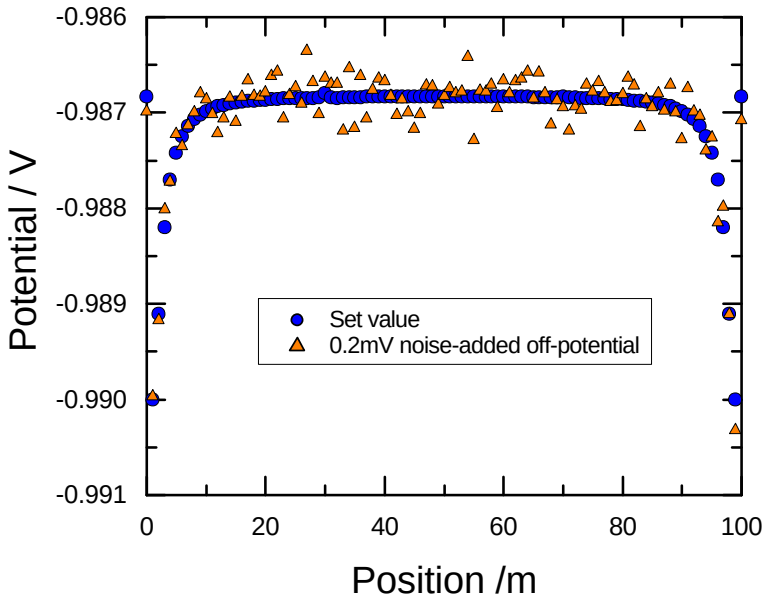

Figure 6-5: Set value and noise-added off-potential on soil surface data.

defects at the 30 m and the 40 m positions could be found. When three defects were assumed initially, no defects could be found. The results are shown in Table 6.2. Figure 6-6 shows χ^2/ν as a function of the number of defects. It indicates that the appropriate number of defects for the current example is two. With the noise data, it is difficult to compare the regression result Table 6.2 with Table 5.2. Apparently, the problem becomes more difficult in estimating the effect of the noise added off-potential data. The common observation is that only two defects can be found in both cases. The most serious defect at the 30 m position can always be found. But the result on other defects vary with the noise-added data, indicating the disturbance of the noise. More refined off-potential data may be necessary to the model. Since the off-potential data are free of IR drop, it will be more reliable to assess pipe condition by using off-potential data if the present model can account for the effect of deposits. Currently, this model can not simulate the influence of scale deposits, but it will be a subject for future research.

Table 6.2: Regression results from the noise-added data by using general form of the objective function (5-25), (5-26) and (5-27). The initial values for each defect was $x_k = 50$ m, $\rho_k = -3.5 \times 10^7$ Ωm, and $\sigma_k = 0.92$ m.

Data Type	Coating Defect	Position x_k / m	Resistivity ρ_k / Ω m	Dimension σ_k / m	χ^2/ν
Set Defect Values					
	1	30	-4.5×10^7	0.316	
	2	40	-3.0×10^6	0.548	
	3	70	-2.0×10^7	0.447	
Regression Result					
Three	1	30.2	-4.36×10^7	0.67	2.94
Three	1	30.1	-4.50×10^7	0.46	2.77
	2	42.8	-3.47×10^7	0.29	
Three	1	49.8	-3.57×10^7	1.20	7.81
	2	50.0	-3.56×10^7	0.92	
	3	53.1	-3.46×10^7	0.10	

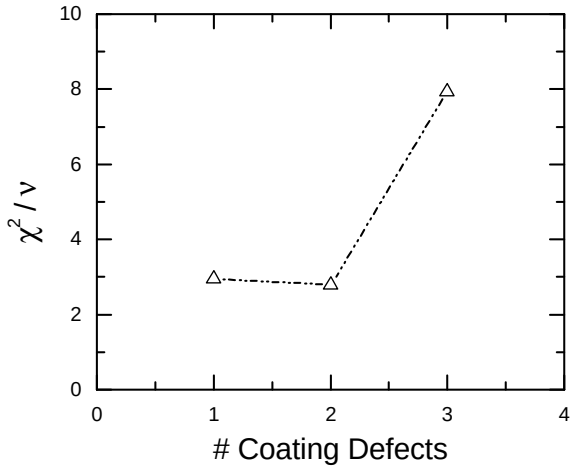

Figure 6-6: Decide the number of defects using noise-added on and off-potential and current density data.

6.3 Conclusions

In this chapter, the effectiveness of the general form of the objective function was studied by using three kinds of survey data. It is concluded that

1. Since the off-potential on soil surface does not vary much on the neighboring soil surface area right above the center line of pipe, few data points need to be measured.

2. Comparing Figure 6-4 with Figure 6-6, it can be find that more coating defects can be found by using noise free data than that with added noise. This result agrees well with the findings from other research, *i.e.,* the impedance analysis.

3. With the general form of the objective function, the more kinds of data sets applied, the more precise the regression results are for the noise free data sets.

4. Since the off-potential data are free of IR drop, it will be more reliable to assess pipe condition by using off-potential data if the present model can account for the effect of deposits.

CHAPTER 7
SUMMARY AND FUTURE WORK

7.1 Summary

Pipeline corrosion costs the U.S. seven billions of dollars. Ninety percent of the cost is the capital, operation and maintenance. To preserve the asset of the pipeline and to ensure safe operations, regular pipeline inspections need to be done to avoid possible failures. In addition, methods to analyze and interpret pipeline survey data to maximize information becomes more important than ever.

In this study, a computer program, which can be used to extract the conditions of the pipe taking into account a wide variety of field survey data, has been developed. The program consists of two parts, the *forward* model and the *inverse* model. The integration of these two models makes the program effective. Besides, this effort established a *proof of concept* which can motivate future developments.

The *forward* model was developed to address how the cathodic protection pipeline system works. The resistivity of pipe coating was approximated by the parameters of the coating defects. The linear boundary conditions were applied to simplify the calculation. The boundary element method with cylindrical elements was developed to reduce the computation task. With the varying potentials on the pipe steel, the on-potential on the soil surface and the current density of the pipe in the axial direction could be obtained. When the anode is disconnected with the pipeline, the off-potential on the soil surface could also be calculated.

The *inverse* model focused on construction of an effective objective function. The scaled objective function possesses the advantages that the weighting strategy

is based on the error structure of each type of data and that the influence of superfluous input information can be reduced. By minimizing the objection function, the parameters to describe the coating conditions were estimated. Several kinds of heterogeneous data sets, *i.e.,* the on-potential, off-potential and the current density data, were applied to the objective function to provide as more information as possible.

Since the *forward* model was applied frequently in the *inverse* calculation, it needed to be precise and fast. The present study shows that the simplified version of the *forward* model can couple well with the *inverse* model in interpreting the pipeline survey data.

7.2 Future Work

Currently, the model was applied to the synthetic data generated for a section of a coated underground pipeline which is electrically connected to a vertical sacrificial anode. For the next step, the synthetic data generated by the *CP3D* model can be used as the pipeline survey data. Comparing the results of the coating conditions obtained from this *inverse* model with the set condition for the *CP3D* model, the robustness of the *inverse* model developed in present study will be further verified.

In addition, an underground pipeline with multi-anode can be simulated by the present model. Other applications for cylindrical shaped object, such as tank, will be another direction to extend the model's applications.

Eventually, a user friendly interface needs to be created for practical applications.

APPENDIX A
BOUNDARY INTEGRAL

A.1 Integral along One Object

When the integral is calculated on one object, it is appropriate to use local coordinate. The integral can be over cylindrical elements or circle elements.

A.1.1 Integral over Cylindrical Elements

There are two kinds of integral over cylindrical elements, depending on the position of the collocation points.

When the collocation points are on the cylinder reference line, the local coordinate of the collocation point P is $(R, 0, z_P)$ and the integration point Q is $(R\cos\theta, R\sin\theta, z_Q)$.

$$|\mathbf{r}_{PQ}| = r_{PQ} = \sqrt{(R\cos\theta - R)^2 + (R\sin\theta)^2 + (z_Q - z_P)^2} \tag{A-1}$$

Substitute equation (A-1) into equation (4-43) to get G_{ij}

$$G_{ij} = l_j(\frac{R}{4\pi})\int_0^1(\sum_{k=1}^{2} q_{jk}N_k(t))dt\int_0^{2\pi}\frac{1}{\sqrt{(R\cos\theta - R)^2 + (R\sin\theta)^2 + (z_j - z_i)^2}}d\theta \tag{A-2}$$

Since $\mathbf{n}_j = \cos\theta\vec{i} + \sin\theta\vec{j}$ at the cylindrical surface by Substituting equation (A-1) into equation (4-44), H_{ij} becomes

$$\begin{aligned} H_{ij} &= l_j(\frac{R}{4\pi})\int_0^1(\sum_{k=1}^{2} u_{jk}N_k(t))dt\int_0^{2\pi}\frac{\partial(\frac{1}{r_{ij}})}{\partial(\mathbf{e}_R)}d\theta \\ &= l_j(\frac{R}{4\pi})\int_0^1\int_0^{2\pi}\frac{(-R)(1-\cos\theta)(\sum_{k=1}^{2} u_{jk}N_k(t))dtd\theta}{[\sqrt{2R^2 - 2R^2\cos\theta + (z_j - z_i)^2}]^3} \end{aligned} \tag{A-3}$$

Where z_j is a function of t. It can be described as

$$z_j = l_p + l_j t \tag{A-4}$$

where l_p represents the length before element j. l_p is a constant if the element j is fixed.

When the collocation points are on the center of the circles, which are the two ends of cylinder, the local coordinates of P, Q points are $(0, 0, z_P)$ and $(R\cos\theta, R\sin\theta, z_Q)$ respectively.

$$\begin{aligned} |\mathbf{r}_{PQ}| &= r_{PQ} = \sqrt{(R\cos\theta - 0)^2 + (R\sin\theta - 0)^2 + (z_Q - z_P)^2} \\ &= \sqrt{R^2 + (z_Q - z_P)^2} \end{aligned} \tag{A-5}$$

Substituting equation (A-5) into equation (4-43), G_{ij} becomes

$$\begin{aligned} G_{ij} &= l_j(\frac{R}{4\pi})\int_0^1(\sum_{k=1}^{2} q_{jk}N_k(t))dt\int_0^{2\pi}\frac{1}{\sqrt{R^2 + (z_J - z_I)^2}}d\theta \\ &= l_j(\frac{R}{4\pi})\frac{2\pi}{\sqrt{R^2 + (z_j - z_i)^2}}\int_0^1(\sum_{k=1}^{2} q_{jk}N_k(t))dt \\ &= [\frac{l_j R}{2\sqrt{R^2 + (z_j - z_i)^2}}]\int_0^1(\sum_{k=1}^{2} q_{jk}N_k(t))dt \end{aligned} \tag{A-6}$$

And Substituting equation (A-5) into equation (4-44), H_{ij} becomes

$$\begin{aligned} H_{ij} &= l_j(\frac{R}{4\pi})\int_0^1(\sum_{k=1}^{2} u_{jk}N_k(t))dt\int_0^{2\pi}\frac{\partial(\frac{1}{\sqrt{R^2 + (z_j - z_i)^2}})}{\partial(\mathbf{e}_R)}d\theta \\ &= \frac{-l_j R^2}{2(\sqrt{R^2 + (z_j - z_i)^2})^3}\int_0^1(\sum_{k=1}^{2} u_{jk}N_k(t))dt \end{aligned} \tag{A-7}$$

A.1.2 Integral over Circle Elements

The collocation points can be on the cylinder side area or the center of circle element as the integral is calculated over circle elements.

When the collocation points are on the cylinder side, P, Q are $(R, 0, z_P)$ and $(r\cos\theta, r\sin\theta, z_Q)$ in local coordinates. Here, r is distance from center of circle O_1 or O_2 to any point on the circle, as shown in Figure 4-8.

$$\begin{aligned} |\mathbf{r}_{PQ}| &= r_{PQ} = \sqrt{(r\cos\theta - R)^2 + (r\sin\theta)^2 + (z_Q - z_P)^2} \\ &= \sqrt{R^2 + r^2 - 2Rr\cos\theta + (z_Q - z_P)^2} \end{aligned} \tag{A-8}$$

Substituting equation (A-8) into equation (4-45), we get G_{ij}

$$G_{ij} = q_j(\frac{1}{4\pi})\int_0^R\int_0^{2\pi}\frac{rdrd\theta}{\sqrt{R^2+r^2-2Rr\cos\theta+(z_j-z_i)^2}} \tag{A-9}$$

At the circle surface $\mathbf{n}_j = \pm\mathbf{e}_z$, where $+\mathbf{e}_z$ refers to the normal vector of the ending circle surface, while $-\mathbf{e}_z$ refers to the normal vector of the beginning circle surface. Substituting equation (A-8) into equation (4-46), we get H_{ij}

$$\begin{aligned} H_{ij} &= u_j(\frac{1}{4\pi})\int_0^R\int_0^{2\pi}\frac{\partial(\frac{1}{\sqrt{R^2+r^2-2Rr\cos\theta+(z_j-z_i)^2}})}{\partial(\pm\mathbf{e}_z)}rdrd\theta \\ &= u_j[\frac{\mp(z_j-z_i)}{4\pi}]\int_0^R\int_0^{2\pi}\frac{rdrd\theta}{[\sqrt{R^2+r^2-2Rr\cos\theta+(z_j-z_i)^2}]^3} \end{aligned} \tag{A-10}$$

When the collocation points are the center of the circle elements, the local coordinates of P, Q are $(0,0,z_P)$ and $(r\cos\theta, r\sin\theta, z_Q)$.

$$\begin{aligned} |\mathbf{r}_{PQ}| &= r_{PQ} = \sqrt{(r\cos\theta)^2+(r\sin\theta)^2+(z_Q-z_P)^2} \\ &= \sqrt{r^2+(z_Q-z_P)^2} \end{aligned} \tag{A-11}$$

Substituting equation (A-11) into equation (4-45), G_{ij} becomes

$$G_{ij} = q_j(\frac{1}{4\pi})\int_0^R\int_0^{2\pi}\frac{rdrd\theta}{\sqrt{r^2+(z_j-z_i)^2}} \tag{A-12}$$

Substituting equation (A-11) into equation (4-46), H_{ij} becomes

$$\begin{aligned} H_{ij} &= u_j(\frac{1}{4\pi})\int_0^R\int_0^{2\pi}\frac{\partial(\frac{1}{\sqrt{r^2+(z_j-z_i)^2}})}{\partial(\pm\mathbf{e}_z)}rdrd\theta \\ &= u_J[\frac{\mp(z_j-z_i)}{4\pi}]\int_0^R\int_0^{2\pi}\frac{rdrd\theta}{[\sqrt{r^2+(z_j-z_i)^2}]^3} \end{aligned} \tag{A-13}$$

A.2 Integral between Different Objects

Integral between an object and its mirror reflection with respect to the soil surface and integral between pipe and anode all belong to the integral between different objects. In order to simplify the calculation, the coordinate transformation

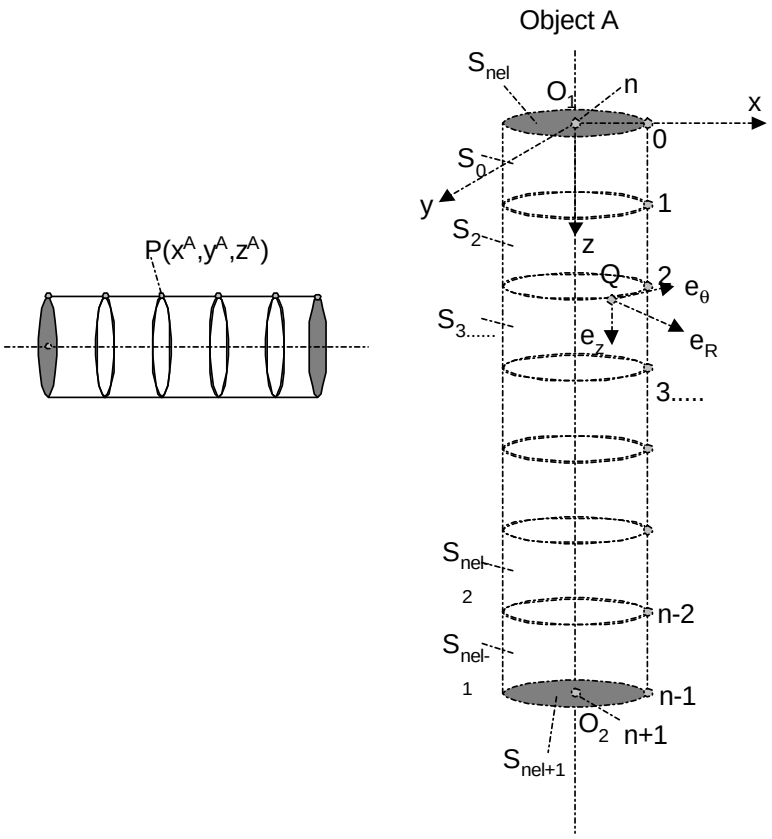

Figure A-1: Integral between different objects.

between two different local coordinates needs to be done. For example, to integrate from collocation point P, which is not belong to object A, to any point on the object A, P's coordinate has to be changed to object A's local coordinate (See Figure A-1). Thus, P's coordinate becomes (x_P^A, y_P^A, z_P^A) in A's coordinate. The equations to obtain matrices G and H are induced below.

A.2.1 Integral over Cylindrical Elements

When the collocation points are on the cylinder side area, the coordinate of P about object A's local coordinate can be simply written as (x, y, z_P). The integration point Q is $(R\cos\theta, R\sin\theta, z_Q)$, which is on the surface of object A.

$$\begin{aligned} |\mathbf{r}_{PQ}| &= r_{PQ} = \sqrt{(R\cos\theta - x)^2 + (R\sin\theta - y)^2 + (z_Q - z_P)^2} \\ &= \sqrt{-2R(x\cos\theta + y\sin\theta) + [x^2 + y^2 + R^2 + (z_Q - z_P)^2]} \end{aligned} \quad \text{(A-14)}$$

Substituting equation (A-14) into equation (4-43), G_{ij} becomes

$$\begin{aligned} G_{ij} &= l_j(\frac{R}{4\pi})\int_0^1(\sum_{k=1}^{2} q_{jk}N_k(t))dt \\ &\cdot \int_0^{2\pi}\frac{1}{\sqrt{-2R(x\cos\theta+y\sin\theta)+[x^2+y^2+R^2+(z_j-z_i)^2]}}d\theta \end{aligned} \tag{A-15}$$

Equation (A-15) can be arranged as

$$G_{ij} = l_j(\frac{R}{\pi})\frac{K(k)}{\sqrt{(\sqrt{x^2+y^2}+R)^2+(z_J-z_I)^2}}\int_0^1(\sum_{K=1}^{2} q_{JK}N_K(t))dt \tag{A-16}$$

Where $K(k)$ is the first kind of complete elliptic integral. For matrix H, substituting equation (A-14) into equation (4-44), we get

$$H_{ij} = l_j(\frac{R}{4\pi})\int_0^1(\sum_{k=1}^{2} u_{jk}N_k(t))dt\int_0^{2\pi}\frac{\partial(\frac{1}{r_{ij}})}{\partial(\mathbf{e}_R)}d\theta \tag{A-17}$$

Equation (A-17) can be arranged as

$$\begin{aligned} H_{ij} &= \frac{l_jR}{\pi}\{\frac{[K(k)-\Pi(k)]}{(-2R)\sqrt{(\sqrt{x^2+y^2}+R)^2+(z_j-z_i)^2}} \\ &- \frac{\Pi(k)(\sqrt{x^2+y^2}+R)}{[\sqrt{(\sqrt{x^2+y^2}+R)^2+(z_j-z_i)^2}]^3}\}\int_0^1(\sum_{k=1}^{2} u_{jk}N_k(t))dt \end{aligned} \tag{A-18}$$

Where $\Pi(k)$ is the third kind of complete elliptic integral.

A.2.2 Integral over Circle Elements

To integrate over circle elements, P's coordinate with respect to object A is still (x, y, z_P). The coordinate of collocation point Q is $(r\cos\theta, r\sin\theta, z_Q)$.

$$\begin{aligned} |\mathbf{r}_{PQ}| &= r_{PQ} = \sqrt{(r\cos\theta-x)^2+(r\sin\theta-y)^2+(z_Q-z_P)^2} \\ &= \sqrt{x^2+y^2+r^2-2r(x\cos\theta+y\sin\theta)+(z_Q-z_P)^2} \end{aligned} \tag{A-19}$$

Substituting equation (A-19) into equation (4-45), G_{ij} becomes

$$G_{ij} = q_j(\frac{1}{4\pi})\int_0^R\int_0^{2\pi}\frac{rdrd\theta}{\sqrt{x^2+y^2+r^2-2r(x\cos\theta+y\sin\theta)+(z_j-z_i)^2}} \tag{A-20}$$

Substituting equation (A-19) into equation (4-46), H_{ij} becomes

$$\begin{aligned} H_{ij} &= u_j\left(\frac{1}{4\pi}\right)\int_0^R\int_0^{2\pi}\frac{\partial\left(\frac{1}{\sqrt{x^2+y^2+r^2-2r(x\cos\theta+y\sin\theta)+(z_j-z_i)^2}}\right)}{\partial(\pm\mathbf{e}_z)}rdrd\theta \\ &= u_j\left[\frac{\mp(z_j-z_i)}{4\pi}\right]\int_0^R\int_0^{2\pi}\frac{rdrd\theta}{[\sqrt{x^2+y^2+r^2-2r(x\cos\theta+y\sin\theta)+(z_j-z_i)^2}]^3} \end{aligned} \tag{A-21}$$

APPENDIX B
CODE STRUCTURE

The code in present work were created and compiled by using Visual C++ 6.0. Object orientation programming method was used. The code structure for the *forward* model and the *inverse* model are shown in Figure B-1 and B-2 respectively.

B.1 Code Structure of the Forward Model

B.2 Code Structure of the Inverse Model

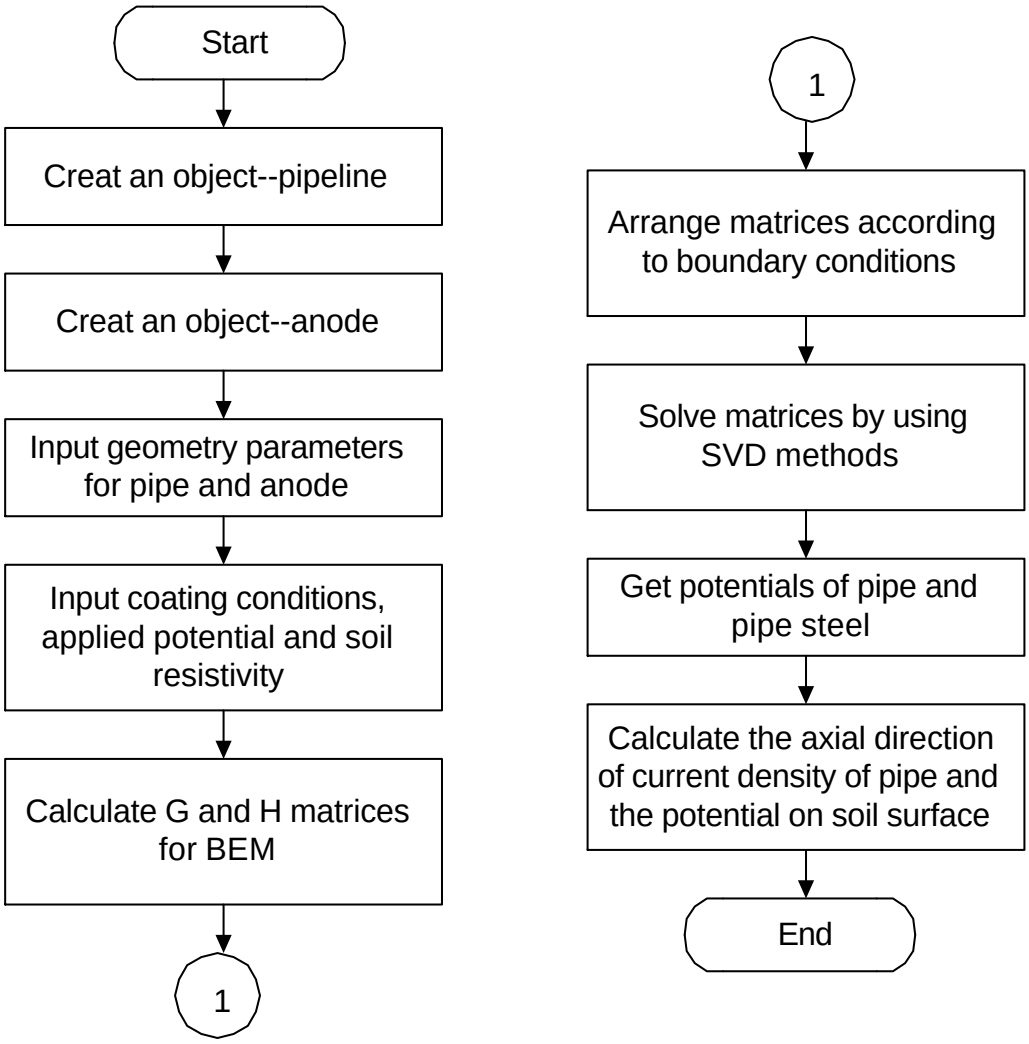

Figure B-1: Code structure of the *forward* model.

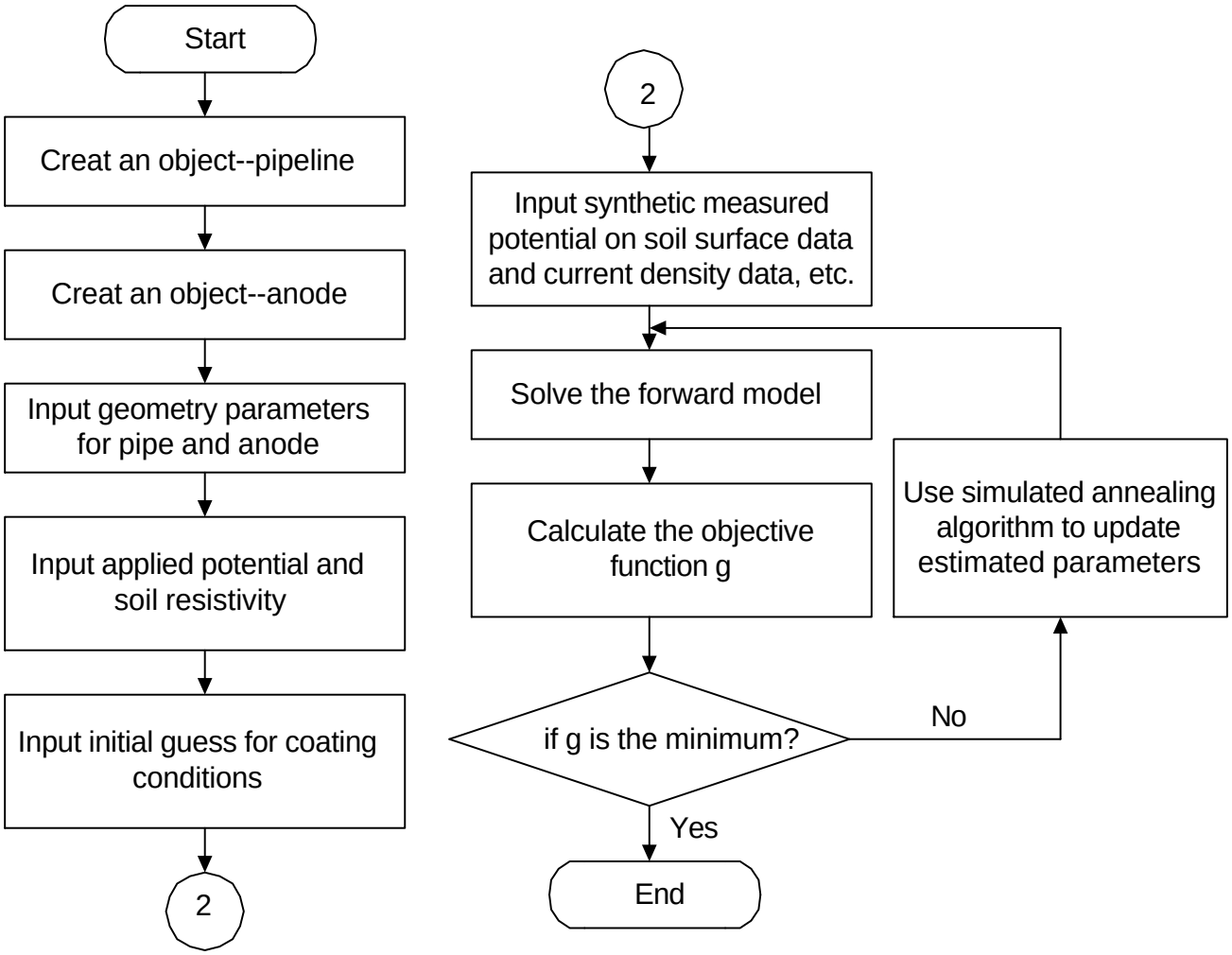

Figure B-2: Code structure of the *inverse* model.

APPENDIX C
INTERFACE

Currently, the interface was made for the *forward* model. Two kinds of windows were created. One was for the inputting conditions, the other is for outputting results.

C.1 Input Windows

The properties of pipeline, anode and coating conditions are input through the three windows, as shown in Figures C-1, C-2 and C-3.

C.2 Output Windows

In the output window, the figures of potential, coating resistivity, and current density can all be shown by pressing the corresponding buttons. See Figure C-4

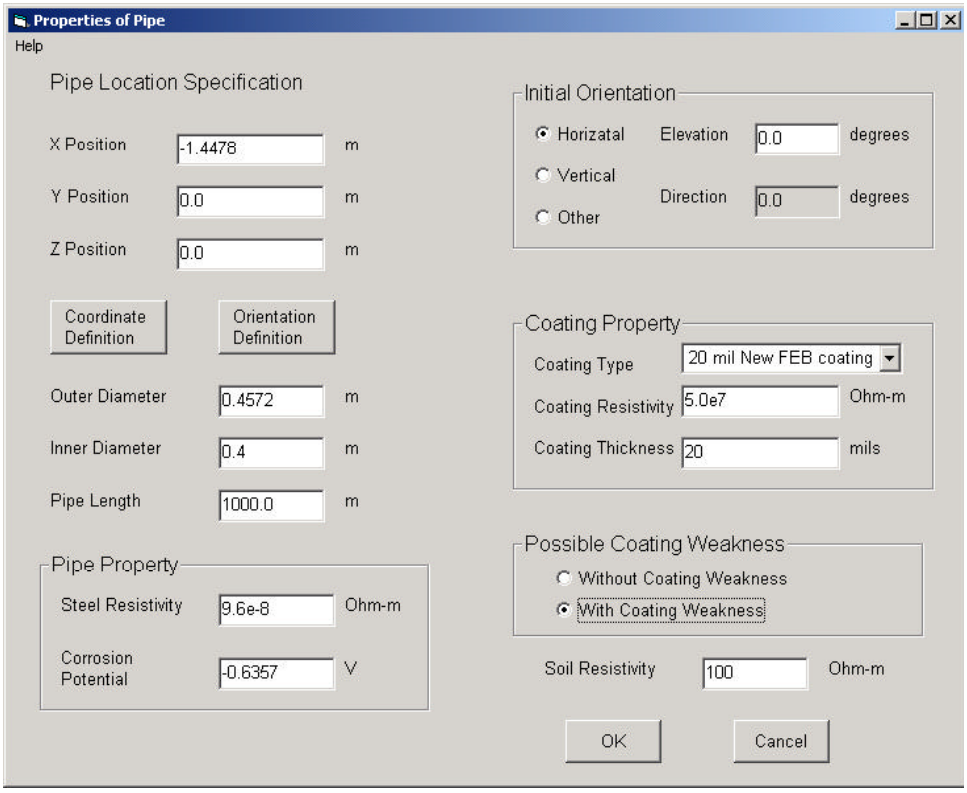

Figure C-1: Window for pipe properties.

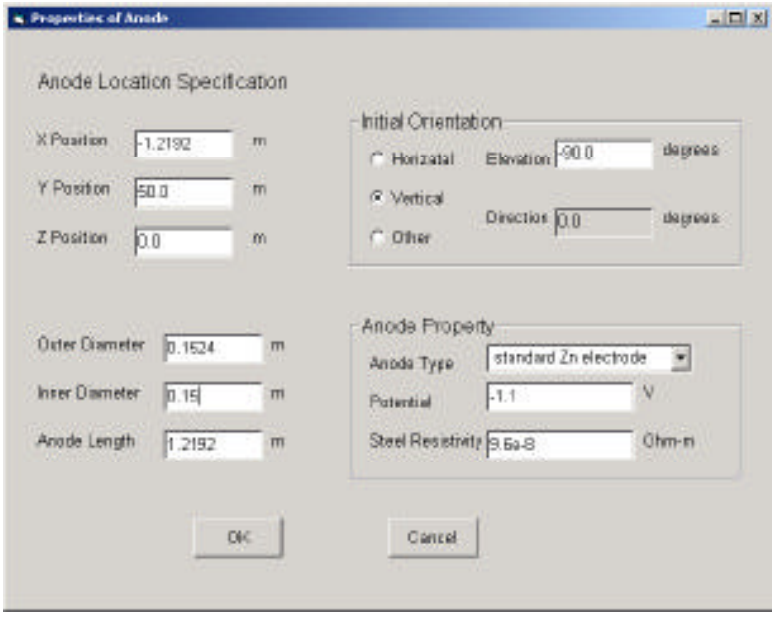

Figure C-2: Window for anode properties.

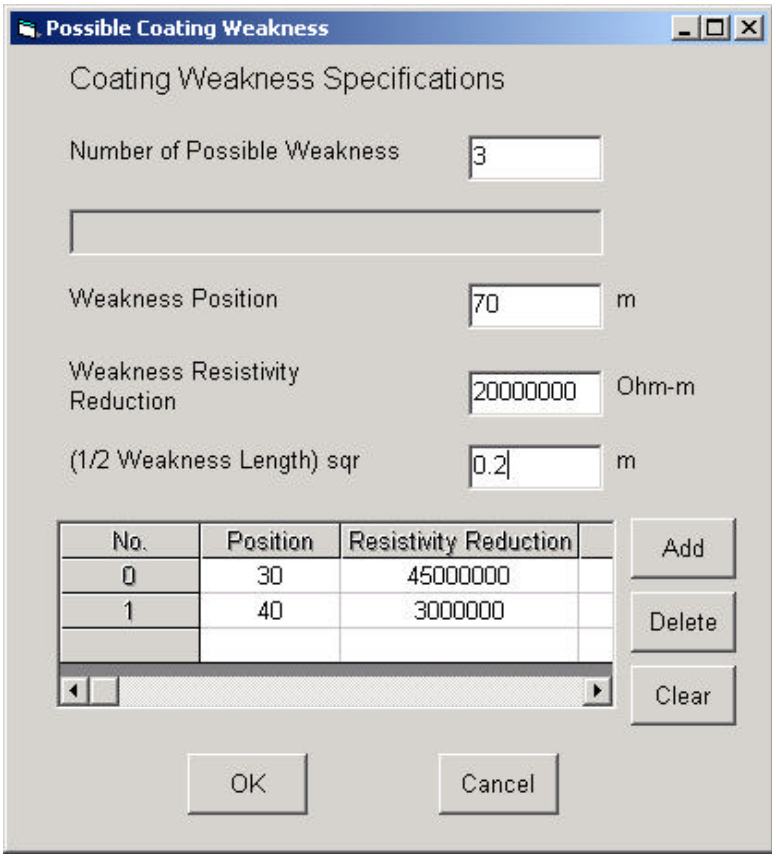

Figure C-3: Window for coating properties.

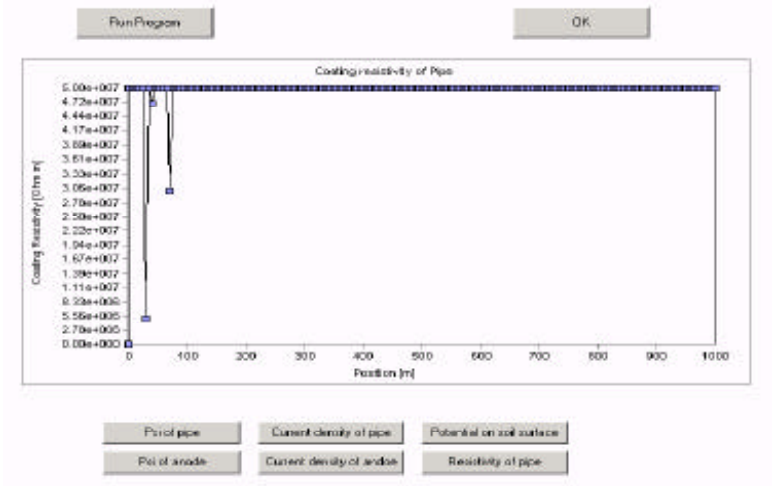

Figure C-4: Window for figures.

REFERENCES

1. D. Riemer and M. Orazem, "Development of Mathematical Models for Cathodic Protection of Multiple Pipelines in a Right of Way," in *Proceedings of the 1998 International Gas Research Conference* (1998) 383–393.

2. J. C. F. Telles, W. J. Mansur, L. C. Wrobel, and M. G. Marinho, "Numerical Simulation of a Cathodically Protected Semisubmersible Platform Using the PROCAT System," *Corrosion*, **46** (1990) 513–518.

3. F. Brichau, J. Deconinck, and T. Driesens, "Modeling of Underground Cathodic Protection Stray Currents," *Corrosion*, **52** (1996) 480–488.

4. G. Koch, M. Brongers, N.G.Thompson, Y.P.Virmani, and J.H.Payer, *Corrosion Cost and Preventive Strategies in the United States*, Technical report, CC Technologies Laboratories, Inc. (2001).

5. G. Prentice, *Electrochemical Engineering Principles* (Englewood Cliffs: Prentice Hall, 1991).

6. D. A. Jones, *Corrosion* (New York: Macmillan Publishing Company, 1992).

7. J. Bockris and D. Drazic, *Electro-chemical Science* (London: Taylor and Francis, 1972).

8. J. Newman, *Electrochemical Systems*, 2nd edition (Englewood Cliffs: Prentice-Hall, 1991).

9. A. W. Peabody, *Control of Pipeline Corrosion* (Houston: NACE International, 1978).

10. S. P. Ewing, "Potential Measurements for Determining Cathodic Protection Requirements," *Corrosion*, (1951).

11. F. Chowdhury and D. T. Vu, "IR Drop-free Readings Offer Best Gauge of CP Effectiveness," *Pipe Line and Gas Industry Features*, **83** (2000).

12. M. Parker and E. Peattie, *Pipeline Corrosion and Cathodic Protection*, 3rd edition (Houston: Gulf Publishing Company, 1984).

13. J. M. Leeds, "New Corrosion Dection Method for Buried Pipe Lines–Part 1," *Pipeline Industry*, (1992) 48–52.

14. M. E. Orazem, J. M. Esteban, K. J. Kennelley, and R. M. Degerstadt, "Mathematical Models for Cathodic Protection of An Underground Pipeline with Coating Holidays .1. Theoretical Development," *CORROSION*, **53** (1997) 264–272.

15. R. Cameron, W. Halliday, and S. Richards, "Airborne Remote Sensing of Pipeline Cathodic Protection Systems," in *The NACE Annual Conference and Corrosion Show* (1992) Paper 385.

16. D. Fasino and G. Inglese, "Discrete Methods in the Study of an Inverse Problem for Laplace's Equation," *IMA Journal of Numerical Analysis*, **19** (1999) 105–118.

17. G. Inglese, "An inverse problem in corrosion detection," *Inverse Problems*, **13** (1997) 977–994.

18. S. Aoki and K. Kishimoto, "Prediction of Galvanic Corrosion Rates by the Boundary Element Method," *Mathematical And Computer Modelling*, **15** (1991) 11–22.

19. C. Brebbia and G. Maier, "Boundary Element Analysis of Galvanic Corrosion," in *Boundary Element VII*, C. Brebbia and G. Maier, editors, volume 1 (New York: Springer-Verlag, 1985) 63–71.

20. K. Amaya, J. Togashi, and S. Aoki, "Inverse Analysis of Galvanic Corrosion - Using Fuzzy a-Priori Information," *JSME International Journal Series a-Mechanics and Material Engineering*, **38** (1995) 541–546.

21. S. Aoki and K. Amaya, "Boundary Element Analysis of Inverse Problem in Corrosion Engineering," in *Boundary Integral Formulations for Inverse Analysis*, D. B. Ingham and L. C. Wrobel, editors (Southampton: Computational Mechanics Publications, 1997) 151–169.

22. J. Nelder and R. Mead, "A Simplex-Method for Function Minimization," *Computer Journal*, **7** (1965) 308–313.

23. J. Waber and B. Fagan, "Methematical Studies on Galvanic Corrosion," *Journal of the Electrochemical Society*, **103** (1956) 64–72.

24. P. Pierson, K. P. Bethune, W. H. Hartt, and P. Anathakrishnan, "A New Equation for Potential Attenuation and Anode Current Output Projection for Cathodically Polarized Marine Pipelines and Risers," *Corrosion*, **56** (2000) 350–360.

25. J. Morgan, *Cathodic Protection*, 2nd edition (Houston: NACE International, 1993).

26. H. B. Dwight, "Calculations of Resistance to Ground," *Electrical Engineering*, **55** (1936) 1319.

27. P. Doig and P. Flewitt, "A Finite Difference Numerical Analysis of Galvanic Corrosion for Seim-Infinite Linear Coplanar Electrodes," *Journal of Electrochem Society: Electrochemical Science and Technology*, **126** (1979) 2057–2063.

28. C. Bribbia and J. Dominguez, *Boundary Element An Introductory Course* (New York: McGraw-Hill Book Company, 1988).

29. C. Brebbia, J. Telles, and L. Wrobel, *Boundary Element Techniques* (New York: Springer-Verlag, 1984).

30. S. Aoki, K. Kishimoto, and M. Miyasaka, "Analysis of Potential and Current-Density Distributions Using a Bounday Element Method," *Corrosion*, **44** (1988) 926–932.

31. J. Telles, L. Wrobel, W. Mansur, and J. Azevedo, "Boundary Elements for Cathodic Protection Problems," in *Boundary Elements VII*, C. Brebbia and G. Maier, editors, volume 1 (New York: Springer-Verlag, 1985) 73–83.

32. F. Brichau and J. Deconinck, "A Numerical-Model For Cathodic Protection Of Buried Pipes," *Corrosion*, **50** (1994) 39–49.

33. K. J. Kennelley, L. Bone, and M. E. Orazem, "Current and Potential Distribution on a Coated Pipeline with Holidays: 1. Model and Experimental Verification," *Corrosion*, **49** (1993) 199–210.

34. M. E. Orazem, K. J. Kennelley, and L. Bone, "Current and Potential Distribution on a Coated Pipeline with Holidays: 2. A Comparison of the Effects of Discrete and Distributed Holidays," *Corrosion*, **49** (1993) 211–219.

35. M. E. Orazem, J. M. Esteban, K. J. Kennelley, and R. M. Degerstedt, "Mathematical Models for Cathodic Protection of an Underground Pipeline with Coating Holidays: 2. Case Studies of Parallel Anode CP Systems," *Corrosion*, **53** (1997) 427–436.

36. R. M. Degerstedt, K. J. Kennelley, M. E. Orazem, and J. M. Esteban, "Traditional Cathodic Protection Design Methods for Coated Pipelines and the Necessity of Computer Modeling," *Materials Performance*, **35** (1996) 16–20.

37. M. E. Orazem, J. M. Esteban, K. J. Kenelley, and R. M. Degerstedt, "Mathematical Models for Cathodic Protection of an Underground Pipeline with Coating Holidays: Part 1 - Theoretical Development," *Corrosion*, **53** (1997) 264–272.

38. D. P. Riemer, *Modeling Cathodic Protection for Pipeline Networks*, Ph.D. dissertation, University of Florida, Gainesville, Florida (2000).

39. D. Riemer and M. Orazem, "Cathodic Protection of Multiple Pipelines with Coating Holidays," in *Procedings of the NACE99 Topical Research Symposium: Cathodic Protection: Modeling and Experiment*, M. E. Orazem, editor, NACE (Houston: NACE International, 1999) 65–81.

40. D. P. Riemer and M. E. Orazem, "Application of Boundary Element Models to Predict Effectiveness of Coupons for Assessing Cathodic Protection of Buried Structures," *Corrosion*, **56** (2000) 794–800.

41. S. Aoki and K. Amaya, "Optimization of Cathodic Protection System by BEM," *Engineering Analysis with Boundary Elements*, **19** (1997) 147–156.

42. M. Ridha, K. Amaya, and S. Aoki, "A Multi-Step Genetic Algorithm for Detecting Corrosion of Reinforcing Steels in Concrete Structure," *Corrosion*, **57** (2001) 794–801.

43. S. Aoki and K. Amaya, "Optimal Cathodic Protection for Ship," in *Boundary Element Technology XI*, R. Ertekin, B. C. A., T. M., and R. Shaw, editors (BETECH, 1996) 345–356.

44. P. Miltiadou and L. C. Wrobel, "A BEM-based Genetic Algorithm for Identification of Polarization Curves in Cathodic Protection System," *International Journal for Numerical Methods in Engineering*, **54** (2002) 159–174.

45. L. Wrobel and P. Miltiadou, "Genetic Algorithms for Inverse Cathodic Protection Problems," (2003). In press.

46. S. Aoki, K. Amaya, A. Nakayama, and A. Nishikawa, "Elimination of Error from Nonuniform Current Distribution in Polarization Measurement by Boundary Element Inverse Analysis," *Corrosion*, **54** (1998) 259–264.

47. H. C. Jongschaap, R. Wytch, J. M. Hutchison, and V. Kulkarni, "Electrical Impedance Tomography: A Review of Current Literature," *European Journal of Radiology*, **18** (1994) 165–174.

48. J. P. Kaipio, V. Kolehmainen, E. Somersalo, and M. Vauhkonen, "Statistical Inversion and Monte Carlo Sampling Methods in Electrical Impedance Tomography," *Inverse Problems*, **16** (2000) 1487–1522.

49. B. Brown, "Medical Impedance Tomography and Process Impedance Tomography: A Brief Review," *Measurement Science & Technology*, **12** (2001) 991–996.

50. Y. Zou and Z. Guo, "A Review of Electrical Impedance Techniques for Breast Cancer Detection," *Medical Engineering & Physics*, **25** (2003) 79–90.

51. A. Tamburrino and G. Rubinacci, "A New Non-Iterative Inversion Method for Electrical Resistance Tomography," *Inverse Problems*, **18** (2002) 1809–1829.

52. L. Borcea, "Electrical Impedance Tomography," *Inverse Problems*, **18** (2002) R99–R136.

53. S. L. Ceccio and D. L. George, "A Review of Electrical Impedance Techniques for the Measurement Of Multiphase Flows," *Transactions of the ASME. Journal of Fluids Engineering*, **118** (1996) 391–399.

54. H. S. Tapp and R. A. Williams, "Status and Applications of Microelectrical Resistance Tomography," *Chemical Engineering Journal*, **77** (2000) 119–125.

55. H. S. Tapp, A. J. Peyton, E. K. Kemsley, and R. H. Wilson, "Chemical Engineering Applications of Electrical Process Tomography," *Sensors and Actuators B*, **92** (2003) 17–24.

56. R. A. Williams and X. Jia, "Tomographic Imaging of Particulate Systems," *Advanced Powder Technology*, **14** (2003) 1–16.

57. T. York, "Status of Electrical Tomography in Industrial Applications," *Journal of Electronic Imaging*, **10** (2001) 608–619.

58. J. E. Molyneux and A. Witten, "Impedance Tomography: Imaging Algorithms for Geophysical Applications," *Inverse Problems*, **10** (1994) 655–667.

59. S. Narayan, M. B. Dusseault, and D. C. Nobes, "Inversion Techniques Applied to Resistivity Inverse Problems," *Inverse Problems*, **10** (1994) 669–686.

60. M. J. Wilt, D. L. Alumbaugh, H. F. Morrison, A. Becker, K. H. Lee, and M. Deszczpan, "Crosswell Electromagnetic Tomography - System-Design Considerations and Field Results," *Geophysics*, **60** (1995) 871–885.

61. S. Narayan and M. B. Dusseault, "Subsurface-to-Surface Resistivity Method for Monitoring Fluid Progression in Improved Oil Recovery Projects," *In Situ*, **23** (1999) 75–106.

62. S. Narayan and M. B. Dusseault, "Sensitivity Studies of Resistivity Monitoring for Shallow Enhanced Recovery Processes - A Numerical Case History," *Journal of Canadian Petroleum Technology*, **39** (2000) 52–61.

63. K. Suzuki, S. Toda, K. Kusunoki, Y. Fujimitsu, T. Mogi, and A. Jomori, "Case Studies of Electrical and Electromagnetic Methods applied to Mapping Active Faults Beneath the Thick Quaternary," *Engineering Geology*, **56** (2000) 29–45.

64. A. Denis, A. Marache, T. Obellianne, and D. Breysse, "Electrical Resistivity Borehole Measurements: Application to an Urban Tunnel Site," *Journal of Applied Geophysics*, **50** (2002) 319– 331.

65. A. Vehtari and J. Lampinen, "Bayesian MLP Neural Networks for Image Analysis," *Pattern Recognition Letters*, **21** (2000) 1183–1191.

66. W. Warsito and L. S. Fan, "Neural Network Based Multi-Criterion Optimization Image Reconstruction Technique for Imaging Two- and Three-Phase Flow Systems using Electrical Capacitance Tomography," *Measurement Science & Technology*, **12** (2001) 2198–2210.

67. M. Bonnet, *Boundary Integral Equation Methods for Solids and Fluids* (New York: John Wiley and Sons Ltd, 1995).

68. F. Hartmann, C. Katz, and B. Protopsaltis, "Boundary Elements and Symmetry," *INGENIEUR ARCHIV*, **55** (1985) 440–449.

69. L. Gray and G. Paulino, "Symetric Galerkin Boundary Integral Formulation for Interface and Multi-zone Problems," *International Journal for Numerical Methods in Engineering*, **40** (1997) 3085–3101.

70. I. Stakgold, *Greens Functions and Boundary Value Problems* (New York: John Wiley & Sons, 1979).

71. S. Aoki, K. Kishimoto, and M. Miyasaka, "Analysis of Potential and Current Density Distributions using a Boundary Element Method," *Corrosion*, **44** (1988) 926–932.

72. F. Brichau, *A Mathematical Model for the Cathodic Protection of Underground Pipelines including Stray Currents*, Ph.D. dissertation, Vrije Universiteit Brussel, Brussels, Belgium (1994).

73. F. Yoshikawa and M. Tanaka, "Boundary Elements in Axisymmetric Potential Problems," in *Boundary Element Methods in Engineering*, C. Brebbia, editor (New York: Springer-Verlag, 1982) 101–111.

74. C. Provatidis, *A Fast Fourier-Boundary Element Mehtod for Axisymmetric Potential and Eleaticity Problems with Arbitrary Boundary Conditions*, Ph.D. dissertation, National Technical University of Athens (1999).

75. B. Berot, F.and Peseux, "Virbo-Acoustic Behavior of Submerged Cylindrical Shells: Analytical Formulation and Numerical Model," *Journal of Fluids and Structures*, **12** (1998) 959–1003.

76. J. W. Gibbs, *The Scientific Papers Vol. II* (New York: Dover Pub. Inc., 1961).

77. J. C. F. Telles and F. A. D. Paula, "Boundary Elements with Equilibrium Satisfaction - a Consistent Formulation for Potential and Elastostatic Analysis," *International Journal of Numerical Methods in Engineering*, **32** (1991) 609–621.

78. W. Press, S. Teukolsky, W. Vetterling, and B. Flannery, *Numerical Recipes in C*, 2nd edition (New York: Cambridge University Press, 1992).

79. W. L. Goffe, G. Ferrier, and J. Rogers, "Global optimization of statistical functions with simulated annealing," *Journal of Econometrics*, **60** (1994) 65–99.

80. P. Agarwal, M. E. Orazem, and L. H. García-Rubio, "Measurement Models for Electrochemical Impedance Spectroscopy: I. Demonstration of Applicability," *Journal of the Electrochemical Society*, **139** (1992) 1917–1927.

81. P. Agarwal, O. D. Crisalle, M. E. Orazem, and L. H. García-Rubio, "Measurement Models for Electrochemical Impedance Spectroscopy: 2. Determination of the Stochastic Contribution to the Error Structure," *Journal of the Electrochemical Society*, **142** (1995) 4149–4158.

82. A. M. Awad, "Properties of the Akaike Information Criterion," *Microelectronics and Reliability*, **36** (1996) 457–464.

83. T.-J. Wu and A. Sepulveda, "The Weighted Average Information Criterion for Order Selection in Time Series and Regression Models," *Statistics & Probability Letters*, **39** (1998) 1–10.

84. Y. Sakamoto, M. Ishiguso, and G. Kitigawa, *Akaike Information Criterion Statistics* (Boston: D. Reidel Publishing Company, 1986).

85. Z. Masilela and J. Pereira, "Using the Direct Current Voltage Gradient Technology as a Quality Control Tool During Construction of New Pipelines," *Engineering Failure Analysis*, **5** (1998) 99–104.

86. W. Fischer, H. Hildebrand, W. Prinz, and W. Schwenk, "Problems Related to the Measurement of IR-Drop Free Potentials in the Presence of Compensating Currents," *Werkstoffe und Korrosion*, **39** (1988) 18–22.

87. R. A. Gummow and P. Eng, "GIC Effects on Pipeline Corrosion and Corrosion Control Systems," *Journal of Atmospheric and Solar-Terrestrial Physics*, **64** (2002) 1755–1764.

88. S. P. Gay, Jr., "The Effects of Cathodically Protected Pipelines on Aeromagnetic Surveys," *Geophysics*, **51** (1986) 1671–1684.

89. W. H. Campbell and J. E. Zimmerman, "Induced Electric Currents in the Alaska Oil Pipeline Measured by Gradient Fluxgate and SQUID Magnetometers," *IEEE Transactions on Geoscience and Remote Sensing*, **GE-18** (1980) 244–250.

90. J. C. Murphy, G. Hartong, R. F. Cohn, P. J. Moran, K. Bundy, and J. R. Scully, "Magnetic Field Measurement of Corrosion Processes," *Journal of the Electrochemical Society*, **135** (1988) 310–313.

91. C. Qiu and M. E. Orazem, "A Weighted Nonlinear Regression-Based Inverse Model for Interpretation of Pipeline Survey Data," *Journal of the Electrochemical Society*, (2003) submitted.

92. G. A. F. Seber, *Linear Regression Analysis* (New York: John Wiley & Sons, 1977).

93. N. R. Draper and H. Smith, *Applied Regression Analysis*, 3rd edition (New York: Wiley Interscience, 1998).

94. L. D. Cox, "How Does the Spike Affect Instant Off Readings?" *Materials Performance*, **3** (1992) 29.

95. M. D. Allen and N. R. Barnes, "Combination of Corrosion-Survey Methods Improves Protection," *Corrosion Science*, (1988) 59–64.

BIOGRAPHICAL SKETCH

Chenchen Qiu was born on December 20, 1971, in Tianjin, China. In 1994, she graduated with a Bachelor of Engineering degree in chemical engineering from Tianjin University, Tianjin, China. From September 1994 to March 1997, she was with the Chemical Engineering Research Center at Tianjin University, where she performed research on bio-material separation and received her Master of Engineering degree. She then joined the Beijing Petro-chemical Engineering Corporation in Beijing, China, where she worked as a process engineer for one and a half years. In pursuit of a high quality education, she came to the University of Florida in May 1999 and joined the Department of Chemical Engineering with Professor Mark E. Orazem as her advisor. She worked on the study of the interpretation of survey data of the cathodic protected buried underground pipeline.